Quantifying Renal Swelling during Machine Perfusion using Digital Image Correlation

Kelly E. Webster

Thesis submitted to the faculty of the Virginia Polytechnic Institute and State University
in partial fulfillment of the requirements for the degree of

Master of Science
In
Mechanical Engineering

John L. Robertson, Co-Chair
Blake N. Johnson, Co-Chair
Robert L. West
Thomas E. Diller

May 5, 2017
Blacksburg, VA

Keywords: Transplant, Kidney, Edema, Machine Perfusion, Digital Image Correlation, Perfusate Composition, Osmolality, Tonicity

Quantifying Renal Swelling during Machine Perfusion using Digital Image Correlation

Kelly E. Webster

ABSTRACT

While machine perfusion of explanted kidneys is theoretically superior to standard cold storage, it may damage potential transplants unless machine-associated swelling is controlled. This thesis presents the effects of perfusate tonicity on renal swelling during hypothermic machine perfusion. Phosphate buffered solution (PBS) and PBS supplemented with 5% w/v mannitol were used as isotonic (289 mOsm/kg) and hypertonic (568 mOsm/kg) perfusates, respectively. Porcine kidney pairs were procured then flushed and machine perfused; the right and left kidneys were assigned opposite perfusates. An experimental methodology was developed to image porcine kidneys undergoing hypothermic machine perfusion (5 °C) for 15 minutes followed by 120 minutes without perfusion to quantify surface displacement (renal swelling) with digital image correlation (DIC). Surface displacement and size (thickness) were compared between the right and left kidneys of each pair. In addition, discharged renal fluids (i.e., filtrate and venous outflow) and biopsies were collected. On average, kidneys perfused with the mannitol solution were smaller in size than the kidneys perfused with PBS ($p < 0.05$) at the start and end of each experiment; however, there was no significant difference between the renal sizes at the end of the 15 minute perfusion interval ($p > 0.05$). Thus, hypertonic and isotonic perfusates yielded different renal swelling outcomes (i.e., physical size and surface displacement), which suggests that perfusate tonicity influences renal swelling. These experiments are the first time *ex vivo* renal surface displacement measurements have been collected during machine perfusion.

Quantifying Renal Swelling during Machine Perfusion using Digital Image Correlation

Kelly E. Webster

GENERAL AUDIENCE ABSTRACT

There is a chronic shortage of transplantable organs in the United States. As more marginal donor organs are being used to increase the number of transplantable organs, there has been a renewed interest in machine perfusion for organ preservation. While machine perfusion of explanted kidneys is theoretically superior to standard cold storage, it may damage potential transplants unless machine-associated swelling is controlled. This thesis presents the effects of perfusate tonicity on renal swelling during hypothermic machine perfusion. Isotonic and hypertonic solutions were used as perfusates. Porcine kidney pairs were procured then flushed and machine perfused; the right and left kidneys were assigned opposite perfusates. An experimental methodology was developed to image porcine kidneys undergoing hypothermic machine perfusion (5 °C) for 15 minutes followed by 120 minutes without perfusion to quantify surface displacement (renal swelling) with digital image correlation (DIC). DIC is a non-contact technique for measuring shape and displacement in three-dimensions. The results from these experiments show that hypertonic and isotonic fluids yielded different renal swelling outcomes (i.e., physical size and surface displacement), which suggests that tonicity influences renal swelling. This indicates that perfusate tonicity is an important factor for improving renal preservation with machine perfusion, which may increase the number of organs available for transplantation.

Acknowledgements

I would like to acknowledge everyone who has helped me complete this thesis work. First and foremost, I would like to acknowledge my committee members. I would like to thank Dr. John Robertson for giving me the opportunity to work in such an interesting and innovative lab space and for all of your exceptional knowledge about everything from histology to organ transplantation; it all greatly helped me with my experiments. Next, I would like to thank Dr. Blake Johnson for introducing me to bio-sensing and all of its applications for organ transplantation. I would also like to thank Dr. Robert West for having brainstorming sessions with me, which became the foundation for using digital image correlation to measure renal surface displacement – this project would never have happened without you. Lastly, I would like to thank Dr. Thomas Diller for always asking the right questions; your knowledge has been invaluable to my development as a researcher. I worked with Dr. Diller during my senior design project and enjoyed the experience so much that I decided to continue my education and pursue a graduate degree.

In addition, I would like to thank those who helped me develop my experimental method in the lab. First, I would like to thank Mr. Charles Aardema, Smart Perfusion Field Engineer, for teaching me about kidney anatomy/function and how to properly prepare kidneys for perfusion. Also, I would like to thank the students in Dr. Scott Case's lab for allowing me to use their digital image correlation equipment and teaching me the basics of image acquisition.

Lastly, I would like thank all of my family and friends who have been so patient and supportive throughout my graduate studies. I would especially like to thank my parents, Bill and Kathy Webster, who have always taught and showed me that working hard and pursuing a passion are essential for loving what you do.

Table of Contents

Chapter 1 - Introduction

There is a chronic shortage of transplantable kidneys in the United States; the demand for kidneys exceeds the supply. In order to alleviate the gap between demand and supply, more marginal donor kidneys are accepted for transplantation. Traditional cold static preservation methods are not as effective at preserving these lower quality kidneys, so many in the transplant community are turning to dynamic preservation methods. Machine perfusion is the most common dynamic preservation method used clinically. While machine perfusion of explanted kidneys is theoretically superior to standard cold storage, it may damage potential transplants unless machine-associated swelling is controlled. A host of factors can impact the magnitude of renal swelling during perfusion such as: perfusion pressure, temperature, and perfusate tonicity.

This thesis presents the effects of perfusate tonicity on renal swelling during hypothermic machine perfusion. An experimental methodology was developed to image porcine kidneys undergoing hypothermic machine perfusion (5 °C) for a 15 minute interval followed by a 120 minute interval without perfusion. Images were post-processed with digital image correlation which calculated the displacement at thousands of 'reference' points over the entire renal surface. It is hypothesized that kidneys perfused with a hypertonic solution will have a different structural response (i.e., surface displacement) to hypothermic machine perfusion than kidneys perfused with an isotonic solution.

Chapter 2 - Literature Review and Theory

2.1 Organ Transplantation in the U.S.

In the United States, kidneys are the most demanded organ for transplantation; 83% of candidates on the current Waiting List are waiting for a kidney (based on OPTN data as of May 16, 2017). For patients with end-stage renal disease (ESRD), a transplant improves quality of life and lowers mortality, compared to dialysis treatment [1,2]. Unfortunately, the demand for transplantable organs has always exceeded the supply; only 20% of candidates on the Waiting List for a kidney receive a transplant [3]. Although the number of candidates on the Waiting List has increased each year, the number of donor organs has plateaued as a result of:

- Fewer ideal donors due to improved highway safety (i.e., helmets, seatbelts, airbags),
- Increased life expectancy of donors due to medical advancements,
- High discard rate of marginal donor organs.

Since living donors only account for approximately 37% of all kidney donations (based on OPTN data as of May 16, 2017 for 2016), the focus for increasing the number of kidneys available for transplantation has been to increase utilization of deceased donor organs.

2.1.1 Kidney quality and allocation. Several numerical systems have been employed to determine which patients will receive transplants and the predicted quality of transplantable organs. Currently, the Kidney Allocation System (KAS) is the process for matching deceased donor kidneys to potential candidates on the Waiting List. Candidates for kidney transplantation

are classified by the Estimated Post Transplant Survival (EPTS) score. The EPTS score ranges from 0 to 100% and is calculated using a formula that incorporates candidate age, time duration on dialysis, diabetes diagnosis, and the number of prior solid organ transplants. Candidates with lower scores are predicted to have longer graft longevity from high quality kidneys than candidates with higher scores [4].

Previously, deceased donor organs were characterized as Standard Criteria Donors (SCD) or Expanded Criteria Donors (ECD). SCD kidneys are "ideal," classically defined as donation from a healthy 35 year old male without hypertension or diabetes, where donation occurred after brain death (such as sudden, catastrophic head trauma, followed by immediate corporeal resuscitation). Kidneys are designated as ECD if the following factors are satisfied [5]:

- Donor age ≥ 60
- Donor age between 50-59, where at least two are true:
    - Death caused by stroke
    - History of hypertension
    - Serum creatinine levels > 1.5 mg/dl.

Donor kidneys are also characterized by when they are donated relative to the mechanism of death: donation after cardiac death (DCD) and donation after brain death (DBD). Donors are classified as DCD if the heart stops beating before organ procurement [5]. DBD donors experience brain death but circulation and respiration are sustained by medical intervention [5]. DBD donors can be either ECD or SCD based on whether or not they match the ECD criteria.

As of December 2014, the classification of deceased donor kidneys changed to better ensure "longevity matching" [4]. Instead of using the SCD and ECD definitions, deceased donor organs are now characterized by the Kidney Donor Profile Index (KDPI). The KDPI score, which ranges from 0 to 100%, quantifies the tendency of graft failure based on 10 donor clinical and demographic characteristics (OPTN Website on Nov. 28, 2016). The lower the KDPI, the less likely the graft is to fail (i.e., the graft will have a longer function time within the recipient). The goal of the new kidney allocation system is to ensure that kidneys with the greatest expected longevity are most frequently transplanted into candidates with the greatest life expectancy [4]. This is achieved by giving candidates with EPTS scores of 20% or less priority for donor kidneys with KDPI scores of 20% or less.

2.2 Organ Storage Methods

The objective of any organ preservation technique is to "maintain function of the organ and tissue during storage so that the graft will function at reperfusion" [3]. The two techniques for organ preservation are static preservation and dynamic preservation.

2.2.1 Static preservation. Static cold storage (SCS) is the most common preservation technique for organ transplantation today. SCS involves flushing an organ with a preservation solution (perfusate) directly after removal from the donor, then storing the organ on ice (0-4 °C) until warmed prior to transplantation. It has been shown that for warm ischemic intervals greater than 20 minutes, SCS is an inadequate preservation method [3]. SCS utilizes hypothermia to

minimize ischemic injury by reducing the metabolism and oxygen requirements [6]. However, retaining the organ at a low temperature may stimulate negative side effects after implantation (i.e., ischemic reperfusion injury (IRI)), such as oxidative stress and inflammation, which have been linked to graft dysfunction [6,7].

Cold ischemia time (CIT) is the length of time between when the organ is first cooled to when it is re-vascularized during transplantation. An increase in CIT has been shown to negatively impact graft survival [8]. The maximum SCS preservation times for organs range from 4-6 hours for lungs and hearts to 24-36 hours for kidneys [9]. Organs that are not transplanted within those intervals are typically either discarded or donated to laboratories for research studies. The difference in SCS preservation times between different organ types is generally due to the organ's sensitivity to ischemic cold storage. For example, hearts and lungs, which have the shortest allowable CIT, are very sensitive to hypoxic injury [6].

2.2.2 Dynamic preservation. Dynamic preservation methods pump fluid into the organ vasculature; the most common type of dynamic preservation is machine perfusion (MP). *Ex vivo* machine perfusion circulates perfusate through the organ via a pressurized perfusate stream. Machine perfusion emulates the physiologic conditions organs experience *in vivo* by providing an environment in which nutrients and oxygen can be exchanged, toxic metabolic products are eliminated, and the vasculature is hydrodynamically stimulated. Additionally, machine perfusion has the ability to control temperature and pressure, and is capable of measuring organ/perfusate parameters over time.

The perfusate stream can be maintained at either a hypothermic or normothermic temperature. For hypothermic machine perfusion (HMP), the perfusate temperature is typically regulated between 1-10 °C. Even at low temperatures, HMP activates and sustains organ metabolism via vascular perfusion [6,10]. For normothermic machine perfusion (NMP), the perfusate temperature is set to body temperature (37 °C). HMP is the only type of machine perfusion that has been approved for use in the United States. NMP is significantly more complex since the organ's metabolism is not reduced during storage and degradative cellular processes (i.e., autolysis linked to ischemia), leading to poor tissue quality, are more common.

Perfusion flow with machine perfusion systems is either continuous or pulsatile. Flow type is either created via a pulsatile pressure waveform (e.g., sine, physiologic) or a constant pressure. The difference between these two flow types will be discussed in greater detail in Section 2.3 Mechanisms of Machine Perfusion.

2.2.3 Existing MP systems. HMP and SCS are currently the only two clinically approved preservation methods for kidneys. There are several pulsatile HMP renal preservation systems on the market: LifePort Kidney Transporter™ (Organ Recovery Systems, Itasca, IL), RM3™ (Waters Medical Systems, Rochester, MN), and Kidney Assist™ (Organ Assist, The Netherlands). Both the LifePort™ and Kidney Assist™ perfuse organ vascular beds with sinusoidal pressure pulse waves, whereas the RM3™ has more of a physiologic pulse wave.

One of the distinct advantages of MP over traditional SCS is its ability to monitor an organ throughout the preservation interval. Perfusion properties collected during this time interval can

act as an additional set of data to help assess organ quality and therefore predict transplant outcome, which is discussed in greater detail in Section 2.7 Assessing Donor Organ Quality. Perfusion properties measured by all systems include: perfusate temperature, flow rate, and pressure. LifePort™ and RM3™ systems additionally calculate vascular renal resistance (R), which is defined as the pressure drop across the renal artery and vein (Δp) divided by the volumetric flow rate (Q),

$$R = \frac{\Delta p}{Q} \tag{1}$$

The LifePort™ and RM3™ use different equations for calculating the renal resistance. The LifePort™ calculates renal resistance (R_{LP}) by using the actual mean pressure (p) and the flow (Q),

$$R_{LP} = \frac{p}{Q} \tag{2}$$

whereas the RM3™ calculates renal resistance (R_{RM3}) by using the systolic (p_s) and diastolic (p_d) pressures and the flow (Q):

$$R_{RM3} = \frac{p_s + 2p_d}{3Q} \tag{3}$$

Renal resistance measured during the HMP interval has been shown to be a risk factor for delayed graft function (DGF) and 1-year graft failure [11]. A high renal resistance may indicate the presence of vascular damage [12].

There have been several studies comparing perfusion parameters (e.g., flow rate, renal resistance) and transplantation outcomes between the LifePort™ and RM3™ systems [13,14]. The two systems generate flow using different mechanisms. The LifePort™ generates flow via a roller pump and the RM3 generates flow via a unidirectional tubing segment (termed "the ventricle") [13]. The different pumping mechanisms result in different arterial pressure waveforms; the RM3™ generates a physiologic pulse wave whereas the LifePort™ generates a sinusoidal pulse wave. It has been shown that the LifePort™ has superior renal graft outcome compared to the RM3™ for deceased donor kidneys [13]. Additionally, kidneys preserved with the RM3™ experienced higher flow rates, and kidneys preserved with the LifePort™ had a significantly lower renal resistance [13].

2.2.4 MP and SCS outcomes. Machine perfusion for abdominal organs was first developed in the 1930's by Dr. Alex Carrel and Charles Lindbergh. With the advancements in preservation machine technology made by Belzer, a significant number of kidneys in the 1970's were preserved with HMP. However, by the 1980's, there was a dramatic phase-out of HMP systems due to two factors: (1) effective, inexpensive SCS preservation solutions were developed, and (2) the "definition of brain death radically changed the deceased donor profile" [15]. Kidneys were only transplanted from DBD donors; kidneys from DCD donors were not accepted for donation [15]. The "pristine" DBD kidneys responded well to SCS, so the more expensive/complex HMP was no longer necessary [15]. Early studies comparing SCS and MP

showed no significant difference in organ transplant outcomes between the two preservation methods [16].

In recent years, there has been a renewed interest in HMP as more marginal donor kidneys are being used to increase the number of transplantable kidneys [15]. Marginal organ grafts (ECD and DCD organs) have less successful graft outcomes than ideal organ grafts; they have higher rates of delayed graft function (DGF) and acute rejection than SCD organs [16] and typically senesce more quickly than SCD organs (as measured by 1, 5, and 10 year graft survival rates). By definition, ECD kidneys have a 70% greater risk of graft failure than SCD kidneys when preserved with standard static cold storage methods [17]. In a recent study by Moers, et al., HMP has shown superior renal graft outcome compared to SCS [18]. Kidneys preserved with HMP had lower rates of DGF and higher rates of 1-year graft survival than SCS preservation [18]. This suggests that HMP provides an advantage over SCS when the donor pool contains a significant number of marginal donors. Currently, the largest percentage of machine perfused kidneys are recovered from marginal donors, as shown in Figure 1 [19].

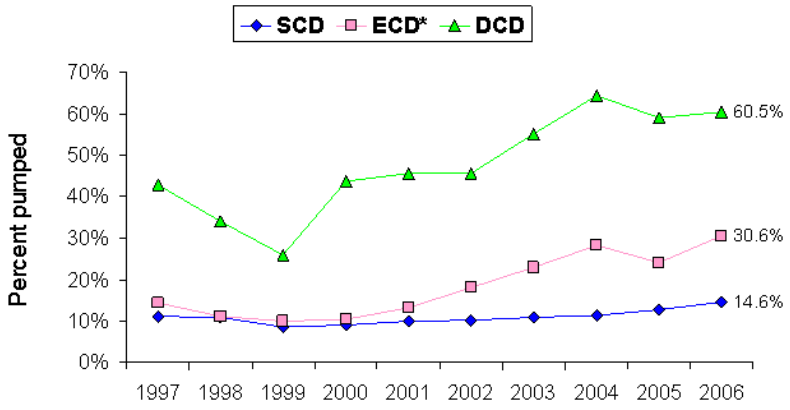

Source: SRTR analysis, May 2007; * includes kidneys from DCD that meet ECD criteria.

Figure 1. Trends in renal machine perfusion from 1997-2006. The plot is from the OPTN/SRTR 2007 Annual Report (Figure II-9. Kidney Pumping Trends).

2.3 Mechanisms of Machine Perfusion

To more fully understand the potential value of MP, it is important to discuss normal physiologic perfusion and how it is controlled. *In vivo*, the heart provides a pressure gradient that pumps fluid throughout the circulatory system [20]. The duration of the cardiac cycle, shown in Figure 2, is broken down into the systolic phase (1/3 of cycle) and diastolic phase (2/3 of cycle). During the systolic phase, the heart contracts, sending a pressure wave from the left ventricle through the arteries. At the end of the systolic phase, the heart begins to relax and the aortic valve closes. Then, during the diastolic phase, the heart is relaxed and arterial pressure decreases exponentially.

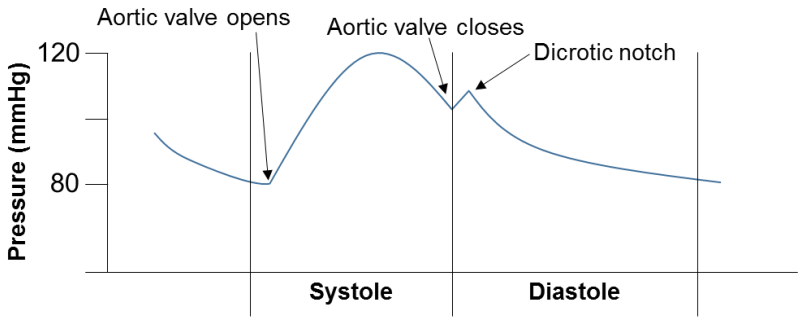

Figure 2. Aortic pressure for one cardiac cycle. The physiologic pressure wave is shown in blue.

Laminar flow is "orderly" and "energy efficient," whereas turbulent flow is "chaotic" and not energy efficient [20]. This makes turbulent flow undesirable because it would increase the workload on the heart and potentially cause blood cell damage [20]. Flow within the arteries is laminar throughout the cardiac cycle, even during the systolic phase [20]. At the end of systole when the flow decelerates as the heart begins to relax, the flow destabilizes. Fully developed turbulence requires a certain amount of time to develop, which isn't possible in the short amount of time during the end of systole (150 ms) [20]. Diastole is characterized by low arterial velocities, so flow is laminar. Then, at the beginning of the next cardiac cycle, the systolic phase re-accelerates and stabilizes the flow.

Flow in the arteries is regulated during the cardiac cycle. The shape of the local velocity profile is dictated by the Womersley number (α), which compares the unsteady inertial forces (numerator) to the viscous forces (denominator),

$$\alpha = \frac{d}{2}\sqrt{\frac{\rho\omega}{\mu}} \tag{4}$$

where d is vessel diameter, ρ is fluid density, ω is heart rate (in radians/s), and μ is fluid viscosity. As α increases, the local velocity profile in the center of the tube becomes flat [20].

There is an important relationship between blood flow and the functional and anatomical characteristics of arteries. Arteries regulate circulation (both flow and pressure) by varying vascular resistance via increasing or decreasing artery diameter. Arterial walls consist of three layers: *intima*, *media*, and *adventitia*. The *intimal* layer is comprised of endothelial cells and a thin layer of elastin. Endothelial cells act as mediators of physiological changes such as thrombogenesis and cellular migration since they are in direct contact with the blood flow [20]. Endothelial cells are responsible for alerting arteries about changes in flow by monitoring hemodynamic forces, such as normal force (pressure) and longitudinal force (shear stress), within the vessel [20]. Endothelial cells contain biosensors that are attached to or embedded in the cell membrane that can sense changes in force that are then converted into meaningful responses [20]. The *medial* layer is comprised of elastin, collagen, and smooth muscle. Elastin and collagen provide "steady tension" to combat transmural pressure, and smooth muscle provides "active tension" for vasoconstriction or vasodilation purposes [20]. The *adventitial* layer is comprised of connective tissue that secures the artery in place within the body.

In the systemic circulation, all vessels share the same relative structure, except for the presence of smooth muscle cells and elastin fibers; elastin is present in all the vessels except the capillaries and the venules [20]. This makes the vessels in the capillaries and venules stiffer than all other vessel types. As blood flows from the aorta to the distal arteries, the diameter of the vessels decreases, which results in a high flow resistance. In order to combat the high resistance, blood pressure drops significantly. The high resistance is mostly caused by the arterioles, which results in a minimal pressure pulse beginning at the capillaries and continuing through the veins to the end of the vena cava [20].

2.3.1 Types of machine perfusion. Machine perfusion is designed to mimic the flow conditions an organ experiences *in vivo* during preservation prior to transplantation. There are two main types of machine perfusion: continuous and pulsatile perfusion. Continuous perfusion provides a constant, steady flow to the organ vessels. Pulsatile perfusion, which includes sinusoidal perfusion and physiologic perfusion, supplies transient pressure waves to organ vessels. All flow types provide hydrodynamic stimulation to the organ during storage/transport.

2.3.2 Pressure waveforms. Continuous perfusion, supplied to the organ by gravity flush or a centrifugal pump, provides a steady, constant-pressure flow through the vessels. Since flow is not periodic in nature, it is more likely to become fully developed turbulent flow. Pulsatile perfusion, supplied to the organ via periodic pressure waves, provides an intermittent, periodic flow through the vessels. This means the driving pressure and velocity gradients are pulsatile. Sinusoidal pulsatile perfusion applies a sinusoidal pressure waveform to the arteries of the explant with a peristaltic pump or pressure waveform generator. The pressure varies during the simulated 'cardiac cycle,' which contains maximum 'systolic' and minimum 'diastolic' pressures. Physiologic pulsatile perfusion applies a physiologic pressure waveform to the perfusate stream using a pressure waveform generator. It closely resembles the physiologic waveform generated by the heart and vascular bed *in vivo*, meaning that it contains all the arterial pressure elements in the cardiac cycle (i.e., systole, diastole, dicrotic notch).

Continuous perfusion is significantly different from pulsatile perfusion since the applied pressure 'waveform' is constant. Sinusoidal pulsatile perfusion yields a pressure waveform similar to a physiologic waveform, since both fluctuate between a maximum and minimum arterial pressure. However, the waveforms have different transient characteristics. For example, only the physiologic waveform has a dicrotic notch.

2.3.3 Transplant outcomes. There are conflicting views and experimental data on which flow type (continuous, pulsatile) results in a superior preservation outcome. According to Yuan, et al., some studies show comparable outcomes between continuous and pulsatile perfusion, whereas other studies show superior outcomes with pulsatile perfusion, including improved microcirculation and organ function [16]. Lee and Mangino hypothesized that superior preservation by pulsatile perfusion, compared to continuous perfusion, is due to the "reduced mean capillary pressures" and the "activation of various gene products" by the normal force and shear stresses acting on the vessel wall [3].

Although it is not fully understood why pulsatile machine perfusion yields superior outcomes compared to SCS [18], it is hypothesized that pulsatile perfusion may induce "protective mechanisms" that aren't present during SCS [16]. While continuous and pulsatile perfusion both have the capability to circulate oxygen and nutrients and remove toxins during storage, pulsatile perfusion is additionally associated with the activation and expression of "flow-dependent, vasoprotective endothelial genes" [16]. Different machine perfusion flow types result in different endothelial gene expression and function, but more studies need to be conducted before any conclusive statements can be made about the perceived benefits of or differences between continuous and pulsatile flow [16].

2.4 Perfusate Types and Composition

All cells and tissues are normally bathed in physiologic fluids derived from and exchanged with blood in blood vessels. Cell and tissue perfusion is critically important in providing nutrients and oxygen and for removal of metabolic and degradative waste products. Whole blood is composed of plasma and formed elements. Plasma consists of proteins - mainly fibrinogen, globulin, and albumin - electrolytes, and water. Fibrinogen is responsible for blood clotting and globulin is a "carrier of lipids and water soluble substances" and contains antibodies to fight infection [20]. Albumin, the most abundant protein of plasma, is responsible for maintaining the balance of the colloid osmotic pressure (oncotic pressure) of the plasma. Interstitial fluid (fluid that bathes all cells and tissues but which is not in the vascular bed) is identical to plasma, except that it lacks the plasma proteins. Therefore, the higher osmotic pressure of the plasma (a result of the presence of proteins) causes water to be pulled from the interstitial fluid into the capillaries containing plasma. The formed elements suspended in plasma are: red blood cells, white blood cells, and platelets. Red blood cells contain hemoglobin, a ferroprotein which carries oxygen throughout the body. White blood cells protect the body against illness by attacking foreign invaders (bacteria, viruses, etc.). Lastly, activated platelets assist in the blood clotting mechanism along with fibrinogen.

The apparent viscosity of whole blood is dependent on tube (vascular) diameter. As the tube diameter decreases, the apparent viscosity decreases (for tubes with a diameter less than 0.5 mm); this is known as the *Fahraeus-Lindqvist effect* [20]. Red blood cells rotate when subjected to a velocity gradient, which causes them to move towards the center of the tube [20]. This creates a cell-free layer close to the wall that is comprised solely of plasma, which has a lower viscosity than whole blood. The cell-free layer has approximately the same cross-sectional area as the central core in tubes with a small diameter. Therefore, the cell-free zone reduces the apparent viscosity [20]. In tubes with a larger diameter (greater than 0.5 mm), the effect of the cell-free layer is reduced. This normal physiological phenomenon is known as "central axial streaming" and is important in distributing plasma-rich blood to organs such as the kidney.

The function of blood *in vivo* is to transport oxygen and nutrients, assist the body with blood clotting, fighting infection, and maintaining osmotic balance. Early studies that utilized heparinized whole blood for initial organ flushing after organ procurement noted that the use of whole blood caused problems upon graft re-implantation, such as vascular stasis [6]. The use of whole blood as a perfusate continues to be problematic. Thus began the search for synthetic

(acellular) preservation solutions [6]. Synthetic preservation solutions, whether for machine perfusion or static cold storage, aim to slow graft metabolism and limit degradation.

Perfusate selected for organ preservation can greatly impact preservation time and organ viability. The drive to increase SCS preservation time, which would lower the discard rate for organs, led to innovations in preservation solutions. Preservation solutions improve organ preservation outcomes; however, they do not actually prevent cellular injury, which still results in primary graft dysfunction [6].

In 1969, Collins, et al. developed a novel perfusate (Euro-Collins) that extended canine kidney preservation time for SCS from 12 hours to 24 hours [21]. In the late 1980's, Belzer's group developed the University of Wisconsin (UW) solution (now ViaSpan®), which extended SCS time to 72 hours for canine kidneys [22]. For human renal transplantation, it has been shown that the UW solution has lower rates of DGF and improved graft function compared to the EuroCollins solution [23]. UW solution is now the 'gold standard' in SCS preservation. Histidine-Tryptophan Ketoglutarate (HTK) solution (now sold as Custodiol® HTK) was developed by Bretschneider in the 1970's for cardiac surgery, but is now being used for renal transplantation [24]. HTK yields comparable results to the UW solution for SCS renal preservation times greater than 16 hours [24].

One of the most important characteristics of preservation solutions is osmotic pressure; if the interstitial fluid osmotic pressure becomes too high during perfusion, tissue edema will occur. The effects of tissue edema are further discussed in Section 2.6 Swelling during Machine Perfusion. The addition of a colloid to the solution is necessary to prevent interstitial edema [10]. For the Euro-Collins solution for SCS, the high concentration of glucose osmotically balances the perfusate, which prevents intracellular swelling [3]. Additionally, the levels of sodium and potassium are similar to *in vivo* cell composition. For the UW solution, the development of edema is controlled by raffinose, lactobionate, and by the addition of hydroxyethyl starch (HES), which is a colloid. UW works well as a preservation solution since it prolongs preservation time and prevents tissue edema. There are two different formulations, one for cold storage and the other for machine perfusion. Unfortunately, UW has a high viscosity, which affects the microcirculation, and a high amount of potassium, which may cause vasoconstriction [16]. HTK uses mannitol to osmotically balance the solution. Additionally, HTK uses histidine as a buffer (superior to UW's phosphate buffer) regulating "membrane stabilization" by tryptophan and employing ketoglutarate as an energy source for anaerobic metabolism [16]. The viscosity of HTK is lower than UW, which may assist in perfusion of microvessels. Euro-Collins, UW, and HTK are all slightly hypertonic, with osmolality measurements of 340, 320, and 310 mOsm/kg, respectively [6].

2.5 Solution Solute Concentration

Cell membranes separate intracellular and extracellular solutions and are selectively permeable. Permeant solutes diffuse across the membrane and non-permeant solutes do not. Water diffuses by osmosis across the membrane to create a state of equilibrium between the intracellular and extracellular spaces. Only non-permeant solutes influence water diffusion across the membrane

since water diffuses from conditions of low solute concentration to high solute concentration [25]. Solution solute concentration can be described by osmolality, osmotic pressure, and tonicity.

2.5.1 Osmolality. Osmolality is a quantitative measure of the concentration of solutes in a solution, reported in units of mOsm/kg (molar concentration of solutes per mass solvent). The osmolality of a solution is measured using an osmometer, which calculates the solution concentration using the freezing point depression; the more solutes in a solution, the lower the freezing point [25]. A typical range for plasma osmolality is 280-295 mOsm/kg [25]. Osmolality as a measurement alone cannot predict the movement water across a membrane; movement is dictated by the difference in osmolality of solutions separated by a semi-permeable membrane.

2.5.2 Osmotic pressure. Osmotic pressure is a another measure of solute concentration, commonly expressed in units of mm Hg [25]. The osmotic pressure of a solution is measured by placing a tube filled with solution into a container of pure water where the interface between the solution and water is separated by a semi-permeable membrane. Due to the solute concentration difference, water will diffuse through the membrane from the pure water side into the solution side by osmosis. Eventually, the pressure generated from the fluid height in the tube will be "large enough to exert the pressure required to force as much water back to the water side of the membrane (by filtration) as crossed into the solution side (by osmosis)" [25]. The pressure exerted by the liquid head at this equilibrium state is the osmotic pressure of the solution [25]. Similar to osmolality, osmotic pressure as a measurement alone cannot predict the movement water across a membrane; movement is dictated by the difference in osmotic pressure of solutions separated by a membrane. The role of osmotic pressure in edema formation will be discussed in Section 2.6 Swelling during Machine Perfusion.

2.5.3 Tonicity. Tonicity is the "semi-quantitative" [25] comparison of solute concentration (i.e., osmolality, osmotic pressure) between a solution and cells; it describes the net movement of water when cells come into contact with a solution [26]. The concept of tonicity can be used to explain the difference in solution solute concentration for both osmolality and osmotic pressure measurements. Isotonic solutions have a solute concentration equal to that of cells, which causes a net-zero transfer of water between the cells and solution. Hypertonic solutions have a solute concentration that is greater than that of cells, which causes a net movement of water out of the cells into the solution. Lastly, hypotonic solutions have a solute concentration that is less than that of cells, which causes a net movement of water into the cells from the solution and results in cell swelling.

One caveat to the tonicity definition is that a solution can be iso-osmotic (i.e., have the same osmolality) with cells but not be isotonic. An osmolality measurement may include both non-permeant and permeant solutes, but only non-permeant solutes dictate water diffusion across a membrane. Thus, tonicity definitions are not solely dependent on the solution osmolality if permeant solutes are present; it is the concentration of non-permeant solutes that determines tonicity.

2.6 Swelling during Machine Perfusion

Swelling of explanted organs has been commonly observed during machine perfusion. While some swelling is expected during the reperfusion phase (as vasculature is refilled with fluid), extreme swelling is detrimental to organ health and is often a sign of tissue edema and lethal intracellular swelling. Proper perfusion parameters (e.g., pressure) and perfusion fluids that are physiologically compatible are essential in reducing the likelihood of swelling during machine perfusion. It must be emphasized that explanted organs do not have access to oxygen or sufficient energy-yielding metabolites to meet tissue metabolic demands, even for a short period of time. It is well-known that loss of tissue perfusion (ischemia) or lack of intracellular energy will lead to tissue deterioration within 20-30 minutes. This thesis will focus on the influence of perfusate solution solute concentration on organ swelling.

2.6.1 Osmotic balance. Fluid exchange between capillaries and the interstitial space is dictated by the "hydrostatic and colloid osmotic pressure difference between the capillary blood and the interstitial fluid" [20]. In normal blood circulation, plasma in the capillaries has a higher osmotic pressure, due to the proteins in the plasma that are not present in the interstitial fluid, which results in the net movement of water from the interstitial fluid into the capillaries [20].

In vivo, edema occurs when excess fluid is accumulated intracellularly (cellular edema) and interstitially (interstitial edema). Interstitial edema is caused by changes in hydrostatic and colloid osmotic pressures, hydraulic conductivity, and the lymphatic outflow system [27]. Interstitial edema is harmful because it "increases the diffusion distance for oxygen and other nutrients," which impacts metabolism and the removal of metabolism byproducts [27]. Interstitial edema can be caused by a reduction in plasma proteins (albumin) due to liver disease or malnutrition. In several tissues, anatomical structures (e.g., kidney capsule) restrict the expansion of tissue during episodes of edema. Since these tissues cannot expand to accommodate the fluid, small increases in the interstitial osmotic pressure yield large increases in the interstitial pressure [27]. This results in compressed capillaries, which lessens perfusion [27].

2.6.2 Renal swelling. Kidneys are highly vascularized organs (1/8 of the cardiac output is devoted to each kidney), so they exist normally in a turgid state within the body. Approximately 25% of renal volume is attributed to hemodynamic pressure and biological fluids (e.g., blood and urine), meaning that organ geometry ("organ turgor") is dependent on perfusion properties [28], especially pressure [29]. Therefore, when kidneys are explanted, they quickly become flaccid as the vasculature collapses due to de-pressurization and fluid drainage.

During machine perfusion, explanted kidneys are re-perfused with a preservation solution via a pressure waveform. Kidney vasculature returns (i.e., fills) to its *in vivo*, pressurized state and the flaccid kidney again becomes turgid (swells). Swelling during machine perfusion is caused by (1) the reintroduction of fluid to the vasculature, and (2) tissue edema. Swelling that occurs during the reintroduction of perfusate to the organ via machine perfusion is caused by the added fluid volume and the re-pressurization of the vasculature. An example of renal swelling caused by the reintroduction of fluid during gravity perfusion is shown in Figure 3. Swelling induced by tissue edema may be caused by: improper perfusate composition (i.e., hypotonic solution), high

fluid flow rates, and non-physiologic perfusion pressures [16]. There are very likely individual variations in explant swelling, due to pathoanatomical differences in the condition of the explant, even when kidneys are perfused under identical conditions.

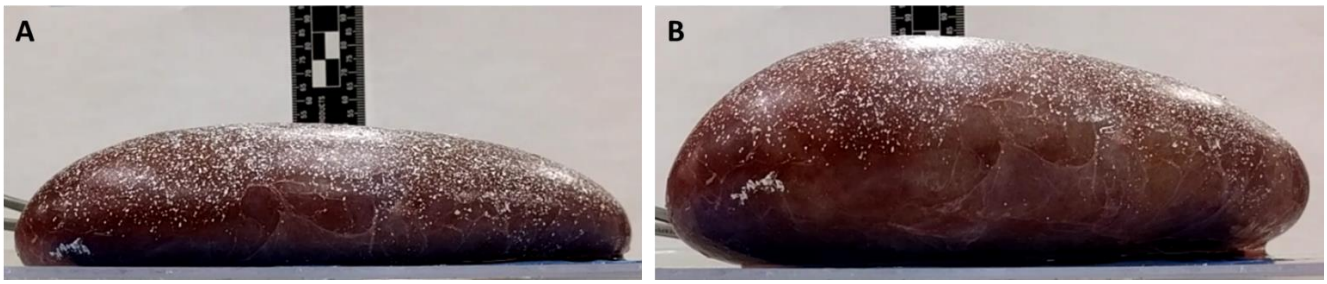

Figure 3. Porcine kidney (A) before and (B) after gravity perfusion. Renal expansion is significant through the thickness. To achieve these results, 500 mL of PBS was perfused at a height of 1.0 m for 5.75 min. While gravity perfusion is a different perfusion mechanism than machine perfusion, the same general swelling trends are observed for both.

Swelling attributed the reintroduction of fluid is expected during reperfusion; however, extreme swelling caused by edema (accumulation of interstitial fluid) compromises normal anatomic structures and may harm the kidney, especially since the intact connective tissue capsule restricts swelling, resulting in pressure-induced damage to the nephron structure. Tissue edema has been linked to: high vascular resistance, low perfusion, and preservation injury.

2.7 Assessing Donor Organ Quality

Due to the shortage of donor organs, it is imperative that no organ is unnecessarily rejected/discarded or damaged by preservation. Donor organ quality is the deciding factor in a surgeon's acceptance or refusal of an organ offer. When a donor kidney is available for transplantation, it is offered to the first candidate on the waiting list. The kidney can either be accepted or declined; if declined, an offer is made to the next candidate on the waiting list.

Currently, the primary factor in determining donor organ quality is subjective. Organ macroscopy, performed by the transplant surgeon, is often viewed as the most important factor in determining whether or not an organ is viable for transplant [30]. Donor medical history (e.g., age, length of time in intensive care unit, cause of death, lab results) is also considered along with visual inspection; however, there is no universal acceptable range for such donor characteristics [30]. A single punch biopsy is collected from the donor organ at the time of procurement to identify the cellular characteristics of the organ. However, the biopsy (3-5 mm in diameter, and less than 5 mm in depth) is unlikely to represent the morphology of the entire organ. The process of biopsy procurement is destructive to the tissue and multiple biopsies (which might be more representative) are rarely procured.

Concerned with the low acceptance rate of donor kidneys, Wolfe, et al. performed an analysis of 4967 'good' kidneys transplanted in 2005 after less than 50 offers [31]. This analysis found that even for 'good' kidneys that did not match ECD or DCD criteria, it took an average of seven offers before kidneys were accepted for transplantation [31]. The most common refusal code was: "patient ill, unavailable, refused, temporarily unsuitable" (22%), followed by "donor

quality/age" (18.9%) [31]. All of the kidneys in the study were of good quality and ultimately transplanted, which raises the question as to why such a large percentage of kidney offers were refused due to donor quality/age. This is an example of "perceived donor quality," [31] which shows that the definition of quality varies between surgeons; a universal standard for quality does not exist.

Machine perfusion measurements can provide additional quantitative data to assist surgeons in making decisions about explant quality and whether to accept or decline organs for transplant. While visual inspection, donor medical history, and biopsy findings are invaluable to the determination of organ health, quantitative parameters could aid in the development of universal standards for organ quality. Unlike SCS, MP has the ability to monitor organ characteristics such as temperature, pressure, renal resistance, and pH (among others) during the preservation interval. These quantitative organ metrics can be used in tandem with visual inspection and biopsy results to aid in the decision making process for accepting or rejecting donor organs. In the future, universal standards could improve the efficiency of graft allocation (i.e., reduce the number of declined offers) and reduce the number of non-use kidneys.

2.8 Quantifying Organ Swelling with Digital Image Correlation

During machine perfusion, kidney swelling is caused by fluid reintroduction and tissue edema. Little has been published on *ex vivo* kidney geometry as a function of perfusion parameters. Helfenstein, et al. reported gross kidney dimensions (length, width, and thickness) as a function of perfusion pressure [29]. However, more detailed measurements are needed to quantify displacement over the entire renal surface.

The kidney surface shown in Figure 4 can be represented as a collection of 3D points that undergo deformation during machine perfusion. The displacement of each point can be tracked over time, which provides a displacement map for the renal surface. Displacement is defined as the change in particle position caused by object deformation. The displacement vector of a particle is the change in particle position, in x-y-z space, before and after deformation. Digital image correlation (DIC) can be used to measure renal surface displacement in three-dimensions (3D) during machine perfusion. DIC is meant to be an investigative tool for mapping surface displacement, not as a clinical tool.

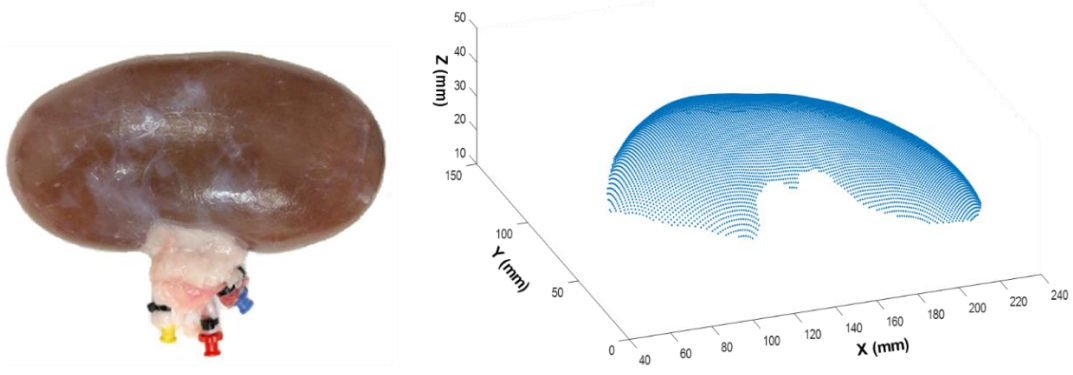

Figure 4. Kidney surface (left) to be represented as a collection of 3D points (right). Measurement of surface displacement over the entire renal parenchyma is highly desirable.

2.8.1 Basic principles. DIC is an optical, and therefore non-contact, technique for measuring shape and deformation in three-dimensions. A sequence of images are captured using an experimental set-up that consists of light sources to illuminate the specimen, sensors (CCD, CMOS cameras) for image collection (i.e., digital image acquisition), a rigid camera support bar, and a computer for image storage and post-processing. A schematic of a typical setup is shown in Figure 5. The number of cameras required for data collection depends on how many planes are investigated. For two-dimensional (2D) DIC, only one camera is required for measuring in-plane displacement. However, 3D DIC requires at least one stereoscopic system, where each stereoscopic system (i.e., stereo rig) consists of a pair of cameras, one right camera and one left camera, mounted on the same support bar [32]. 3D DIC is capable of measuring shape and both in-plane and out-of-plane displacement.

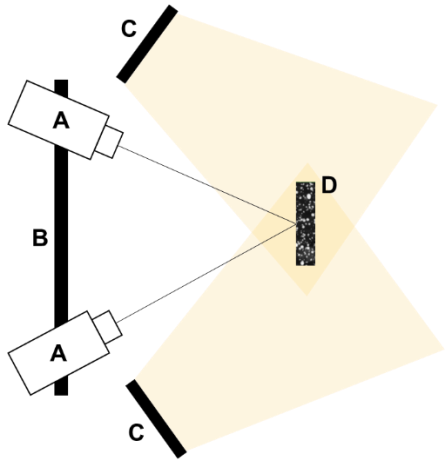

Figure 5. Typical experimental set-up of 3D DIC equipment (overhead view). Equipment consists of (A) two cameras/sensors, (B) rigid support bar, (C) light sources, and (D) speckled specimen. The sensors are connected to a computer for image acquisition and storage.

2.8.2 System calibration. A system calibration is performed prior to data collection that establishes the relationship between an object, camera sensors, and camera orientation. More specifically, it defines the relationship between the world, camera, and sensor coordinate systems. The intrinsic camera parameters (e.g., focal length, principal point, distortion parameters) and extrinsic stereo rig parameters (e.g., rotation matrix, translation vector) are estimated as a result of the calibration process [33]. For a 3D stereo-system, "once the cameras are calibrated, the sensor plane locations in the two views for the same object point can be used to determine an accurate estimate for the three-dimensional position of the common object location" [34].

Calibration involves collecting images of a calibration plate that is rotated and translated within the field of view. The calibration plate consists of points in a "predetermined grid spacing" [34]; a calibration plate with a common 2D dot pattern is shown in Figure 6. For each image collected of the calibration plate, the point locations are extracted from the sensor plane. These extracted values are compared to theoretical values that are calculated using a "mathematical calibration model" [35]. The theoretical point locations are determined using estimated camera/stereo rig

parameters. The estimated parameters that minimize the difference between the extracted and theoretical point locations are the optimal estimated parameters.

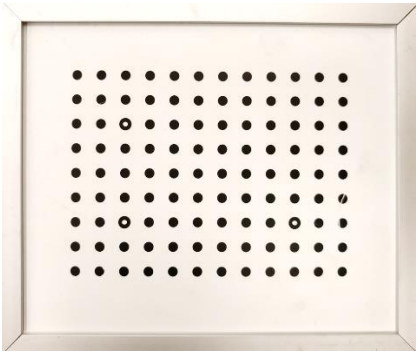

Figure 6. Calibration plate with dot pattern from Correlated Solutions, Inc. (Irmo, SC). Point spacing is 9 mm.

The calibration score is the average error "between the position where a target point was found in the image, and the theoretical position where the mathematical calibration model places the point" [35]. The lower the score, the better the calibration; scores less than 0.05 pixels are considered acceptable. Once the camera system has been calibrated, the equipment cannot be moved or bumped, as this can change the camera parameters and thus the system would need to be re-calibrated.

2.8.3 Specimen preparation. A high-contrast, stochastic pattern ('speckle pattern') is applied to the surface of the object being measured. An example of two speckle patterns is shown in Figure 7, where two different speckling techniques were used. The speckle pattern must be unique; subset tracking depends on being able to match uniquely patterned subsets. There are many studies reported in the literature that discuss how speckle pattern parameters (i.e., speckle size, density) impact measurement accuracy [36]. A speckle size of approximately 5 pixels with 5 pixel spacing is preferred [37].

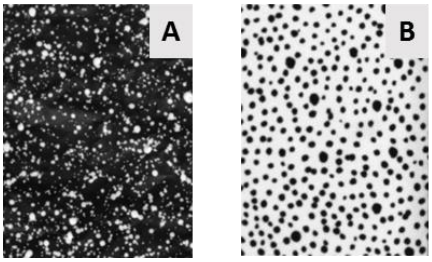

Figure 7. Example speckle patterns. Techniques include (A) white spray paint on a black surface, and (B) black marker dots on a white surface.

2.8.4 Image collection. During an experiment, grayscale images are captured of the speckled object before, during, and after deformation at a given sampling rate. Each individual grayscale image is made up of pixels, and each pixel contains a grayscale (intensity) value. This "digitized image intensity field" is the data output from the grayscale images that is used for DIC [34]. In the set of collected images, a single image collected prior to deformation (while the

object is undeformed) is defined as the 'reference image' of the object. All subsequent images are defined as 'deformed images' since they are collected as the object deforms.

2.8.5 2D digital image correlation. The most basic principle of DIC is subset matching between images. A grayscale image (in the sensor plane) is divided into small subsets of pixels and the subsets are tracked over time. Reference subsets in the reference image are matched in all subsequent deformed images by "pattern matching"; the speckle pattern (i.e., pixel intensity) in the reference subset is matched to a deformed subset in the deformed image that has the 'same' speckle pattern [38]. The difference in position of the subset between the reference and deformed subsets is displacement. All displacement measurements are calculated with respect to the original reference image. In this study, displacement measures tissue swelling.

Two-dimensional (2D) DIC tracks the reference subset from the reference image in all subsequent deformed images. First, a reference subset of n pixels (N x N pixels) is selected in the reference image, centered at $P(x_0, y_0)$. A "searching area" [38] is then defined in the deformed image of interest. A deformed subset is iteratively moved around the searching area. At each deformed subset position within the searching area, a correlation coefficient is calculated. The correlation coefficient is used to calculate the similarity/difference between the reference subset and the deformed subset. The position of the "correlation coefficient extreme" [38] is found with an optimization algorithm and represents the best estimated location of the deformed subset (i.e., where it best matches the reference subset), as shown in Figure 8. The deformed subset is centered at $P(x_0', y_0')$ on the deformed image. The displacement (u, v) that occurs between the reference image subset and the deformed image subset is calculated as the difference in position between the reference subset center and the deformed subset center at the optimal correlation coefficient,

$$u = x_0' - x_0 \tag{5}$$

$$v = y_0' - y_0 \tag{6}$$

where u is x-displacement and v is y-displacement. This entire process is completed for all desired points on the reference image. However, these displacement values are in terms of the sensor coordinates in the image plane and are in units of pixels, not a physical dimension. The image plane displacements (pixels) are converted into object displacements (metric units) by multiplying the image plane displacements by scale factors [34].

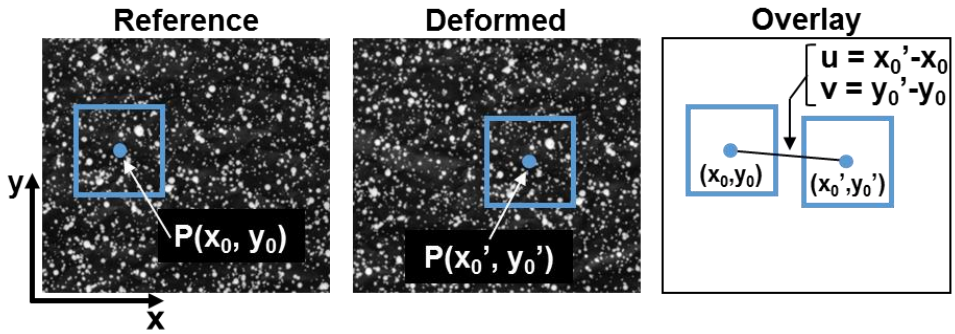

Figure 8. A single subset tracked from the reference image to the deformed image. The overlay depicts the reference and deformed subsets in the same field of view (i.e., the reference and deformed images are overlaid).

2.8.6 3D digital image correlation. Three-dimensional (3D) DIC utilizes many of the same principles used in 2D DIC. Since there are two cameras in a stereo set, pattern matching must occur across both camera images and a common 3D point must be identified. To determine the initial 3D shape of an object, one of the cameras is selected as the master (e.g., Camera 1). Subsets are selected in the Camera 1 reference image and are matched in the reference image of Camera 2 using 2D DIC principles described previously. Next, a skew ray is projected through the center point of each matching subset in Camera 1 and Camera 2; the location where the skew rays intersect is the 3D location of the common object point for the matching subset pair, as shown in Figure 9 [34]. The collection of 3D points over the entire object is the initial object shape [34].

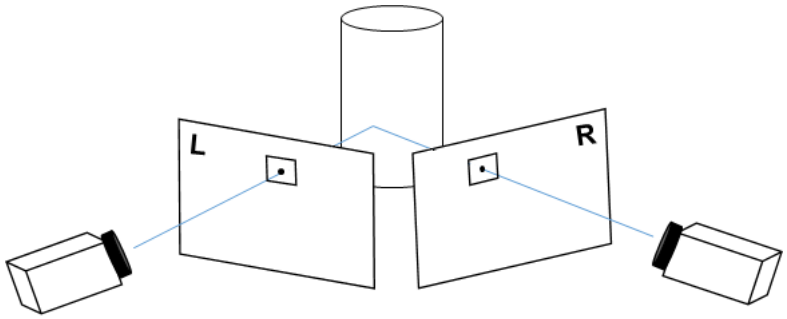

Figure 9. Finding a common object point using 3D DIC. A skew ray is projected from the camera pinhole through the center of the matching subset in both the right and left image planes. This diagram is an artistic representation of 3D DIC.

The same reference subsets used to identify the initial object shape in Camera 1 and Camera 2 are used to determine the deformed object shape in 3D. For a given reference subset in the Camera 1 reference image, 2D DIC principles are used to find the matching subset in the first Camera 1 deformed image. For the same reference subset in the Camera 2 reference image, 2D DIC principles are used to find the matching subset in the first Camera 2 deformed image. Next, a skew ray is projected through the center point of the matching subset in the Camera 1 and Camera 2 deformed images; the intersection of the rays is the 3D position of the of the deformed object point. This process for locating the common object point for each subset is repeated for

all subsets in all deformed images. The 3D displacement field is calculated by subtracting the undeformed 3D object points from the deformed 3D object points for each image set.

2.8.7 Correlation coefficient. There are several different correlation criteria that exist for evaluating the similarity/difference between the reference subset and potential deformed subsets. These include: cross-correlation (CC), sum of squared differences (SSD), sum of absolute difference (SAD), and parametric sum of squared differences (PSSD). Choosing the proper correlation criteria depends on the DIC software package being used and the experimental testing conditions (e.g., light intensity may vary during the experiment).

The correlation coefficient implements the intensity (gray scale) values of the reference and deformed images to evaluate the similarity between the reference and potential deformed subset. Thus, it is important to have a unique speckle pattern over the entire object surface so each subset is filled with a unique set of intensity values. "For a square subset containing *n* discrete pixels," $F(x_i, y_i)$ is the intensity value of the *i*th pixel in the reference subset and $G(x_i', y_i')$ is the intensity value of the *i*th pixel in the deformed subset [38]. For simplicity, the intensity values $F(x_i, y_i)$ and $G(x_i', y_i')$ will be referred to as F_i and G_i, respectively. All summations across a subset are from $i = 1$ to $i = n$ in the following correlation coefficient definitions.

This thesis will focus on the sum of squared differences correlation criteria. As opposed to the cross-correlation coefficient, all sum of squared differences coefficients are minimized; the optimal location of the deformed subset is located where the difference in intensity values between the reference and deformed subsets is at a minimum, as shown in Figure 10. The three different sum of squared differences correlation criteria are: direct sum of squared differences (SSD), normalized sum of squared differences (NSSD), and zero-mean normalized sum of squared differences (ZNSSD). The correlation coefficient equations are as follows [38]:

$$C_{SSD} = \sum (F_i - G_i)^2 \tag{7}$$

$$C_{NSSD} = \sum \left(\frac{F_i}{\sqrt{\sum {F_i}^2}} - \frac{G_i}{\sqrt{\sum {G_i}^2}} \right)^2 \tag{8}$$

$$C_{ZNSSD} = \sum \left(\frac{\overline{F_i}}{\sqrt{\sum \overline{F_i}^2}} - \frac{\overline{G_i}}{\sqrt{\sum \overline{G_i}^2}} \right)^2 \tag{9}$$

where $\overline{F_i}$ and $\overline{G_i}$ are equal to $F_i - \bar{F}$ and $G_i - \bar{G}$, respectively. The direct sum of squared differences (SSD) is not recommended since it is affected by changes in lighting during data collection [35]. The NSSD is the most recommended since it is not affected by changes in lighting during data collection [35]. The ZNSSD is also recommended since it is not affected by changes in lighting during data collection; however, it may fail to converge more frequently than the NSSD criteria [35].

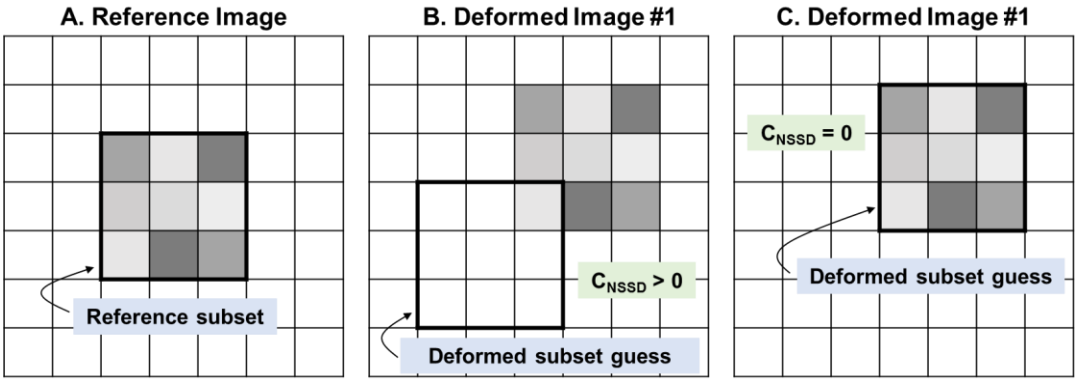

Figure 10. Matching subset intensity values using normalized sum of squared differences (NSSD). As a 3x3 subset (containing 9 pixels) is moved within the deformed image, the NSSD correlation coefficient (C_{NSSD}) is calculated, which compares the intensity values for each pixel within the deformed subset to the reference subset. As shown in (B), the deformed subset guess does not have the same intensity values as the reference subset and thus C_{NSSD} is greater than zero. However, in (C), the deformed subset has the same intensity values as the reference subset and thus C_{NSSD} is zero. Since the deformed subset in (C) has a lower C_{NSSD} than (B), the optimal/matching deformed subset is located at the position shown in (C).

2.8.8 Sources of error. Error in the 3D DIC data stems from two sources: (1) correlation errors and (2) reconstruction errors [33]. Correlation errors "influence the accuracy of the image correlation," meaning they are associated with the uncertainties that arise from subset matching in different images [33]. Correlation errors include statistical and systematic errors (bias) [33]. Statistical errors are mostly attributed to camera image noise [33]. Noise in the system can be reduced by implementing the proper focus, contrast and lighting, F-stop, stereo-angle, and lens [39]. Once the system set-up is optimized, noise minimization is achieved by optimizing the speckle pattern quality [39]. Systematic errors occur when the incorrect correlation model is used. Reconstruction errors stem from errors in the system calibration. Since the 3D coordinate data is generated using parameters determined during system calibration, errors in the calibration result in systematical errors that appear in the 3D coordinates [33]. Calibration errors may be caused by "statistical uncertainties of the calibration parameters or an insufficient calibration model" [33].

2.8.9 Quantifying error. Displacement accuracy can vary widely depending on the experimental set-up and speckle pattern quality, even from experiment-to-experiment. There are two main ways to estimate displacement accuracy (i.e., noise): (1) field-of-view (FOV) rule-of-thumb, and (2) static image displacement measurements [40]. The rule-of-thumb for displacement accuracy is,

$$1/50{,}000 \times FOV \tag{10}$$

$$1/25{,}000 \times FOV \tag{11}$$

for in-plane and out-of-plane displacements, respectively. However, this method does not incorporate variations in experimental set-up that may cause noise.

A more conservative estimate of the displacement accuracy can be achieved through measurement by obtaining several static images of the speckled object prior to deformation. Since the object is not being deformed, the displacement on the surface of the object should be zero; however, noise present in the system will result in displacements that deviate from zero. For a single static image, the average and standard deviation of displacement along the X, Y, and Z axes show how much noise is present. A method for calculating the average noise is to create an interval that contains 95% of the displacement, assuming a normal distribution,

$$\mu \pm 2\sigma \tag{12}$$

where μ is the average displacement along one axis and σ is the standard deviation of displacement along the same axis. Since the interval may contain positive and negative values, it is important to find the average of the absolute deviation from zero. Therefore, if the interval does not contain zero, then the average displacement is simply the average of the interval, μ. However, if the interval does contain zero, then the average displacement is the larger absolute bound of the interval divided by two since the absolute interval actually ranges from zero to the larger absolute bound. This method results in an absolute average displacement that is not artificially lowered by negative displacements.

2.8.10 DIC for biological tissues. DIC has previously been used for measuring the *ex vivo* structural response of soft biological tissues such as the brain [32], ligaments [41], skin [42], and arteries [43]. While there are cases where a natural pattern exists on the surface of biological tissues (e.g. liver [44]), most tissue experiments require the application of a high-contrast pattern (i.e., speckles). Some common speckling materials are spray paint, face paint, powder, and dye. The application of speckles to biological tissue is challenging. According to Lionello, et al. the following criteria must be met in order to generate a successful speckle pattern on the surface of a soft biological tissue [41]:

- Dehydration is not required nor induced,
- Mechanical response is unchanged after speckle application,
- Speckles are retained on the surface, even during large deformations.

Therefore, DIC is a viable method for measuring the structural response of soft tissues, as long as the speckling method is correctly implemented.

Chapter 3 - Experimental Methods

A series of eight experiments were performed to evaluate the surface deformation of kidneys, associated with tissue swelling, using digital image correlation. All experiments followed the same protocol: kidney procurement, kidney surface preparation, and kidney perfusion coupled with data collection.

3.1 Experimental Design

3.1.1 Perfusate. To determine how perfusate type influences renal expansion, isotonic and hypertonic perfusates were used. Phosphate buffered solution (PBS), a salt-based solution, was used as an isotonic perfusate since it is commonly used for cell culture applications (PBS is iso-osmotic to plasma). A recipe for 1X PBS is located in Appendix A. To create a hypertonic solution, mannitol (D-Mannitol, Sigma® Life Science) was added to PBS in a 5% w/v concentration (50 g/L). Mannitol is a sugar alcohol commonly used to sweeten sugar-free foods and it is used clinically in humans as a diuretic and is administered by intravenous injection. Mannitol Injection, USP has a 25% concentration of mannitol for clinical use [45]. Mannitol is effective as a diuretic because it is cannot permeate through the cell membrane and it is filtered and excreted by the kidneys [45]. As a result, urine volume output is increased [45]. For simplicity, mannitol will frequently be abbreviated as "MAN" throughout the results section of this thesis.

3.1.2 Experiment series. In order evaluate how perfusate types influence renal swelling, the right and left kidneys were each perfused with a different perfusate (i.e., isotonic or hypertonic). For a single experiment, a pair of kidneys was procured from the same pig. The protocol alternated the kidney side (right or left) receiving each perfusate type and alternated the order in which the kidneys were perfused. Alternating the kidney side and perfusion order is designed in the experimental series to compensate for these factors.

A series of eight experiments were performed, as shown in Table 1. Since two kidneys could not be perfused at once, the order of perfusion (i.e., first or second) dictated which kidney from the kidney pair was perfused first and second. The kidney number columns (i.e., "Kidney #1" and "Kidney #2") shows the order that the kidney pair was perfused. Within these two columns, the kidney side and perfusate type are indicated (e.g., "R_PBS" is the right kidney perfused with PBS). The date column is the date that the experiment was performed. Experiments 5-8 were simply repeats of Experiments 1-4.

Table 1: Experimental design for eight experiments

Experiment #	Date	Kidney #1	Kidney #2
1	02/09/17	R_PBS	L_MAN
2	03/08/17	L_MAN	R_PBS
3	02/22/17	R_MAN	L_PBS
4	02/24/17	L_PBS	R_MAN
5	03/01/17	R_PBS	L_MAN
6	03/02/17	L_MAN	R_PBS
7	03/03/17	R_MAN	L_PBS
8	03/07/17	L_PBS	R_MAN

Prior to each experiment, perfusate control samples (i.e., unused perfusate) were collected for osmolality measurements. Additionally, the pH of each perfusate was measured (Ion 6 Acorn series, Oakton®, Vernon Hills, IL) prior to experimentation to ensure consistency in the

perfusate recipe. The mannitol solution consistently had a lower pH than the PBS; however, both were within the pH range of 7.3 – 7.5 (with a target PBS pH of 7.4). The measured pH values from all experiments are listed in Appendix B.

During each experiment, images were acquired to be later evaluated with a DIC software (Vic-3D, Correlated Solutions, Inc., Irmo, SC) to measure surface displacement. Additionally, renal fluid samples from the ureter (filtrate) and renal vein (venous outflow) were collected during the perfusion interval; the osmolality and composition of the renal fluids were later measured. After the conclusion of the perfusion experiment, sample biopsies were collected. The fluid osmolality in tandem with the sample biopsies was used to identify the presence or absence of tissue edema.

Each experiment was peformed for a duration of 135 minutes; 15 minutes of active machine perfusion followed by 120 minutes without perfusion. Kidneys were machine perfused with perfusate at a temperature of 5 °C and a target systolic/diastolic pressure of 120/100 mm Hg.

3.2 Kidney Protocol

3.2.1 Kidney procurement. All porcine kidneys were procured from an abattoir (Gunnoe's, Goode, VA). Kidneys were procured at ~7:15 AM on the same day as the perfusion experiments were performed. The kidney pair was removed *en bloc*, and the meat inspector (non-invasively) stamped the right kidney to uniquely identify it from the left kidney, as shown in Figure 11. Next, the fat and connective tissue were removed from the kidneys, but the capsule was left intact. The renal vein, renal artery, and ureter were then catheterized with female Luer-lock adapters. The adapters were secured in the vasculature with zip ties. The ventral renal surface was tied with suture to differentiate the ventral surface from the dorsal surface. The right kidney was tied with two pieces of suture and the left with one to differentiate between the right and left kidneys. A fully prepared kidney pair is shown in Figure 11.

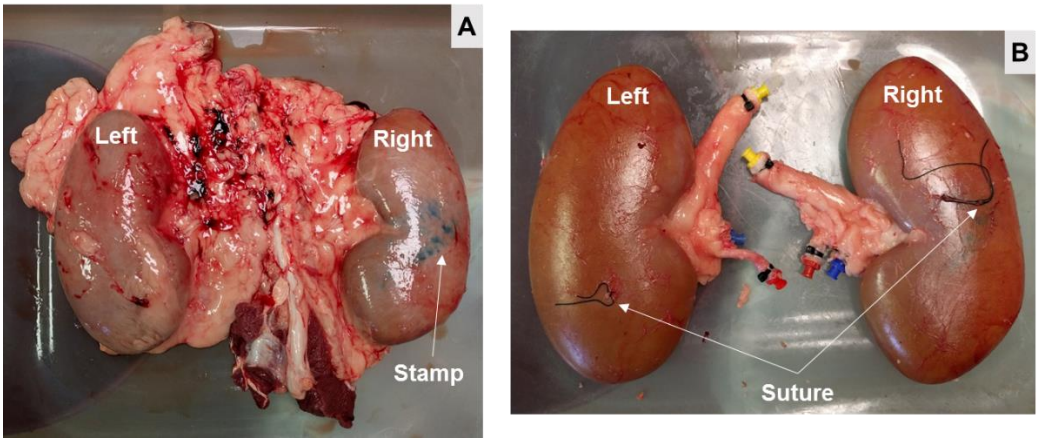

Figure 11. Kidney preparation for flush. (A) Kidneys are procured *en bloc* and the right kidney is stamped to indicate kidney side. (B) A fully prepared kidney pair after connective tissue and fat are removed; suture is tied to the ventral surface and Luer-lock adapters (colored red, blue, and yellow) are connected to the vasculature (renal artery, vein, and ureter, respectively).

After the kidneys were prepared, they were gravity-flushed with room temperature (25 ^{o}C) perfusate. Two funnels (one for mannitol, one for PBS) were attached to a coat rack; the height

was consistent across all experiments. The perfusate was poured into the funnels, which were at a height of approximately 1 meter above the kidneys, as shown in Figure 12. The funnel tube was outfitted with a male Luer-lock adapter, which was inserted into the renal artery of each kidney. Then the right and left kidneys were simultaneously flushed with 1.0 L of the perfusate prescribed by the experimental design, inverting the kidneys after every 250 mL of perfusate was perfused. After the flush, each kidney was placed into its own plastic bag and submerged in a cooler filled with ice. Kidneys were stored on ice during transport back to Virginia Tech, a 90 minute drive.

Figure 12. Flush at slaughterhouse. (A) Funnels are attached to a coat stand (~1 m above kidneys) and filled with perfusate; the funnel tubing is attached to the renal artery. Both the right and left kidneys are flushed simultaneously. (B) Tubing is attached to the renal artery and both the renal vein and ureter are unobstructed and drain freely. The renal surface becomes lighter in color as blood is flushed from the kidney vasculature.

3.2.2 Renal surface preparation for DIC. Since kidneys do not have a unique, natural surface pattern, the renal surface had to be prepared for DIC imaging by dying and applying a speckle pattern to the dorsal surface. The normal renal surface is a light tan-pink color after being flushed, so the tissue does not have significant contrast. To provide substrate contrast, methylene blue solution (Methylene Blue Indicator: 1% w/v, Fisher Science Education) was sprayed onto the surface with a spray bottle and evenly distributed by manually rubbing it over the surface of the kidney. Then, the surface was convectively dried with a fan to speed up the drying process, as shown in Figure 13. After the kidneys were sufficiently dry, they were dyed a second time with the methylene blue solution to further darken the kidney surface. One dying treatment was not sufficient to darken the surface. The kidneys were stored in plastic containers

on ice in a cooler with its top removed. This kept the kidneys as cool as possible during the surface preparation process, as shown in Figure 13.

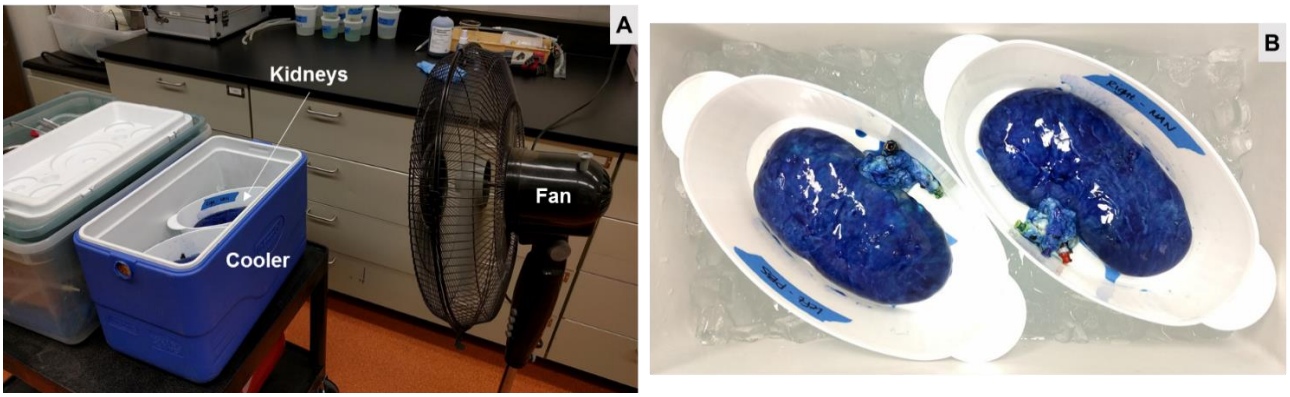

Figure 13. Drying the dyed kidney surface. (A) A fan assists in drying the chilled kidneys. (B) Drying kidneys are placed in plastic containers and stored on ice in a cooler with its top removed.

After the surface was dyed a dark blue and given sufficient time to dry, the kidneys were then spray painted with white paint (Stops Rust® Flat Protective Enamel, Rust-Oleum). A sputtering technique with the spray paint nozzle was used to generate a speckle pattern with distinct drops of paint. The combination of a dark-blue dyed kidney surface and white speckles yielded a high-contrast speckled surface for DIC imaging. The full chronological series of surface preparation is shown in Figure 14.

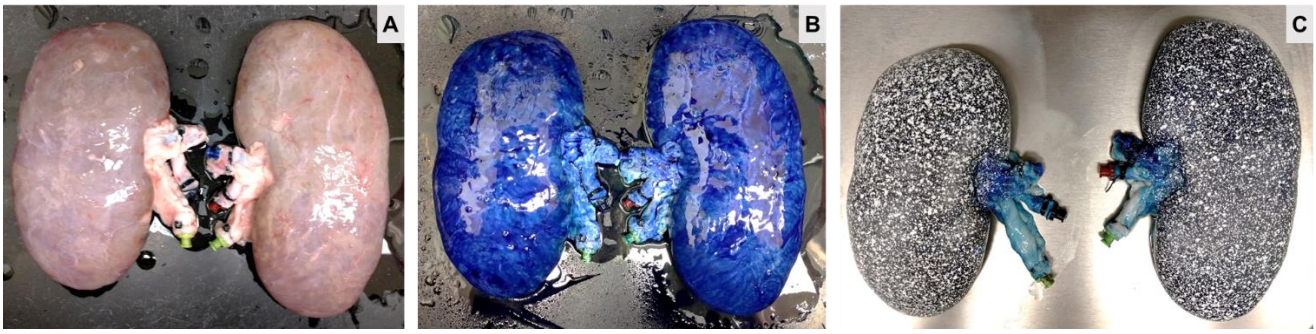

Figure 14. Kidney surface preparation for DIC. The original kidney surface in (A) is dyed with methylene blue indicator (B) and after drying is speckled with white spray paint (C).

3.3 Equipment Set-up

3.3.1 DIC system set-up. Equipment for the DIC system was arranged around the set-up of the perfusion circuit. Equipment consisted of: camera sensors (Prosilica GX, Allied Vision Technologies, Stadtroda, Germany) connected to the computer via Ethernet cables, lenses (XENOPLAN 1.9/35-0901, Schneider-Kreuznach, Bad Kreuznach, Germany) set to an aperture of 8.0, rigid camera mounting bar, tripod (Velbon (Tokyo, Japan) and Manfrotto (South Upper Saddle River, NJ) components), two light sources (Hilio, Litepanels®, Shelton, CT), and a computer. As shown in Figure 15, the sensors were attached to the camera support bar and the sensors' line of sight was perpendicular to the floor. The two light sources were situated to provide indirect light to the kidney surface. Directly lighting the kidney was ineffective and

resulted in glare caused by moisture on the renal surface. Overhead fluorescent lights were used to provide additional lighting.

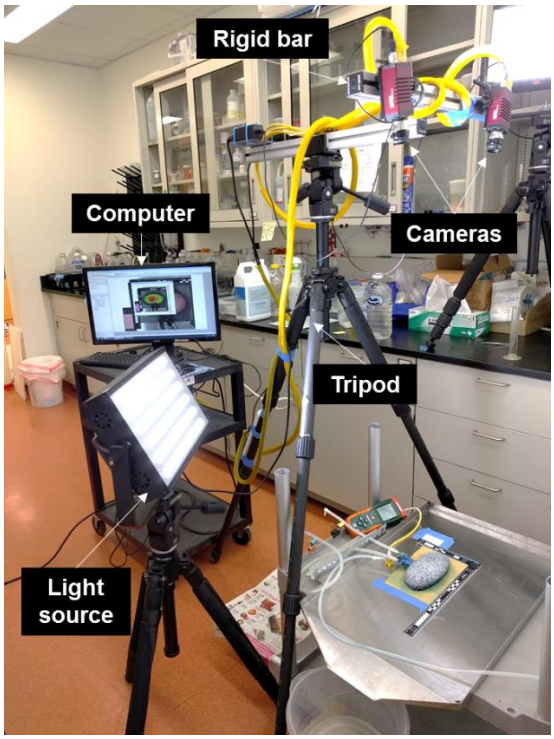

Figure 15. DIC equipment set-up. Equipment consists of cameras attached to a rigid support bar, tripod, light sources, and a computer.

The DIC system was calibrated for every experiment (i.e., calibrated for each kidney pair) prior to experimentation. Approximately 35-40 images were collected of the calibration plate (12x9 points with 9 mm spacing, Correlated Solutions, Inc., Irmo, SC). Each image was collected with the plate in a different orientation. An example of a calibration image is shown in Figure 16. Images were collected using the Vic-Snap software (Correlated Solutions, Inc., Irmo, SC). After all calibration images were collected, the images were used to calibrate the system. If the resulting calibration score was less than 0.05 pixels, then the calibration was successful. A list of the calibration scores for all experiments is located in Appendix C. From this point forward, the equipment (i.e., tripod, light sources) was not touched or bumped.

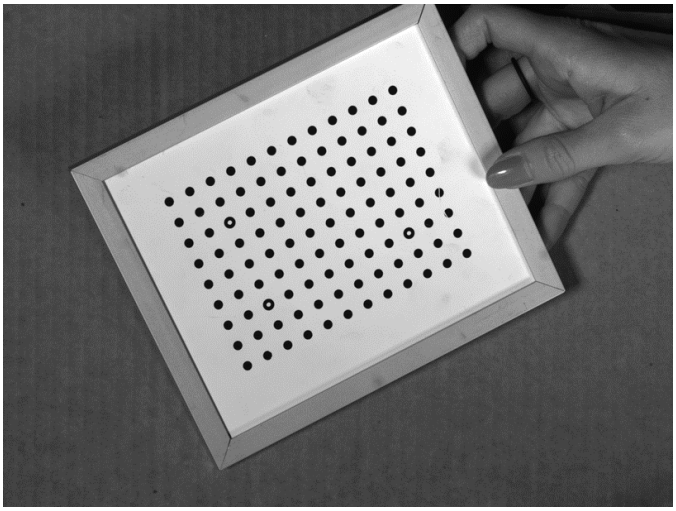

Figure 16. Collected calibration image. The calibration plate is tilted at an angle; each image collected for calibration shows the plate in a different orientation.

The area where the kidney would be placed within the field of view was then staged to prepare for experiments. A piece of 320-grit sandpaper was taped to a metal sheet; this prevented the kidney from sliding. Next, a group of reference speckles (white paper speckled with marker) was taped to the metal sheet; this served as the location of the origin. Lastly, a reference ruler was placed into the field of view. A picture of the staged kidney area is shown in Figure 19 in Subsection 3.3.3 Kidney testing position set-up.

3.3.2 Perfusion circuit set-up. The machine perfusion circuit used was an open circuit driven by a peristaltic pump. Temperature was regulated by a heat exchanger, as shown in Figure 17. An open circuit design was used so renal fluids (i.e., filtrate and venous outflow) would not mix with the renal artery inflow. Components included: a peristaltic pump (Sarns™ 8000 Roller Pump, 3M, Somerset, NJ), heater-cooler (Hemotherm®, Cincinnati Sub-Zero, Cincinnati, OH), heat-exchanger (BIOtherm™, Medtronic, Minneapolis, MN), and manometer (Differential Pressure Manometer, Extech® Instruments, Nashua, NH). A perfusion system flow diagram is shown in Figure 18, which indicates the direction of perfusate flow. For each experiment, the heater-cooler was set to 5 ^{o}C so perfusion was hypothermic. The peristaltic pump RPM was adjusted to generate a target systolic/diastolic pressure wave of 120/100 mm Hg; the pressure was measured with a manometer placed anterior to the renal artery. In between the first and second experiments for a kidney pair, the perfusion circuit was flushed with 4 L of RO water to remove any remnants of the first perfusate from the lines. Before each experiment, the tubing lines were de-bubbled.

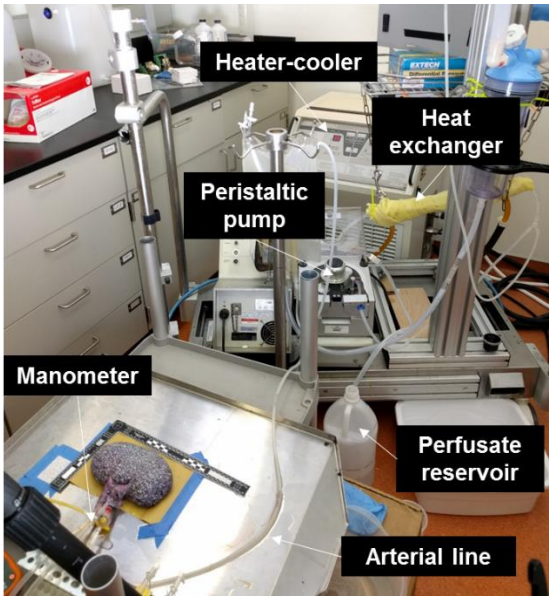

Figure 17. Perfusion circuit set-up. Components in the perfusion circuit include: perfusate reservoir, heat exchanger, heater-cooler, peristaltic pump, and manometer.

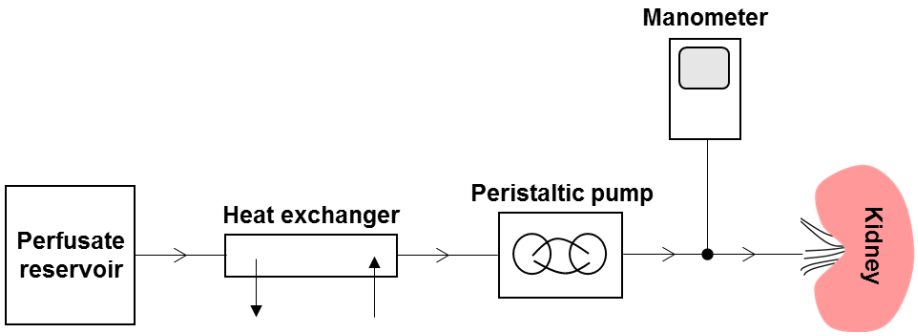

Figure 18. Open-circuit perfusion diagram. Perfusate is stored in the perfusate reservoir, and is then pumped through the heat exchanger by the peristaltic pump; the pump outflow (i.e., arterial line) sends the pressure wave to the renal artery and the pressure is measured by the manometer.

3.3.3 Kidney testing position set-up. Before each experiment, the kidney to be perfused was removed from the cooler and placed onto the swatch of sandpaper with the dorsal surface facing upwards. With the perfusion lines prepared (i.e., de-bubbled), the peristaltic pump outflow tube (arterial line) was connected to a stop-cock that was connected to the manometer and renal artery, as shown in Figure 19. Additionally, drain tubes were connected to the renal vein and ureter. The drain tubes allowed for easy sample collection of the venous outflow and filtrate; the tubing discharged two separate streams into a waste bucket.

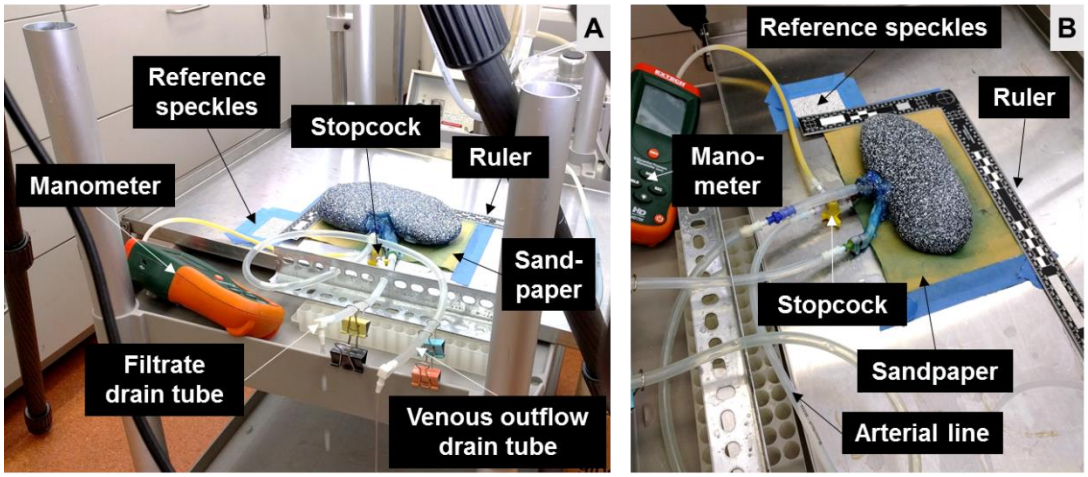

Figure 19. Kidney perfusion set-up. The kidney is placed onto a swatch of sandpaper that is secured to the metal sheet. Reference speckles and a ruler are also placed on the metal sheet for DIC imaging. The arterial line is connected to the stopcock that is connected to the renal artery and drain tubes are connected to the ureter and renal vein to drain the filtrate and venous outflow, respectively. The manometer is connected to the stopcock to measure perfusion pressure. (A) and (B) are images of different vantage points for two separate experiments.

3.4 Data Collection

First, several test images with the kidney in the testing position were collected with the calibrated DIC system. Vic-Snap (Correlated Solutions, Inc., Irmo, SC) was used to acquire images; a shutter speed of 80 ms was used for all image acquisition. This set of sample images was then correlated in the DIC software (Vic-3D, Correlated Solutions, Inc., Irmo, SC) to ensure a proper speckle pattern, lighting, and shutter speed. If the software was able to correlate a 3D surface, then the experiment was ready to begin. As previously stated, each experiment was 135 minutes in duration (15 min perfusion, 120 min without perfusion); the image sampling rate was 500 ms for the first 17 minutes and 20 s for the remaining 118 minutes. At the cross-over between the sampling rates at 17 minutes, there was a 20.5 s gap in image collection. The ischemic interval (time between procurement and start of perfusion) varied; a table of the ischemic intervals for each experiment located is in Appendix D.

With the proper initial sampling rate selected (500 ms) in Vic-Snap, image acquisition was started. This allowed for the collection of 10-20 seconds of undeformed images. Then, the peristaltic pump RPMs were gradually increased to start perfusion. The manometer indicated the perfusion pressure and it took approximately 2 minutes of adjusting the pump RPMs to reach a steady pressure waveform of 120/100 mm Hg. After the pressure stabilized, the pump was not re-adjusted throughout the entire experiment, even as the pressure changed as a result of changes in renal resistance. So, regardless of changes in resistance of the kidney, the flow remained the same, as shown in Appendix E, which altered the pressure in all of the experiments. The only time it was necessary to re-adjust (reduce the pump RPMs) was if the systolic pressure increased to greater than 150 mm Hg; high systolic pressure has the capability to overperfuse the kidney

and to tear the renal capsule. Initial and final perfusion pressures for each experiment are located in Appendix E.

During the 15 minutes of perfusion, 0.6 mL fluid samples (venous outflow, filtrate) were collected every two minutes until 16 minutes elapsed time (i.e., samples collected at 2, 4, 6, 8, 10, 12, 14, 16 minutes). These samples were subsequently used to assess perfusate and filtrate osmolality. The 0.6 mL vials were placed under the fluid stream from the discharge tubing, which allowed samples to be collected without bumping the testing set-up or the kidney. At 15 minutes elapsed time, the peristaltic pump was turned off and thus began the 120 min of DIC data collection without perfusion. At 17 minutes elapsed time, the image sampling rate was reduced to 20 s. After the experiment for one kidney was concluded, the contralateral kidney was perfused using the same set-up and procedure.

Once both kidney pair experiments were finished, sample biopsies were collected. As shown in Figure 20, the kidney was dissected; a small slice containing both the cortex and medulla was removed from the kidney and then immediately preserved in 10% neutral-buffered formalin. After the tissue was fixed, a small sliver of the biopsy was dissected and placed into a biopsy cassette and returned to 10% neutral-buffered formalin to await processing. Additionally, the renal fluid samples were frozen at the completion of both experiments.

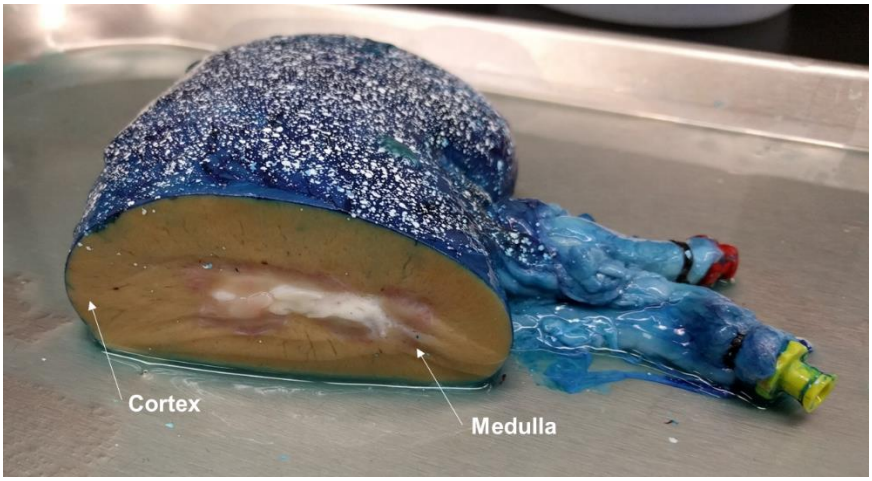

Figure 20. Kidney cross-section. A biopsy slice is removed that contains the cortex and medulla.

3.5 Sample Post-processing

3.5.1 Fluid post-processing. Osmolality was measured for all renal fluid samples. Just prior to osmolality testing, the samples were thawed on the bench and brought to room temperature. The osmolality of each 0.6 mL sample was measured using an osmometer (The Advanced™ Micro-Osmometer, Model 3MO Plus, Advanced Instruments, Inc., Norwood, MA). The osmometer used 20 μL of the sample and had an accuracy of ± 2 mOsm/kg.

Raman spectroscopy was implemented to determine sample composition for all samples in a single experiment performed on February 17, 2017. This experiment was not included in the deformation study due to a pump malfunction, but the same protocol was followed as all other

experiments. It was of interest to determine if the osmotic agent (mannitol) was present in the filtrate, which would determine if the kidney still had remaining filtering function. A Raman spectrometer (PeakSeeker™, Agiltron, Woburn, MA) with a 785 nm laser was used. Raman spectrometry uses a laser to measure chemical bond deformation in the unique molecules that are present in a substance. Wavenumbers associated with medium and very strong peaks for mannitol are 473, 872, and 1034 cm^{-1} [46]. Each sample was scanned 10 times with an integration time of 15 sec and a 15 sec delay between scans.

3.5.2 Biopsy post-processing. Biopsies were transferred from buffered formalin to a short tap water rinse, and then immersed in an aqueous solution of 70% ethanol. Subsequently (on an automated tissue processor), tissues were sequentially dehydrated in a graded series of alcohols, and then transitioned to xylene and infiltrated with paraffin polymer. Three micron sections were cut, de-paraffinized, rehydrated, and then stained with hematoxylin-eosin solution. An experienced renal pathologist was given the encoded slides and performed a 'blinded grading' of major histoanatomical features, using a semi-quantitative scoring procedure (1=minimal feature change, 2=mild feature change, 3=moderate feature change, 4=marked feature change, 5=severe feature change).

3.5.3 DIC image post-processing. The DIC software Vic-3D (Correlated Solutions, Inc., Irmo, SC) was used to perform digital image correlation with the acquired images. This involved several steps: (1) Area of Interest (AOI) selection, (2) subset and step size selection, (3) correlation, and (4) coordinate transformation. AOI selection, shown in Figure 21, is the process of selecting the area to be analyzed; in this case, the AOI was the renal surface and the reference speckles. Subset size, step size, and noise level were identical for all experiments; a subset size of 45 pixels (45x45 pixels), a step size of 7 pixels, and a noise level of 6.0 were used. The correlation parameters were also the same for all experiments. A normalized squared differences (NSSD) correlation criterion was used with an optimized 8-tap interpolation. After the correlation was completed, a coordinate transformation was performed using the "3-point selection" method; the origin and x-axis were drawn and then a point in the xy-plane was selected. As depicted in Figure 21, the origin and x-axis are located on the reference speckles. The 'reference speckle origin' created a z-axis that was zero on the same surface that the kidney was supported on; this resulted in meaningful z-coordinate measurements. After the displacement field was generated for all experiments, the data was then exported and analyzed.

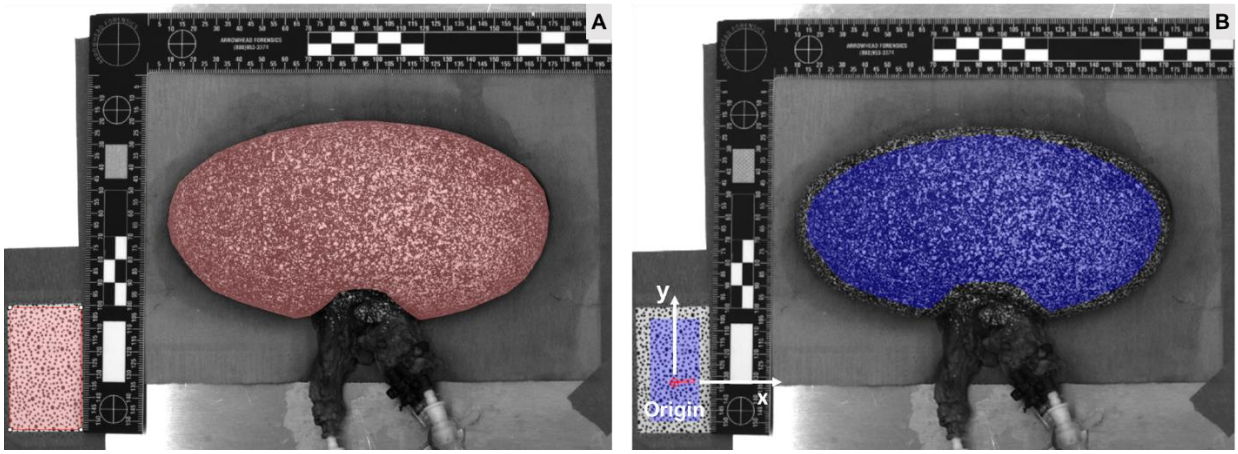

Figure 21. AOI selection and coordinate transformation. (A) Two linked areas of interest (kidney and reference speckles) are created. (B) Coordinates are transformed by selecting an origin and x-axis; the x- and y-axes are labeled.

3.6 DIC Data Analysis

There are several different methods to extract and/or export displacement data from the DIC software and manipulate it to present in a meaningful form. This section will detail the (1) quantitative methods to compare renal displacement for PBS and mannitol and (2) visualization methods to analyze renal shape.

3.6.1 Definitions and notations. First, this subsection will present the background necessary for interpreting displacement results. X, Y, Z coordinates for all data points are only reported for the reference (i.e., initial) image. Calculated displacements in all subsequent deformed images along the x-, y-, z-axes are reported as U, V, W, respectively. Again, U, V, W displacements are calculated with respect to the reference image (i.e., reference image has zero displacement). The resulting deformed coordinates along the x-, y-, z-axes are Xp, Yp, Zp, respectively,

$$Xp = X + U \tag{13}$$

$$Yp = Y + V \tag{14}$$

$$Zp = Z + W \tag{15}$$

where X, Y, Z are the initial coordinates of a point and U, V, W are the displacements of that same point. Equations 13, 14, and 15 are applied to every point to determine the deformed coordinates of all points. Z-coordinate displacement (W) is the change in position of a point and the deformed z-coordinate (Zp) is the physical dimension (thickness) of a point, which is indicative of a kidney's thickness.

Most of the analyses in this thesis focus on three distinct time points during image collection: "initial," "maximum" (abbreviated as "max"), and "final." These three time points capture critical instances during the experimental perfusion intervals as shown in Figure 22. The "initial" time point refers to the first image collected (reference image), which contains no

displacement. The “maximum” time point refers to the last image collected during machine perfusion; this is the image that contains the maximum z-displacement (W) of all the collected images. The “final” time point refers to the last image that was collected after 120 minutes without perfusion.

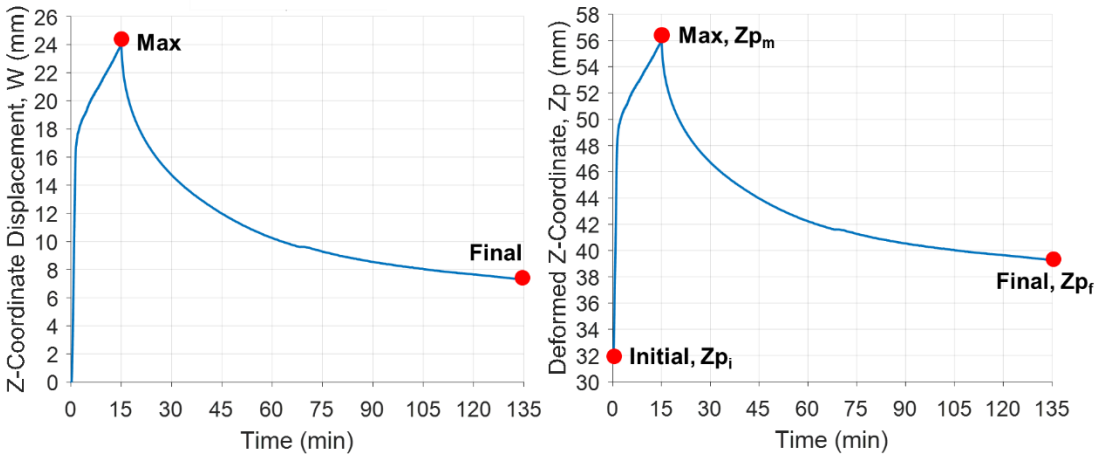

Figure 22. Selection of maximum and final data collection points for z-coordinate displacement (left) and the selection of initial, maximum, and final data collection points for the deformed z-coordinate (right). The maximum (abbreviated “max”) data collection point is the last image collected during perfusion.

Several percent difference calculations will be reported for certain measurements: “percent difference,” “percent increase,” and “percent decrease.” In the context of this thesis, “percent difference” refers to the percent difference between any measurement and the initial measurement; “percent increase” refers to the percent difference between the maximum measurement and the initial measurement; “percent decrease” refers to the percent difference between the final measurement and the maximum measurement.

Each kidney is referenced by an identifier (e.g., “K1-R-PBS-020917”) that describes its experimental testing conditions. The notation for the kidney identifier is:

“Kidney #” - “Kidney Side” - “Perfusate” - “Experiment Date”

The kidney number describes the order of perfusion (first or second; i.e., K1 or K2); the kidney side describes whether it is the right or left kidney (i.e., R or L); the perfusate describes the perfusate type (PBS or mannitol; i.e., PBS or MAN); and the experiment date is the date the experiment was conducted.

3.6.2 Data loss. Two experiments experienced significant (greater than 5%) data loss; an example is shown in Figure 23. Data loss refers to the contour holes that appear in the 3D surface when subsets cannot be correlated. The main reason for data loss was surface wetting, shown in Figure 23, which occurs naturally when kidneys are perfused. Surface wetting created droplets of water (which were relatively dark in color because of the methylene blue) on the kidney surface that would temporarily or permanently remove the spray paint speckle pattern,

especially when they run down the side of the kidney. Another cause of data loss was the quality of the speckle pattern, especially near the renal poles. The application of spray paint near the poles had a greater tendency to be more of a mist than a spatter pattern due to the sweeping technique used for spattering.

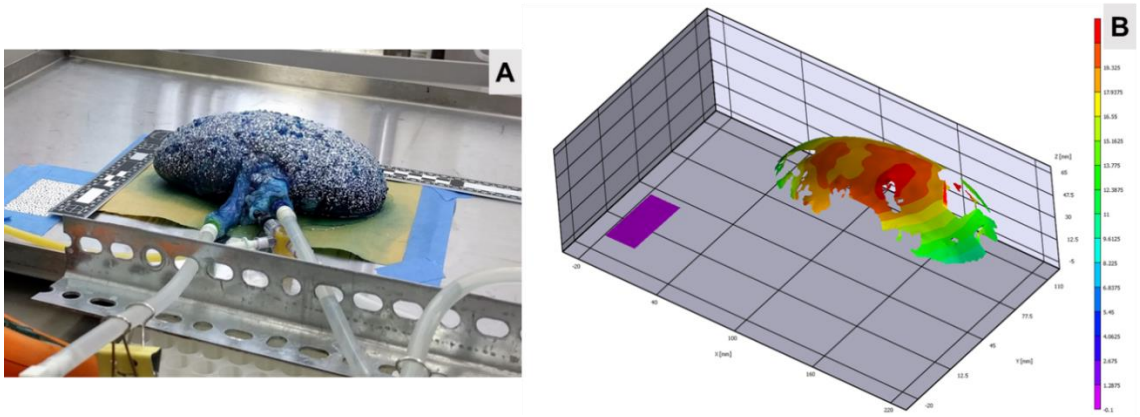

Figure 23. Data loss potentially caused by surface wetting. (A) Surface wetting of K1-L-MAN-030817; the wet spots are droplets of perfusate that have naturally appeared on the surface. (B) Resulting 3D surface of K1-L-MAN-030817 where contour holes are apparent.

A plot of the percent data loss (i.e., percent decrease in the number of data points) between the initial image and the maximum and final images is shown in Figure 24. Kidneys K1-R-MAN-022217 and K1-L-MAN-030817 both experienced significant data loss during the experiment. Thus, in future sections of this thesis, these two kidneys and their experiment pairs (K2-L-PBS-022217 and K2-R-PBS-030817) were removed from most of the analyses since the analysis type would be skewed by data loss. These two experiments will be noted as "Experiments 02-22-17 and 03-08-17." Each section will mention if any of the data was dropped from the analysis.

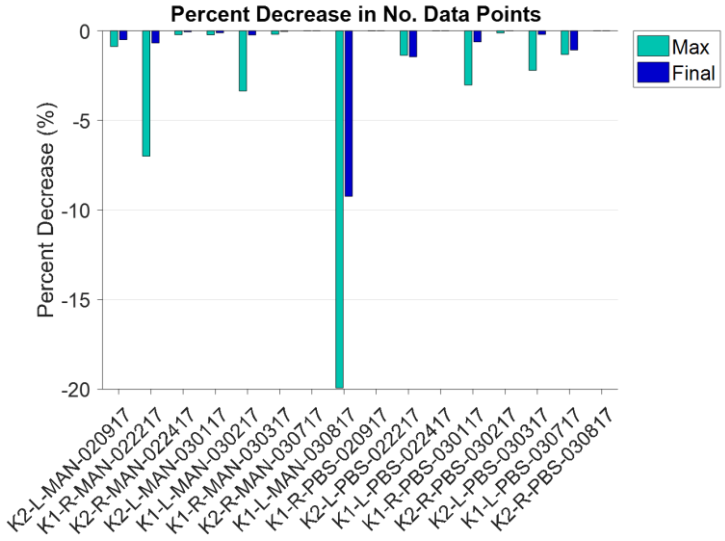

Figure 24. Percent decrease in the number of data points with respect to the initial image. A large percentage of data loss occurred for kidneys K1-R-MAN-022217 (-20%) and K1-L-MAN-030817 (-7%).

3.6.3 Point tracking method. The first quantitative method used for comparing PBS and mannitol was point tracking. One of the major benefits of DIC is its ability to track the position of a single point over time without placing a distinct fiducial marker at that point on the object. This means that any point on the speckled object can be identified and subsequently located in all collected images (i.e., point tracking). The "Inspect Point" tool (Correlated Solutions, Inc., Irmo, SC) was used to select the point of maximum z-displacement (W) in the last collected image of perfusion, as shown in Figure 25. This point will be referred to as P0. With P0 tracked over all images, it was possible to export data from the point for all images. Since the largest displacement component was along the z-axis, the variables of interest were W and Zp. Since P0 is not affected by data loss, all experiments were used for this analysis.

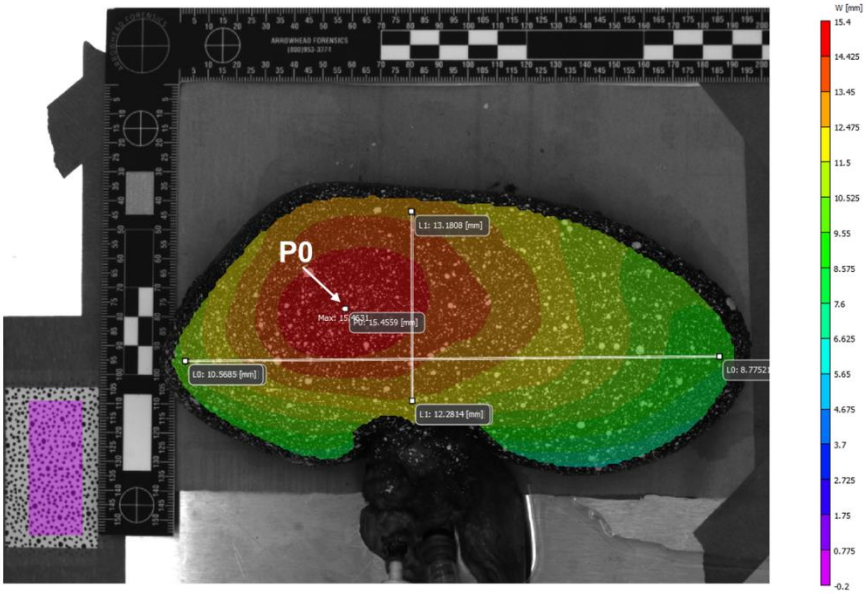

Figure 25. P0 selection where the maximum z-displacement (W) occurs. P0 is selected in the last image of perfusion; the location of P0 varies from kidney to kidney.

3.6.4 Average method. The second quantitative method used for comparing PBS and mannitol involves averaging the point data. All data points in X, Y, Z space were exported for the initial, maximum, and final images. This resulted in a 3D point cloud of the renal surface for each image, as shown in Figure 26. For specific exported images (i.e., initial, maximum, final), the data values over the entire image (e.g., W, Zp) were averaged. For example, there might be 7,000 data points over the renal surface, but by taking the average, the variable of interest (Zp or W) can be represented by a single value. Since the average is affected by data loss, Experiments 02-22-17 and 03-08-17 were removed from the analysis.

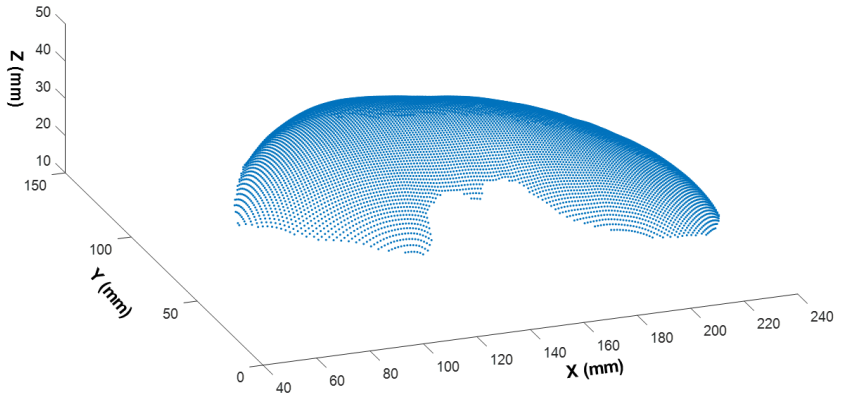

Figure 26. Renal surface represented by 3D data points.

3.6.5 Volume estimation method. The third quantitative method used for comparing PBS and mannitol was volume estimation. Using the same exported data as the average analysis, renal volume was estimated at the initial, maximum, and final images. While the data points were not evenly spaced in a grid over each image, the spacing was fairly consistent, which allowed every data point to be treated as a rectangular prism,

$$V = l \times w \times h \tag{16}$$

where l and w are the length (1.1 mm) and width (1.1 mm) of the square area in the xy-plane bounding the data point and h is the deformed z-coordinate (Zp) of the data point. An example of the square area is shown in Figure 27. Thus, the estimated volume of the kidney (V) is the sum of the rectangular prisms at each data point; a visualization of this technique is shown in Figure 27. This is an extremely crude volume estimation method, but since the kidneys do not expand significantly along the x- and y-axes, most of the volume change occurs through the thickness (z-axis) of the kidney.

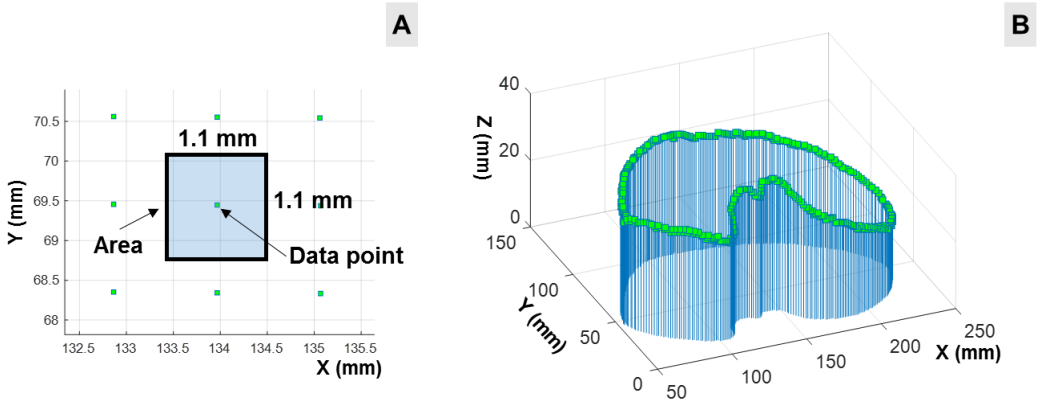

Figure 27. Volume estimation method. (A) Area of a square in the xy-plane that surrounds each data point. (B) Visualization of the volume estimation; rectangular prisms are created for each data point by multiplying the xy-plane area by the deformed z-coordinate. (B) Only includes the kidney border for visualization purposes; the volume method is applied to all data points over the kidney surface.

3.6.6 Maximum z-displacement (Wmax) tracking. To better visualize how the renal surface reacts to machine perfusion, a MATLAB® code (MathWorks Inc., Natick, MA) was developed that plots and tracks the location of the maximum z-displacement (Wmax) in each image. To complete this analysis, all data points were exported for each image being analyzed. The data boundaries in the xy-plane for the initial, maximum, and final images were also plotted using the boundary function in MATLAB®, with a shrink factor of 1.0. An example of the data boundary with respect to the data points is shown in Figure 28. The purpose of tracking the maximum z-displacement (Wmax) is to locate the position on the renal surface that is being most affected structurally by machine perfusion. It is hypothesized that tracking these points over time can show how and where a kidney is most impacted by perfusion.

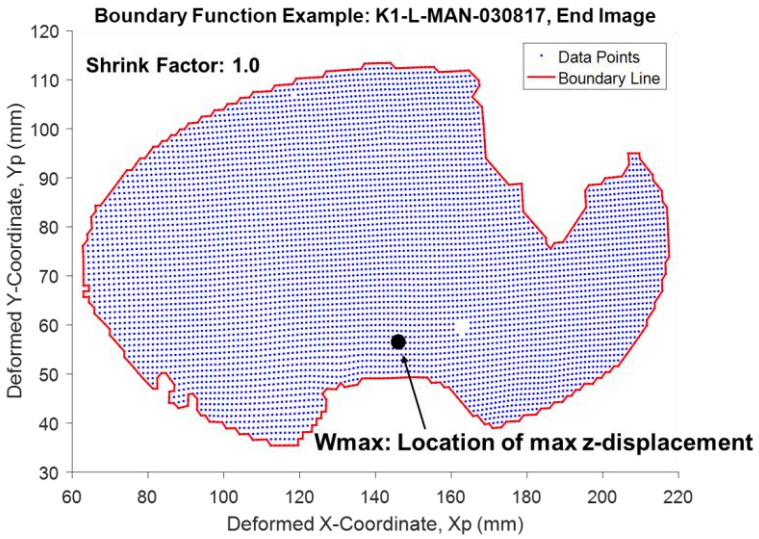

Figure 28. Boundary of data points. The MATLAB® boundary function is used with a Shrink Factor of 1.0 to bound the kidney surface data points, which shows the 'outline' of the contour. The locations of maximum z-coordinate displacement (Wmax) are plotted within the boundary lines to show where they occur with respect to the kidney anatomy.

3.6.7 Line slices. None of the other analysis techniques used have explicitly examined the renal shape during perfusion. The "Inspect Line" tool (Correlated Solutions, Inc., Irmo, SC) was used to examine renal shape across the length and width of the kidney, as shown in Figure 29. L0 was placed along the length from pole to pole and L1 was placed along the width from the hilus to the lateral border. The "Inspect Line" tool extracts 200 points from the start to the end of each line segment with any variable desired. In this case, the z-displacement (W) and deformed z-coordinate (Zp) were plotted as a function of the deformed x-coordinate (Xp) and deformed y-coordinate (Yp) for lines L0 and L1, respectively. The z-displacement (W) shows how points along the line deform and the deformed z-coordinate (Zp) shows the actual renal thickness.

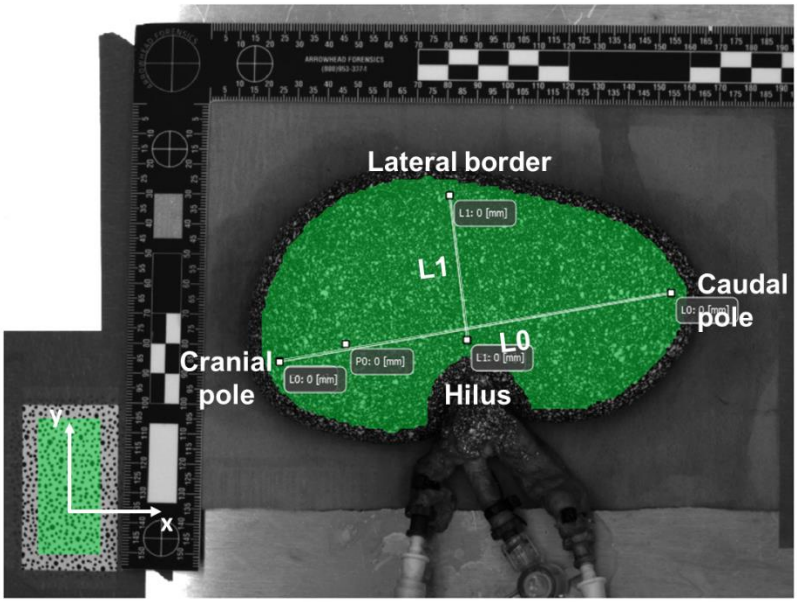

Figure 29. Inspect line tool to evaluate renal shape. L0 is placed from pole to pole and L1 is placed from the hilus to the lateral border. 200 points are evaluated along the length of the line.

3.6.8 Statistical analysis. Since each experiment was conducted with the right and left kidneys from the same pig, the paired t-test was used to determine the statistical significance of average differences between PBS and mannitol measurements. For each experiment (i) the difference in the measurement (y) between mannitol (MAN) and PBS is,

$$d_i = y_{MAN,i} - y_{PBS,i} \tag{17}$$

The sample mean difference ($\bar{d}$) for all n experiments is,

$$\bar{d} = \frac{\sum_{i=1}^{n} d_i}{n} \tag{18}$$

The sample mean difference is an estimator of the true mean difference, δ. The set of null and alternative hypotheses are listed in Table 2. The conclusions for if the null hypothesis is rejected are shown in the third column of Table 2. The significance level (α) used for all statistical analyses was 0.05; the null hypothesis was rejected for a p-value < 0.05. The "Matched Pairs" analysis tool was used in JMP Pro 12.0 (SAS®, Cary, NC). P-values for all experiments are included in Appendix F.

Table 2: Null and alternative hypotheses for the paired t-test

Null Hypothesis (H_0)	Alternative Hypothesis (H_a)	Conclusion if H_0 is rejected (p-value < 0.05)
$\delta = 0$	$\delta > 0$	MAN yields larger results
$\delta = 0$	$\delta < 0$	PBS yields larger results
$\delta = 0$	$\delta \neq 0$	MAN and PBS yield different results

3.6.9 DIC displacement accuracy. Using the methods described in Subsection 2.8.9 Quantifying error, the rule-of-thumb approximations for displacement accuracy are ~1 μm in-plane and ~2 μm out-of-plane for a field of view of 0.0533 m^2. The measured displacement accuracy was completed using the sixth static image for all experiments. There was variation among the experiments; a table of the variation is located in Appendix G. The average displacement accuracy for all experiments are ~2.7 μm in-plane and ~6.8 μm out-of-plane. Since the scale of the displacements experienced by the kidneys was so much larger than the measured noise, the displacement measurements were not strongly impacted by the noise.

Chapter 4 - Results and Discussion

This section presents and discusses the experimental results that were obtained through renal fluid collection, renal biopsy, and DIC analysis.

4.1 Biological Samples

4.1.1 Renal fluids. Drained renal fluids (i.e., filtrate and venous outflow) were collected during machine perfusion and the osmolality of all the samples was measured. The filtrate and venous outflow osmolality are plotted against elapsed perfusion time for PBS and mannitol in Figure 30 and Figure 31, respectively. The control samples (i.e., unused perfusate) are plotted as well, which give an idea of how the outflow is related to the inflow. The inflow into the renal artery is equal to the osmolality of the unused (control) perfusate. Several of the experiments are missing fluid samples, especially filtrate. The absence of a fluid sample indicates that the kidney was not discharging fluid at that time point. The kidneys perfused with PBS produced significantly less filtrate than the kidneys perfused with mannitol. This is an expected outcome since mannitol is a diuretic.

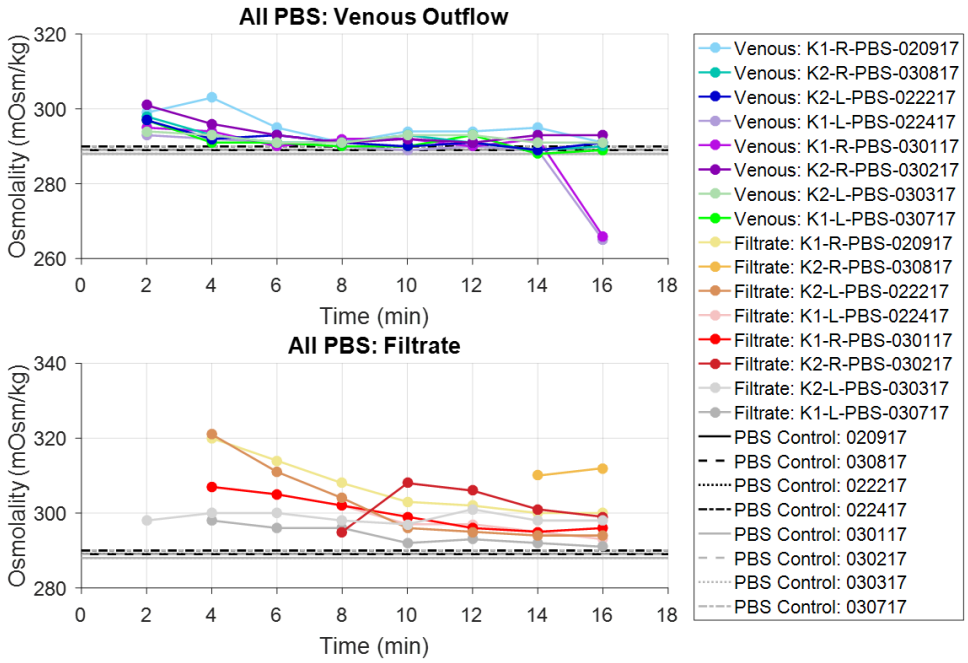

Figure 30. All renal fluid samples collected from kidneys perfused with PBS. (Top) Venous outflow samples for all time points. (Bottom) Filtrate samples for all time points. Several data points are missing for the PBS filtrate since many of the kidneys did not have significant flow from the ureter.

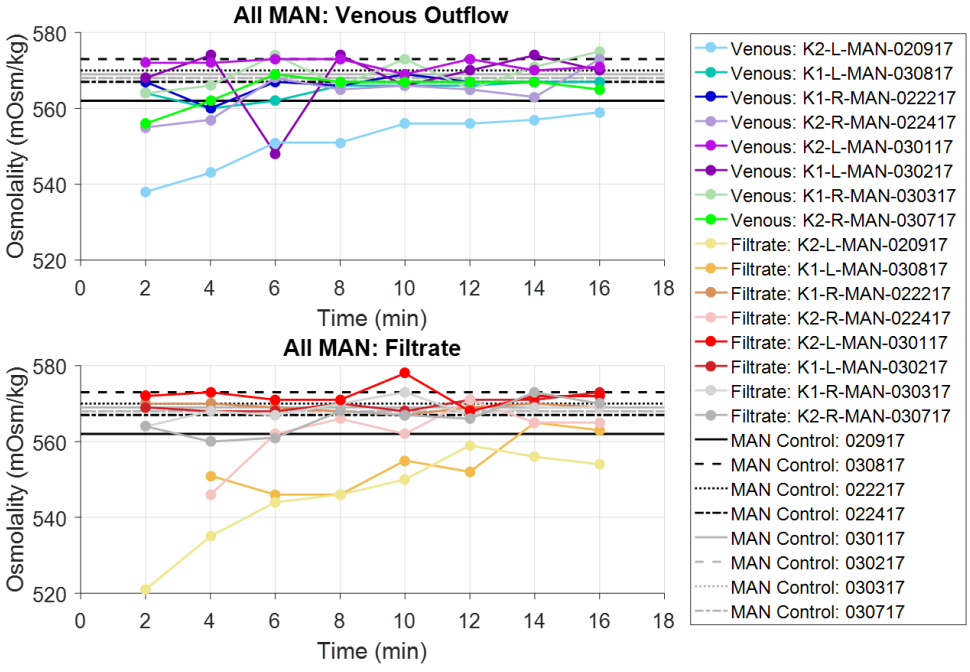

Figure 31. All renal fluid samples collected from kidneys perfused with mannitol. (Top) Venous outflow samples for all time points. (Bottom) Filtrate samples for all time points. A few data points are missing for the MAN filtrate; however, kidneys perfused with mannitol produced a substantially higher volume of filtrate.

The average at each time point is also plotted in Figure 32, which shows the general trend for filtrate and venous outflow for mannitol and PBS. However, since many of the PBS filtrate points are not present, the average may be strongly influenced by the lack of measurements at the early time points. Figure 32 suggests that over time, the discharged renal fluids (filtrate, venous outflow) approach the osmolality of the unused perfusate. For the mannitol, this means that the renal fluids are increasing in osmolality whereas for the PBS, the renal fluids decrease in osmolality. The change in osmolality measurements over time could be from decreasing amounts of retained, whole blood in the fluid samples over time as the perfusate is continuing to flush out the vasculature. This suggests that blood has a lower osmolality than mannitol (as expected) and blood has a higher osmolality than PBS. This may be why the solution of blood and perfusate start either greater than or less than the control.

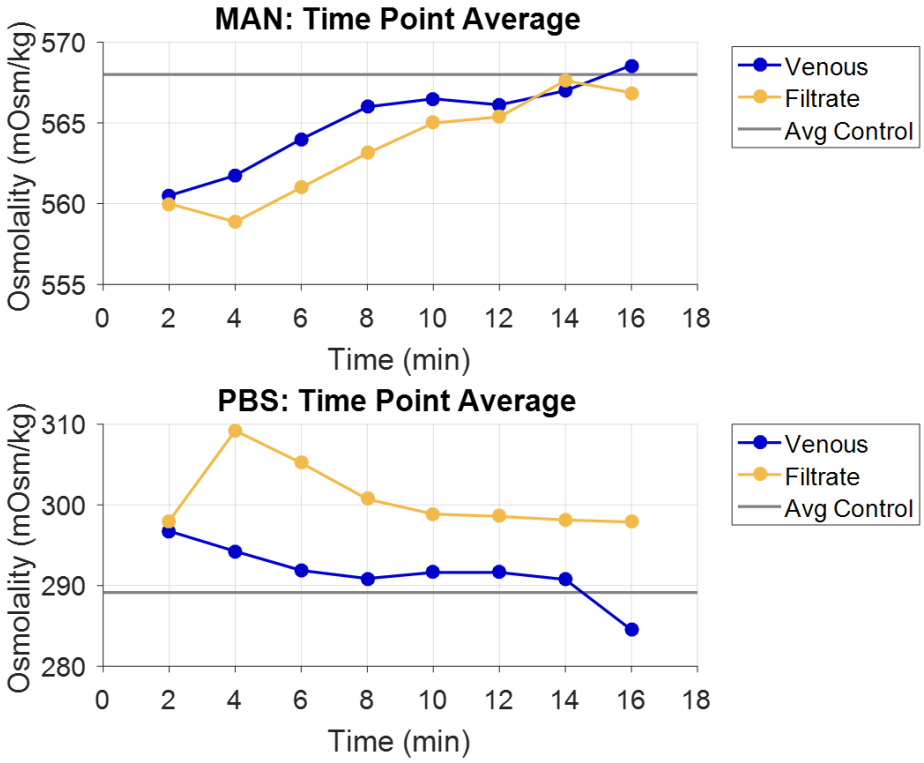

Figure 32. Time point average of renal fluid samples collected from kidneys perfused with (top) mannitol and (bottom) PBS. The average at every sample collection time was calculated. Both the mannitol and PBS tend to trend towards the osmolality of the control.

For a single experiment (02-17-17), the discharged renal fluid samples were also scanned with Raman spectroscopy to determine the composition of the fluids. All spectra were baselined and vector normalized. The mannitol and PBS control spectra in Figure 33 are significantly different. Thus, the mannitol can be distinctly identified in a set of Raman spectra.

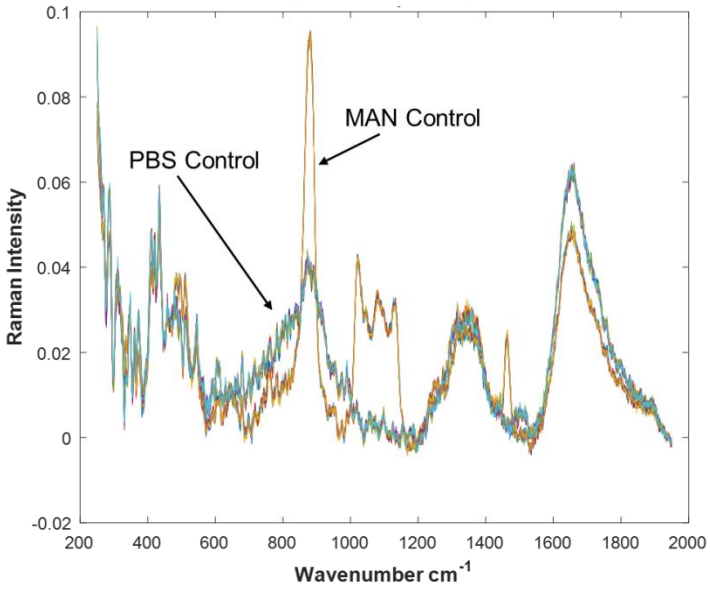

Figure 33. Raman spectra of PBS and mannitol controls. Each control has 10 associated scans; the PBS scans are a blue color and the mannitol scans are a red-orange color. The PBS and mannitol have unique spectra; Raman spectroscopy can differentiate between the two perfusates.

To determine if mannitol is present in the filtrate, a peak analysis was performed. Since ten scans were performed for each sample, the average intensity value of the ten scans at relevant wavenumbers (473, 872, 1034 cm^{-1} [46]) associated with mannitol were plotted. Next, the average intensity values at each wavenumber were summed. The result is Figure 34, which contains the samples for mannitol, PBS, and controls, separated with a vertical dashed line. The samples collected from kidneys perfused with mannitol showed a significantly larger "sum" peak than samples collected from kidneys perfused with PBS. This proves that the mannitol is present in all of the renal fluids collected from kidneys perfused with mannitol. More importantly, there is mannitol present in the filtrate, which shows that the renal glomeruli are actively filtering the mannitol; there is residual kidney function even after hours of static cold storage.

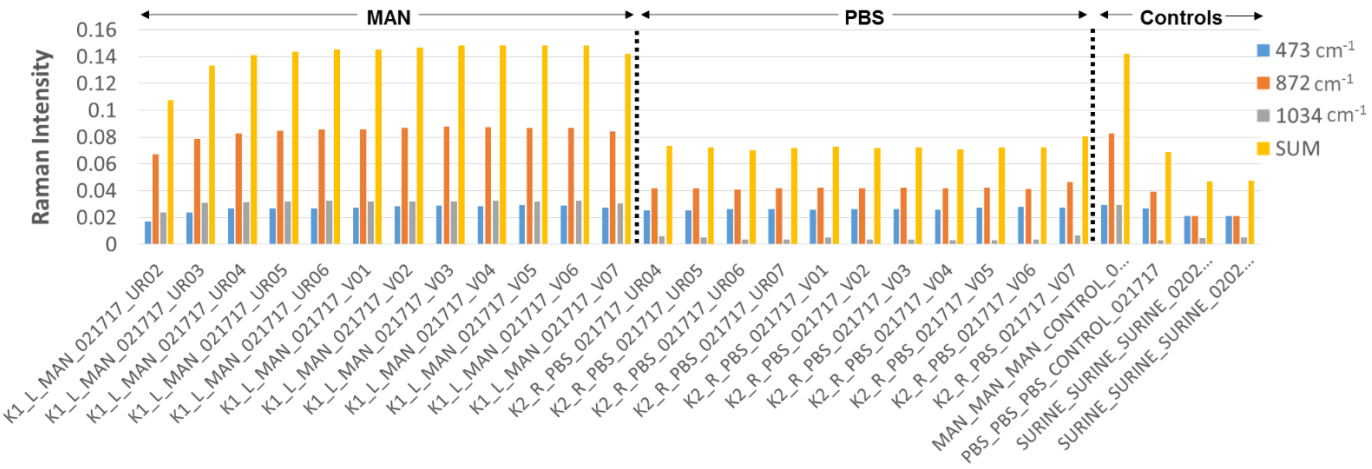

Figure 34. Raman spectroscopy peak analysis for renal fluid samples. The mannitol, PBS, and control samples are separated by dashed black lines. The "sum" bar for each sample is the sum of the intensities for the three wavenumbers associated with mannitol (473, 872, 1034 cm^{-1}). Thus, it is expected that the samples containing mannitol have larger magnitude intensity sums than the PBS samples. Surine (synthetic urine) controls are plotted for reference. "UR" is an abbreviation for urine; the notation has since been changed to "Filtrate." "V" is an abbreviation for venous outflow.

4.1.2 Renal biopsy. Biopsies of perfused porcine kidneys were collected and prepared for histopathological evaluation, as detailed in Subsection 3.5.2 Biopsy Post-processing. The scored results for all renal biopsies are shown in Appendix H. The interpretation of the morphology of these biopsies was provided by Dr. John Robertson, an experienced and qualified veterinary/translational pathologist. His interpretation follows.

"The histomorphology of kidneys perfused with physiologic phosphate-buffered saline (PBS) differed from the histomorphology of kidneys perfused with PBS with additional mannitol, a known osmotically-active agent.

The most prominent lesion seen in PBS-perfused kidneys (Figure 35) was varying degrees of cell swelling, with formation of intracellular vacuoles and dilution of the cell cytoplasm (blue arrow). Cell swelling occluded the lumens of some tubules. Acute tubular necrosis was also seen, associated with both single cell and multicellular hyperchromasia, and nuclear pyknosis (red arrow). Necrotic cells in some tubules sloughed into tubular lumens. These lesions are typically associated with periods of ischemia and a loss of nutrients (oxygen and energy-yielding metabolites) in mammalian cells; lesions tend to get more pronounced over extended periods of time. A semi-quantitative grading system was used to score the severity and distribution of these lesions and this is noted in an accompanying tabular figure in Appendix H.

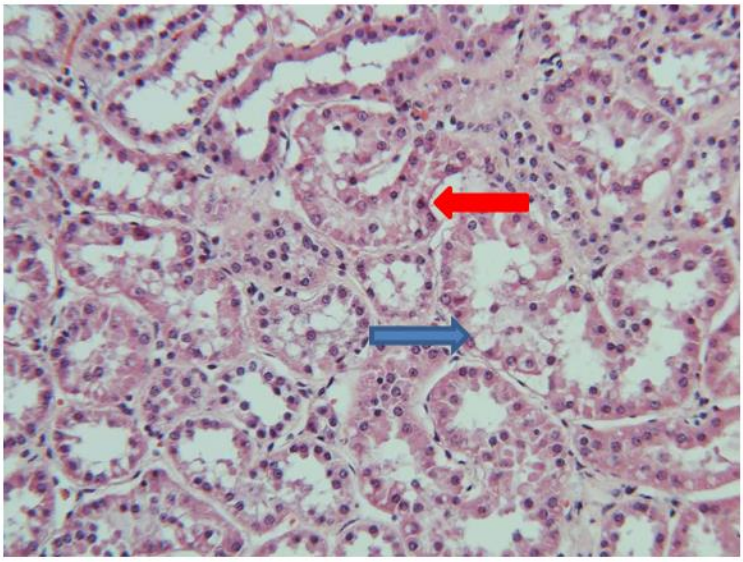

Figure 35. PBS-perfused kidney biopsy (K2-L-PBS-022217). The red arrow indicates nuclear pyknosis and the blue arrow indicates cytoplasm dilution.

Perfusion of kidneys with a solution of PBS and 5% mannitol resulted in diffuse dilation of tubular lumens and flattening of tubular epithelial cells (blue arrow) (Figure 36). Note that the cell swelling associated with perfusion solely with PBS solution is not a prominent feature in the biopsies of kidneys that were perfused with PBS + mannitol. Some tubules contain hyaline, proteinaceous (pink) debris (red arrow) that is likely derived from sloughed tubular epithelial cells showing slight degeneration due to prolonged ischemia. Hematoxylin-eosin stain, original magnification 200X."

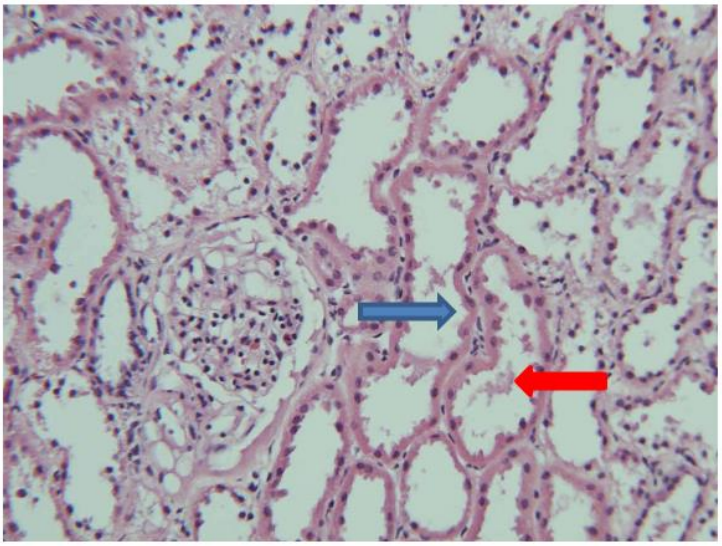

Figure 36. Kidney perfused with PBS and 5% mannitol solution (K2-L-MAN-020917). The red arrow indicates hyaline debris and the blue arrow indicates tubule lumen dilation and tubule epithelial cell shrinkage.

4.2 Digital Image Correlation

4.2.1 Point tracking method. The point of maximum z-displacement, P0, was extracted from the DIC point data for all images. P0 is an important location to evaluate because it is where the largest amount of z-displacement occurs over the entire renal surface for all collected images. Thus, it is the location where the kidney expands the most through the thickness. Since P0 is not affected by data loss, kidneys from all experiments were used in the analysis. As a note, percent differences in this section are calculated using the deformed z-coordinate.

The z-displacement (W) and deformed z-coordinate (Zp) are plotted as a function of time in Figure 37. There is a large increase in W and Zp during the 15 minute perfusion interval followed by a decrease over the 120 minute interval without perfusion. While these plots are beneficial for identifying trends over time, it is difficult to compare the W and Zp response of kidneys perfused with mannitol and kidneys perfused with PBS. Thus, the rest of this section will focus on three data collection times ("initial," "maximum," and "final") for each experiment.

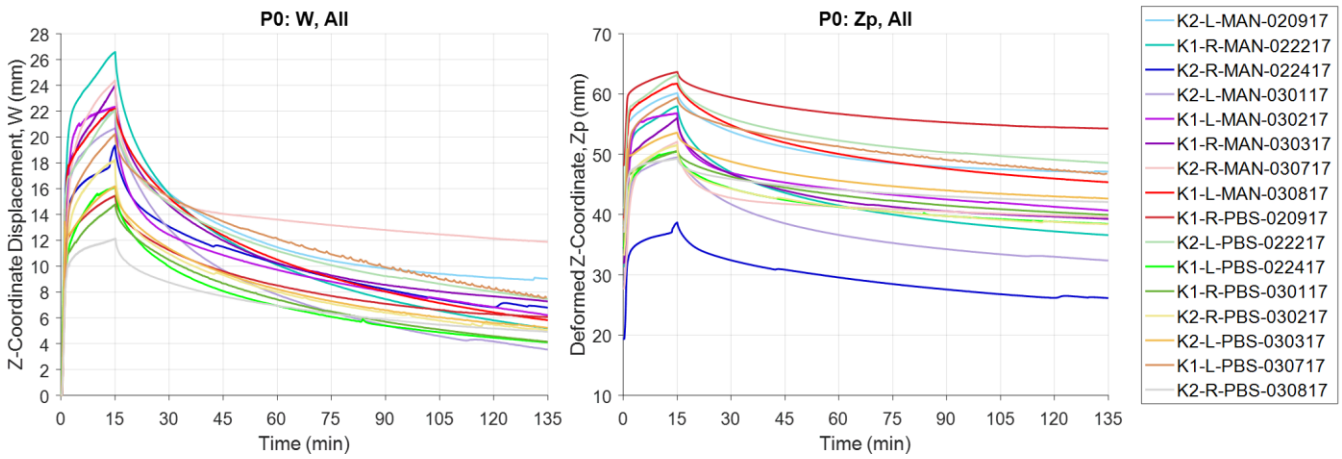

Figure 37. P0 (left) z-coordinate displacement and (right) deformed z-coordinate as a function of time for all kidneys. There is a sharp increase in W during the 15 minute perfusion interval followed by a steady decline during the interval without perfusion.

The results for P0 are displayed as a pair of plots in a single figure; the plot on the left is of measurements for all kidneys and the plot on the right is of the average PBS and mannitol measurements. For the plot containing all measurements, kidneys perfused with mannitol are located on the left side of the plot and kidneys perfused with PBS are located on the right side of the plot, divided by a red vertical line. The average measurements of kidneys perfused with mannitol and the average measurements of kidneys perfused with PBS are compared to evaluate how perfusate tonicity impacts renal swelling during perfusion. Statistical significance between the mannitol and PBS averages was calculated using the paired t-test. Statistical significance (p-value less than 0.05) is indicated by an asterisk. No statistical significance is indicated with "ns" for "not significant." Error bars are the 95% confidence interval calculated using the critical value, *t*, unless otherwise noted. The measurements collected for P0 (i.e., W, Zp, percent difference, percent increase, percent decrease) are shown in Figures 38-41.

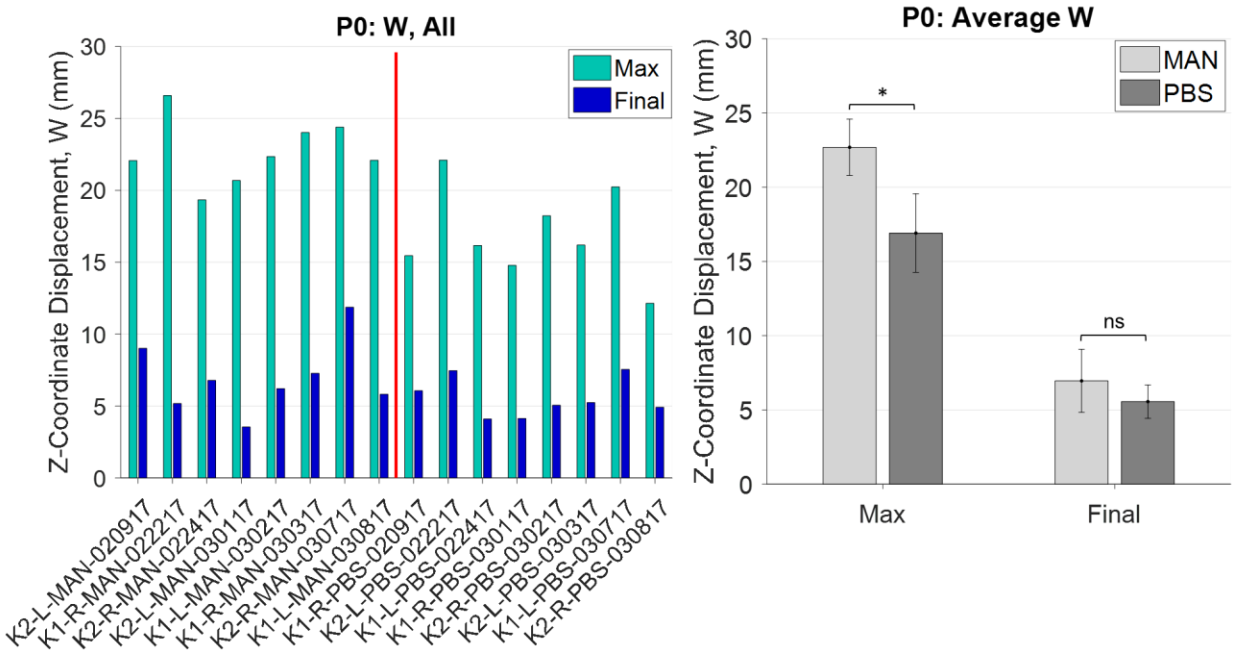

Figure 38. P0 z-coordinate displacement (W) for: (left) all kidneys and (right) mannitol and PBS averages. Mannitol and PBS yield statistically different z-coordinate displacements at the maximum data collection time but not at the final data collection time.

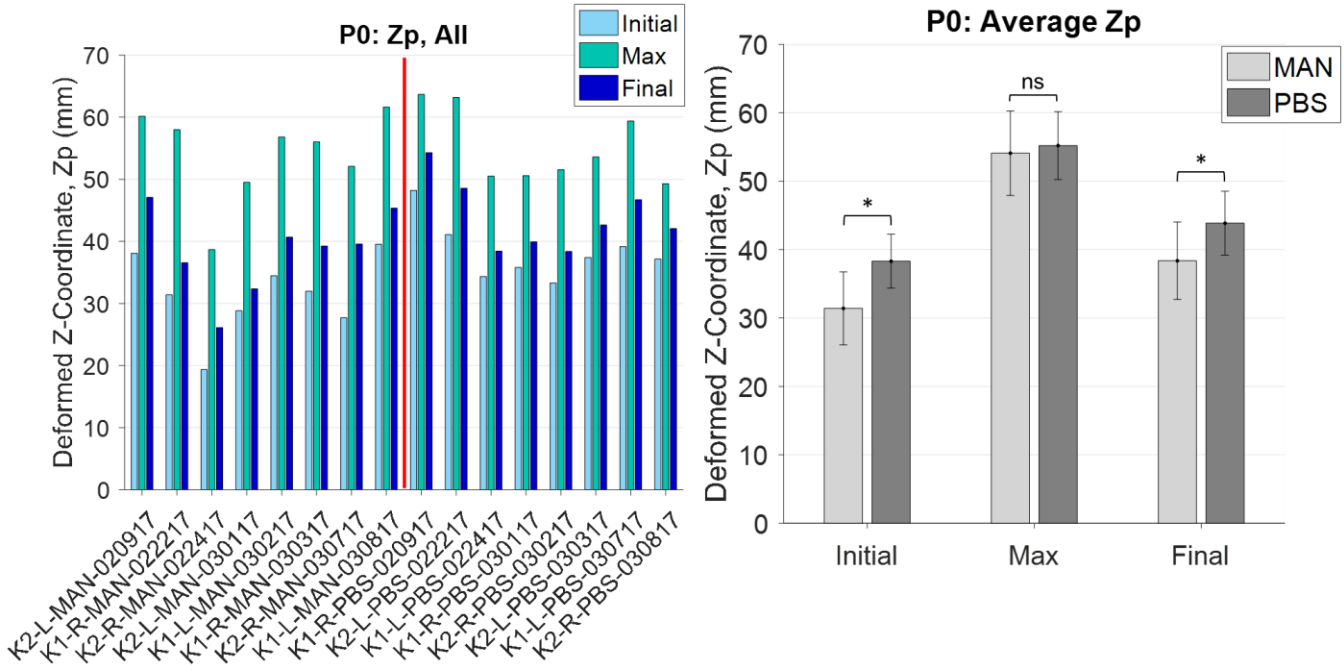

Figure 39. P0 deformed z-coordinate (Zp) for: (left) all kidneys and (right) mannitol and PBS averages. Mannitol and PBS yield statistically different deformed z-coordinates at the initial and final data collection times but not at the maximum data collection time.

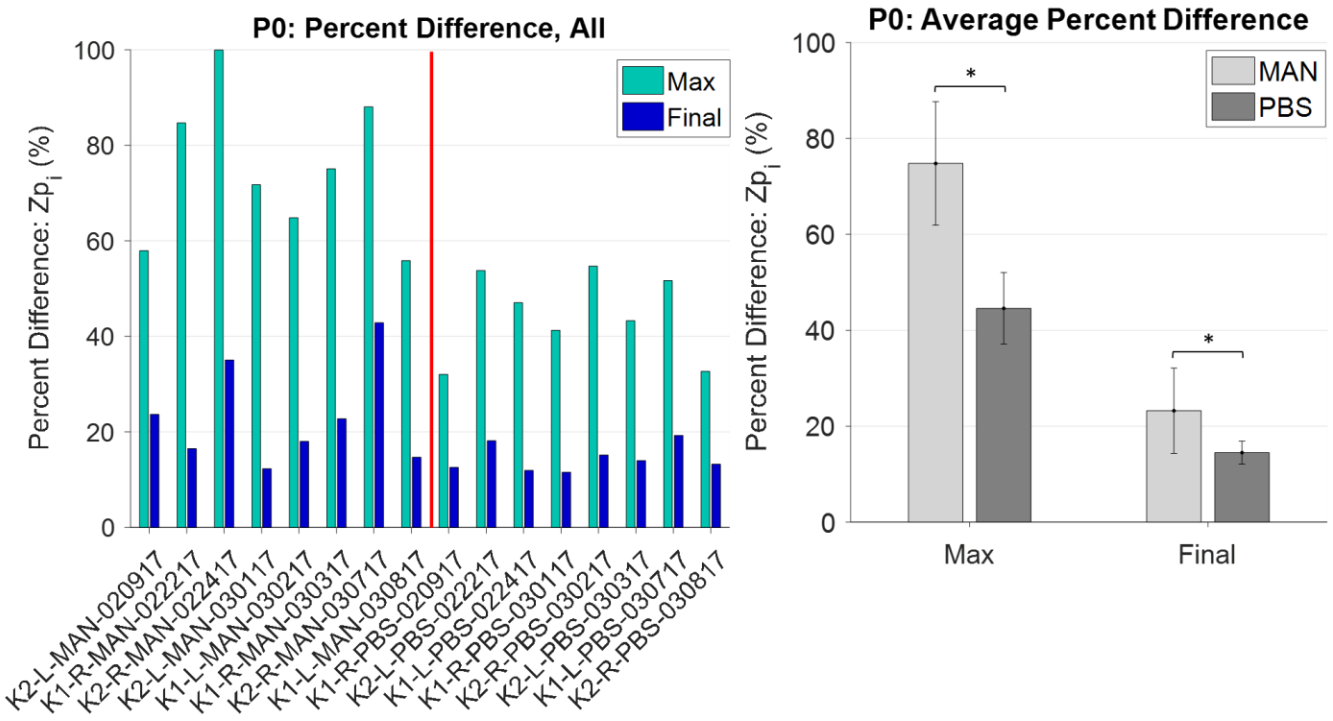

Figure 40. P0 percent difference for: (left) all kidneys and (right) mannitol and PBS averages. Mannitol and PBS yield statistically different percent differences at the maximum and final data collection times.

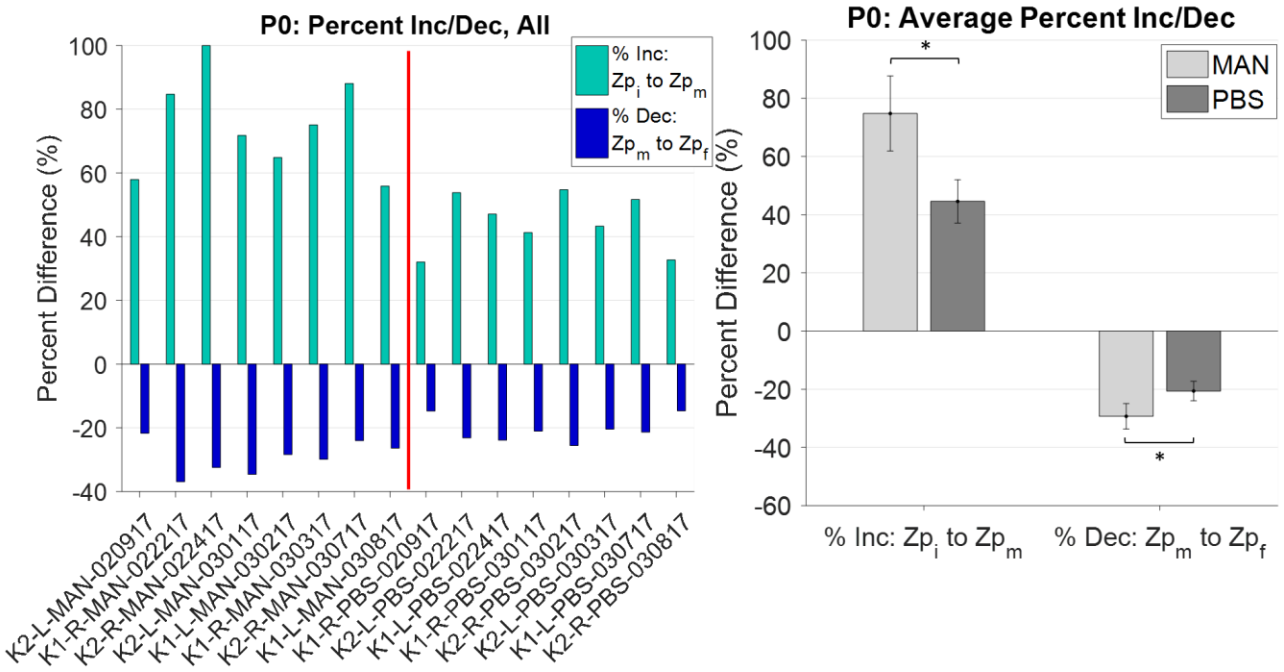

Figure 41. P0 percent increase/decrease for: (left) all kidneys and (right) mannitol and PBS averages. Mannitol and PBS yield statistically different percent increases/decreases.

At P0, kidneys perfused with mannitol have a larger maximum z-displacement than kidneys perfused with PBS and there is no difference in final z-displacement for mannitol and PBS. The presence of z-displacement at the final data collection time shows that the kidneys do not fully return to their original size; the machine perfused kidneys retained fluid. At P0, kidneys perfused with mannitol have a smaller initial and final deformed z-coordinate (smaller thickness) than kidneys perfused with PBS. However, there is no difference in the maximum deformed z-coordinate for mannitol and PBS. This suggests that there is a physical threshold for renal thickness (the renal capsule) for kidneys perfused at 120/100 mm Hg for 15 minutes, regardless of perfusate type. Additionally, the fact that the initial deformed z-coordinate is smaller for kidneys perfused with mannitol than kidneys perfused with PBS indicates that the initial flush at the abattoir impacts the kidney's morphology and its reaction/sensitivity to perfusion. Also, it is possible that the mannitol perfusate continues to act passively as the kidney is stored on ice (i.e., after the flush, perfusate within the vasculature 'passively' draws water out of the intracellular space).

At P0, kidneys perfused with mannitol have a greater percent difference between the initial and final deformed z-coordinate than kidneys perfused with PBS. So, while the PBS kidneys have a larger deformed z-coordinate, the final deformed z-coordinate is closer to the to the initial deformed z-coordinate than for kidneys perfused with mannitol. At P0, kidneys perfused with mannitol have a larger percent increase and percent decrease in the deformed z-coordinate, which indicates that the kidneys perfused with mannitol have a more elastic response to perfusion (i.e., they are more sensitive/willing to respond to perfusion). Conversely, the PBS kidneys have a smaller percent increase and percent decrease in the deformed z-coordinate, which indicates that the PBS kidneys do not respond structurally to perfusion as well as the mannitol kidneys do. The difference in response could be caused by edema present in the PBS kidneys since edema restricts perfusion.

4.2.2 Average method. The average measurement over the entire kidney surface was calculated for each collected image. Since P0 only shows trends at one location, it is important to additionally have a metric that incorporates data over the entire renal surface. Since the average is affected by data loss, kidneys from Experiments 02-22-17 and 03-08-17 were removed from the data analysis. As a note, percent differences in this section are calculated using the deformed z-coordinate.

The results for the 'average method' are displayed as a pair of plots in a single figure; the plot on the left is of measurements for all kidneys and the plot on the right is of the average PBS and mannitol measurements. For the plot containing all measurements, kidneys perfused with mannitol are located on the left side of the plot and kidneys perfused with PBS are located on the right side of the plot, divided by a red vertical line. The average measurements of kidneys perfused with mannitol and the average measurements of kidneys perfused with PBS are compared to evaluate how perfusate tonicity impacts renal swelling during perfusion. Statistical significance between the mannitol and PBS averages was calculated using the paired t-test. Statistical significance (p-value less than 0.05) is indicated by an asterisk. No statistical significance is indicated with "ns" for "not significant." Error bars are the 95% confidence

interval calculated using the critical value, *t*, unless otherwise noted. The measurements collected using the average method (i.e., W, Zp, percent difference, percent increase, percent decrease) are shown in Figures 42-45.

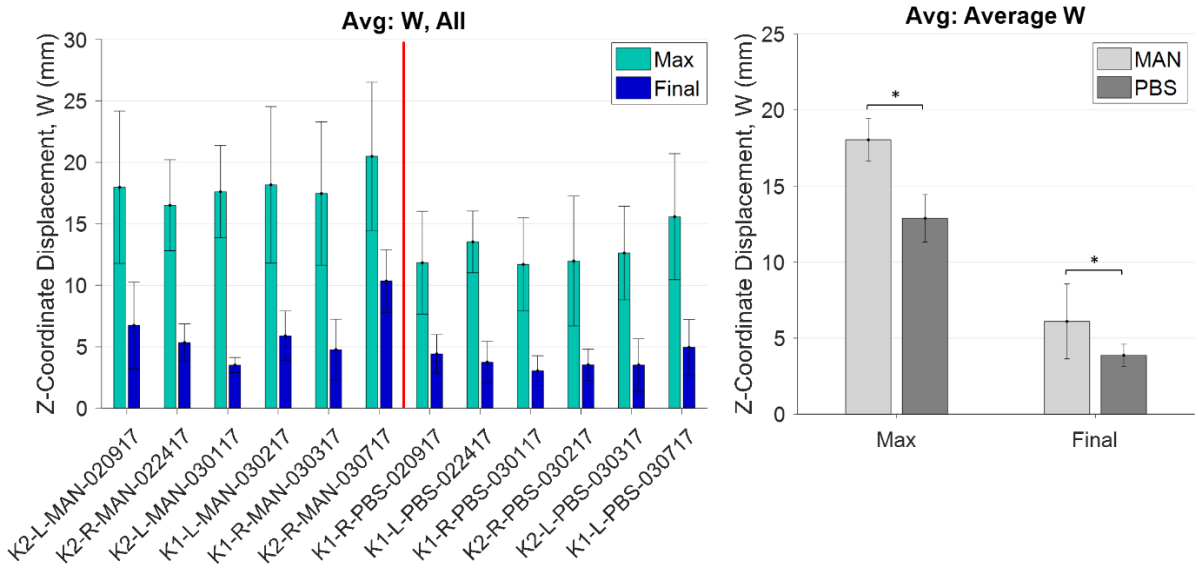

Figure 42. Average method z-coordinate displacement (W) for: (left) all kidneys and (right) mannitol and PBS averages. Mannitol and PBS yield statistically different z-coordinate displacements at the maximum and final data collection times. Error bars in the left plot are 2σ, where σ is the standard deviation; this shows the spread of the displacement data over the entire renal surface.

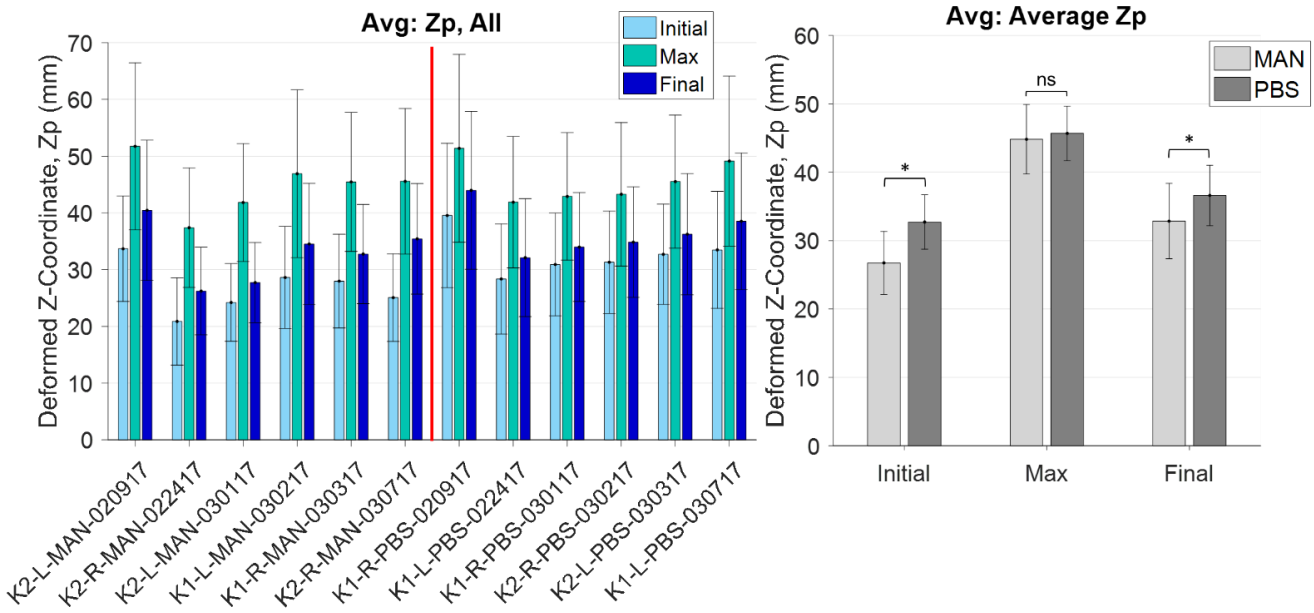

Figure 43. Average method deformed z-coordinate (Zp) for: (left) all kidneys and (right) mannitol and PBS averages. Mannitol and PBS yield statistically different deformed z-coordinates at the initial and final data collection times but not at the maximum data collection time. Error bars in the left plot are 2σ, where σ is the standard deviation; this shows the spread of the deformed z-coordinate data over the entire renal surface.

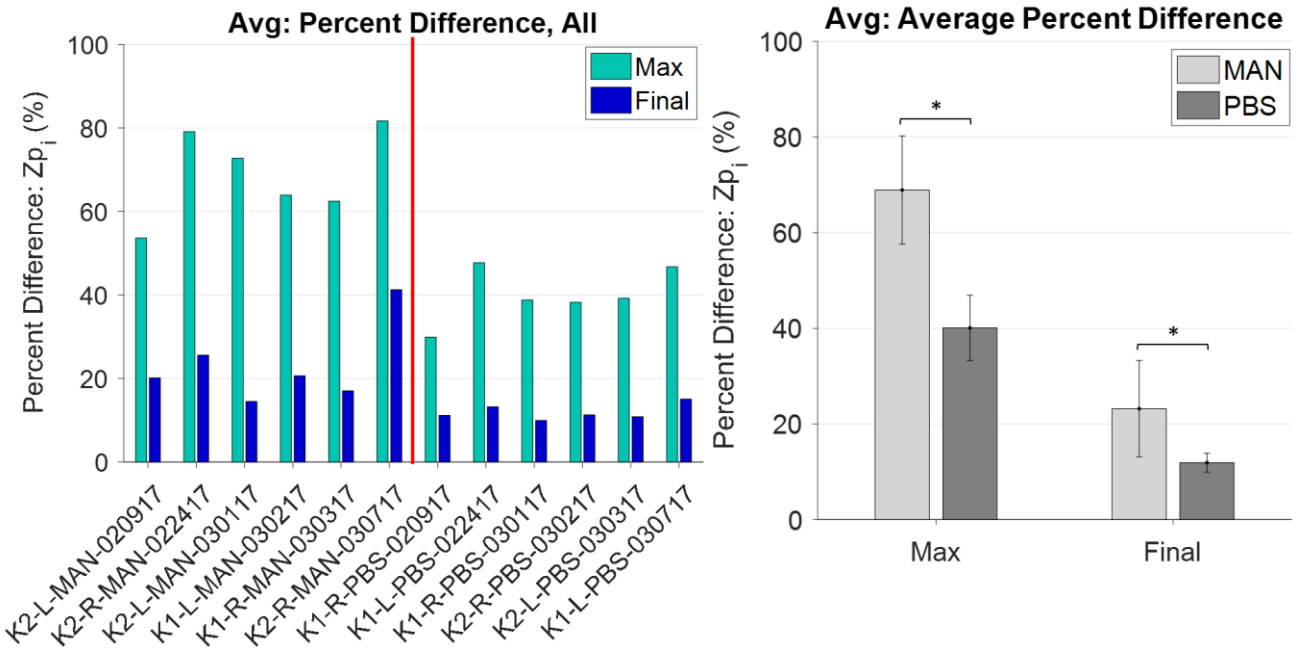

Figure 44. Average method percent difference for: (left) all kidneys and (right) mannitol and PBS averages. Mannitol and PBS yield statistically different percent differences at the maximum and final data collection times.

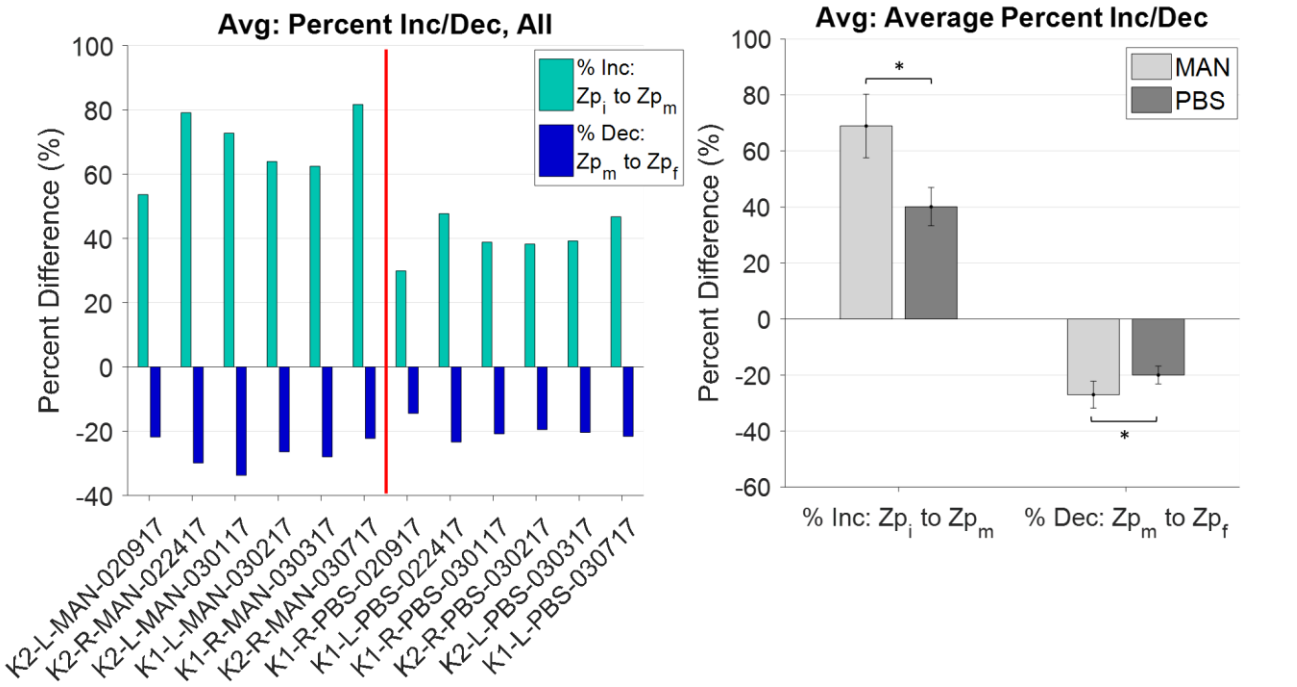

Figure 45. Average method percent increase/decrease for: (left) all kidneys and (right) mannitol and PBS averages. Mannitol and PBS yield statistically different percent increases/decreases.

For the average method, kidneys perfused with mannitol have larger maximum and final z-displacements than kidneys perfused with PBS. Otherwise, all of the trends for the average method are identical to those found from the analysis of P0 in the previous subsection. On average, kidneys perfused with mannitol have a lower initial and final deformed z-coordinate (thickness). However, there is no difference in the maximum deformed z-coordinate between kidneys perfused with mannitol and kidneys perfused with PBS. On average, kidneys perfused with mannitol have a larger percent difference between the initial and final deformed z-coordinate than kidneys perfused with PBS. On average, kidneys perfused with mannitol have a larger percent increase and percent decrease compared to kidneys perfused with PBS.

4.2.3 Volume estimation method. The renal volume was estimated by assuming each data point in 3D space was a rectangular prism; the volume was summed over all data points to determine the total estimated renal volume. Since volume is affected by data loss, kidneys from Experiments 02-22-17 and 03-08-17 were removed from the data analysis. As a note, percent differences in this section are calculated using volume.

The results of the estimated renal volume are displayed as a pair of plots in a single figure; the plot on the left is of measurements for all kidneys and the plot on the right is of the average PBS and mannitol measurements. For the plot containing all measurements, kidneys perfused with mannitol are located on the left side of the plot and kidneys perfused with PBS are located on the right side of the plot, divided by a red vertical line. The average measurements of kidneys perfused with mannitol and the average measurements of kidneys perfused with PBS are compared to evaluate how perfusate tonicity impacts renal swelling during perfusion. Statistical significance between the mannitol and PBS averages was calculated using the paired t-test. Statistical significance (p-value less than 0.05) is indicated by an asterisk. No statistical significance is indicated with “ns” for “not significant.” Error bars are the 95% confidence interval calculated using the critical value, *t*, unless otherwise noted. The measurements collected using the estimated renal volume method (i.e., volume, percent difference, percent increase, percent decrease) are shown in Figures 46-48.

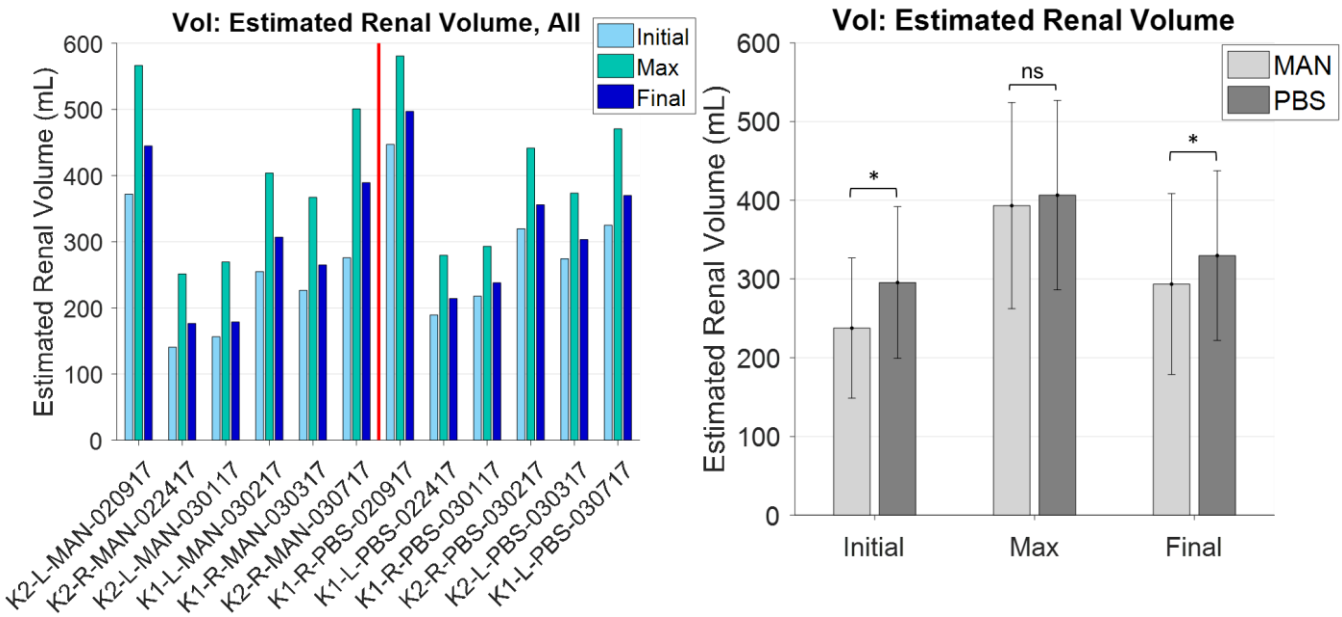

Figure 46. Estimated renal volume for: (left) all kidneys and (right) mannitol and PBS averages. Mannitol and PBS yield statistically different estimated renal volumes at the initial and final data collection times but not at the maximum data collection time.

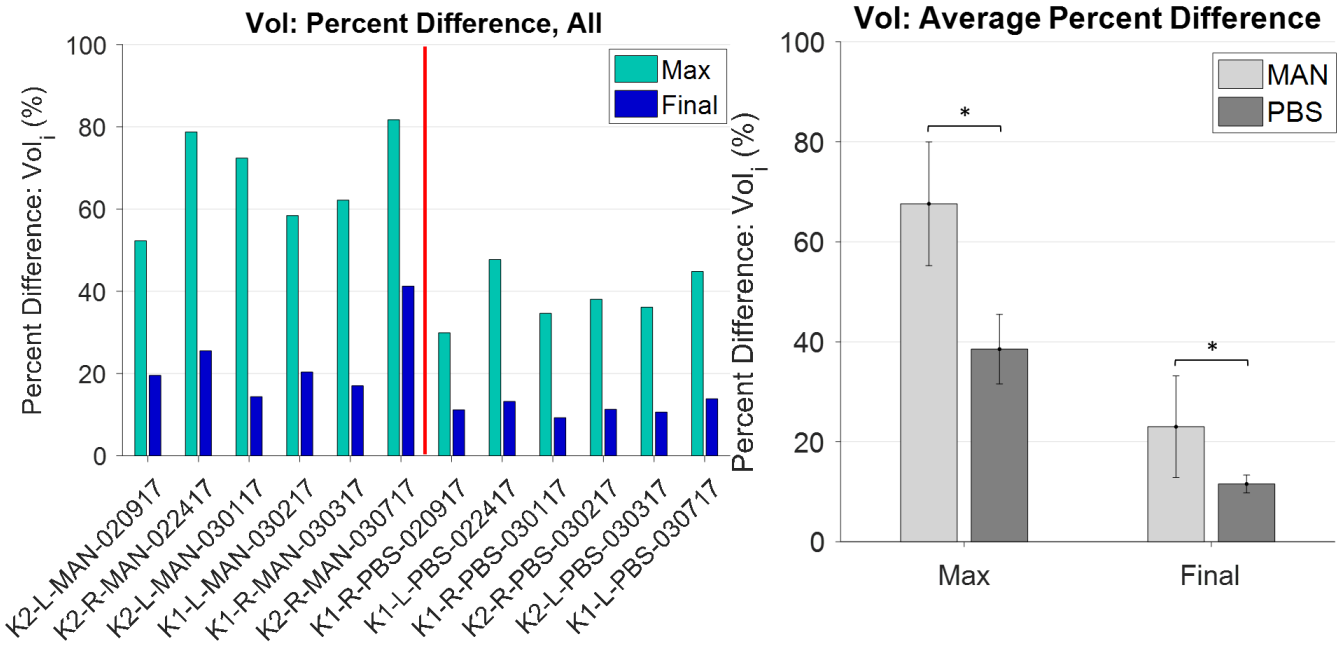

Figure 47. Estimated renal volume percent difference for: (left) all kidneys and (right) mannitol and PBS averages. Mannitol and PBS yield statistically different percent differences at the maximum and final data collection times.

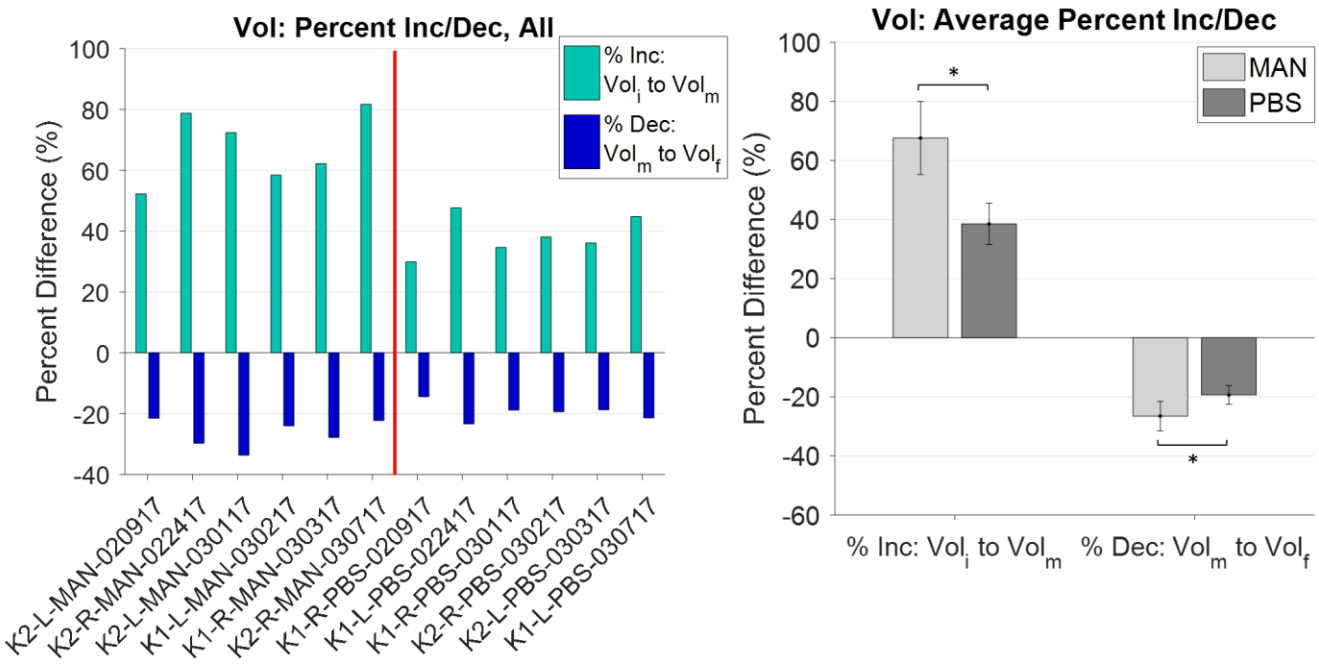

Figure 48. Estimated renal volume percent increase/decrease for: (left) all kidneys and (right) mannitol and PBS averages. Mannitol and PBS yield statistically different percent increases/decreases.

Kidneys perfused with mannitol have a smaller renal volume than kidneys perfused with PBS at the initial and final data collection times. However, there is no difference in the maximum volumes for kidneys perfused with mannitol and kidneys perfused with PBS. This suggests that there is a volume threshold (i.e., maximum capacity volume) that cannot be exceeded, regardless of perfusate type, at the last image during perfusion. Also, since the initial volume is smaller for kidneys perfused with mannitol than kidneys perfused with PBS, the initial flush at the abattoir impacts the initial renal volume.

Kidneys perfused with mannitol have a larger percent increase and percent decrease than kidneys perfused with PBS, which suggests that they are more sensitive to perfusion and can accommodate for structural changes during perfusion.

4.2.4 Maximum z-displacement (Wmax) tracking. The location of the maximum z-displacement (Wmax) was determined for each collected image and plotted within the data boundary to show where Wmax occurs relative to the renal anatomy. Two examples are shown in Figure 49 for the right and left kidneys in a pair (note, the right and left kidneys are mirror images of each other). All other plots are located in Appendix I. In addition to Wmax data points, each consecutive data point in time is linked with an arrow to show the direction of Wmax movement over the renal surface. The location of Wmax is important because it shows locations where the kidney is most significantly impacted structurally by perfusion. The data boundary does not show contour holes within the boundary.

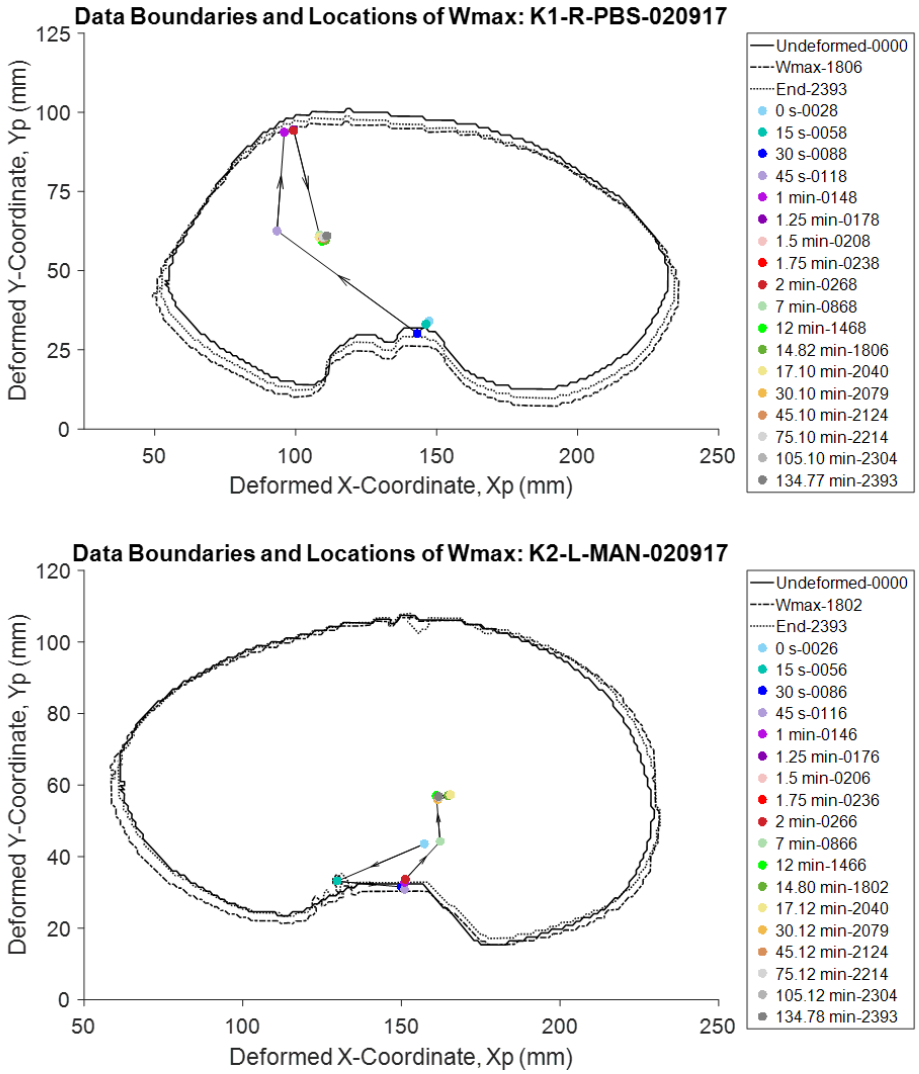

Figure 49. Maximum z-displacement tracking. The kidney pair from 02-09-17 is shown as an example; (top) the right kidney is perfused with PBS and (bottom) the left kidney is perfused with mannitol. The legend includes the data boundaries at the undeformed (initial), maximum (Wmax), and final (end) time points. Each Wmax data point corresponds to an elapsed time and the points are linked with directional arrows indicating transient movement. In the legend, the last four digits are the image number associated with the image collection time.

All boundary and Wmax locations plots are shown in Figure 50. These plots show the relative location of the maximum z-displacement with respect to the renal anatomy. Note that conclusions about the data boundaries' size should not be made; the plots have different scales. The displacement starts at the hilus for all kidneys and the majority of kidneys show translation of Wmax towards the center and/or lateral border. Three of eight PBS kidneys have maximum z-displacements that do not deviate from the hilus, suggesting that only relatively small displacements/expansion occurred over normal areas due to edema. Other than this, there are no trends that define the mannitol or PBS kidneys from one another; there are no distinct trends that separate the surface response by perfusate tonicity. The data boundary does expand / contract /

shift, so there are displacements in the xy-plane, but they are small compared to the displacement that occurs through the thickness.

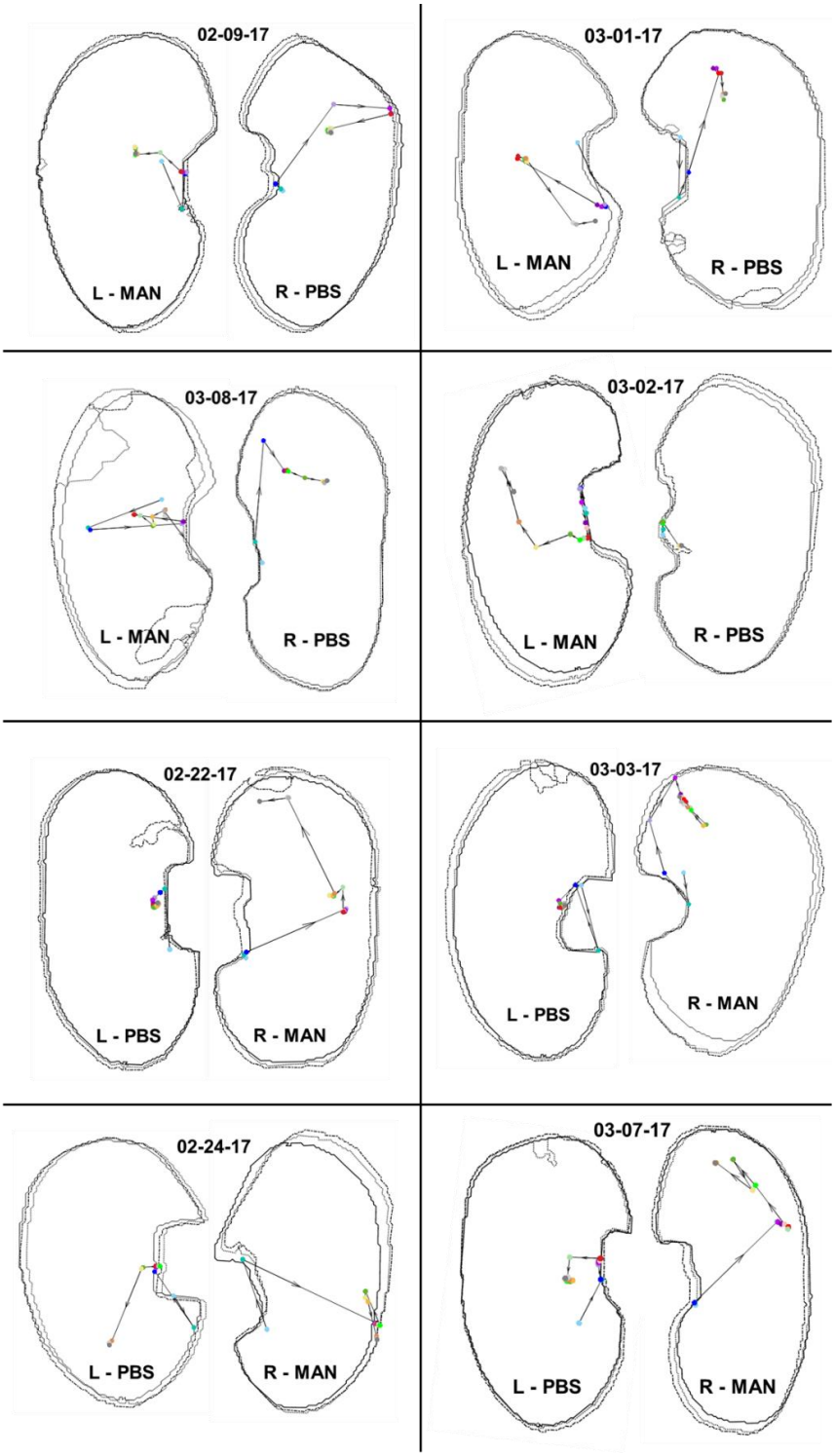

Figure 50. Maximum z-displacement tracking for all kidneys in the xy-plane. The maximum z-displacement at certain data collection times is shown, connected with transient vectors showing the direction of change. The cranial pole is at the top of each plot and the caudal pole is at the bottom.

4.2.5 Line slices. Line slices across the renal surface can aid in the visualization of the physical renal surface. Figures 51-53 show the comparison of all PBS and mannitol renal surfaces for the initial, maximum, and final images. In all L0 plots, the left kidneys are plotted as a mirror image so the orientation for cranial/caudal is the same for all kidneys regardless of the kidney side (right/left). The x-axis is translated to zero to have a common starting point. The position relative to kidney anatomy is written along the x-axis (cranial/caudal and hilus/lateral border). Mannitol kidneys are plotted with a solid line and PBS kidneys are plotted with a dashed line. The deformed z-coordinate is plotted as a function of Xp and Yp for L0 and L1, respectively. The deformed z-coordinate is the shape (thickness) of the kidney along the line slice. There is more variety in shape for L0 than L1, possibly because of cysts or other naturally occurring surface features. In Figure 51, most kidneys have large 'bumps' on the surface in L0, which is likely caused by the line slice being positioned near the maximum displacement, coupled with surface abnormalities. In Figure 52, the majority of kidneys have deformed z-coordinates in L1 that are higher at the hilus than the lateral border, suggesting that there is significant perfusion at the hilus. In Figure 53, the surface shapes that become apparent in L0 maximum are retained. Other than the height of the deformed z-coordinate plots, there are no significant differences present in the shape for kidneys perfused with mannitol and kidneys perfused with PBS.

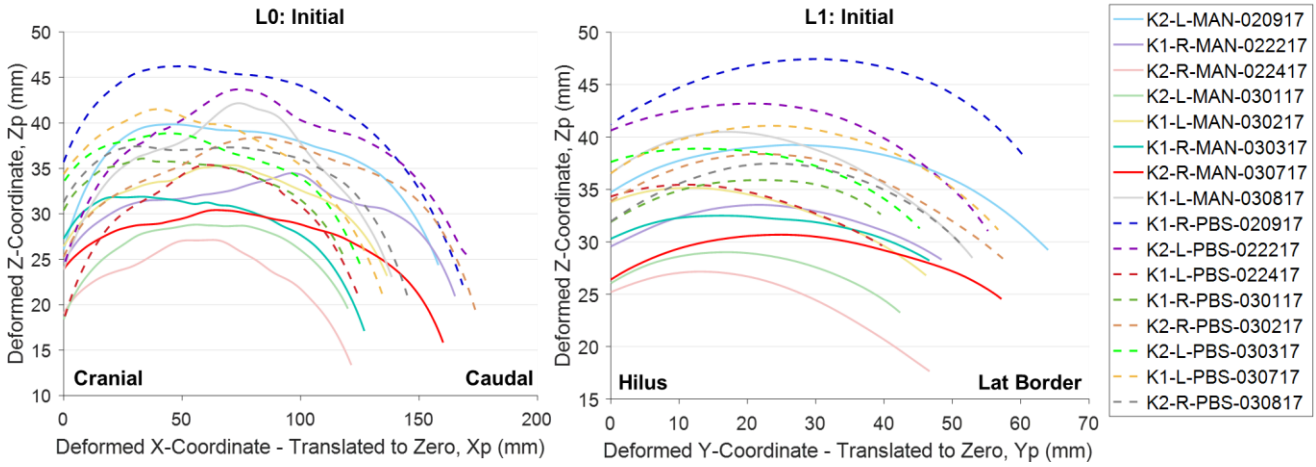

Figure 51. (Left) L0 and (right) L1 line slices at the initial collection time for all kidneys. For the most part, the PBS kidneys are 'larger' in thickness than the mannitol kidneys.

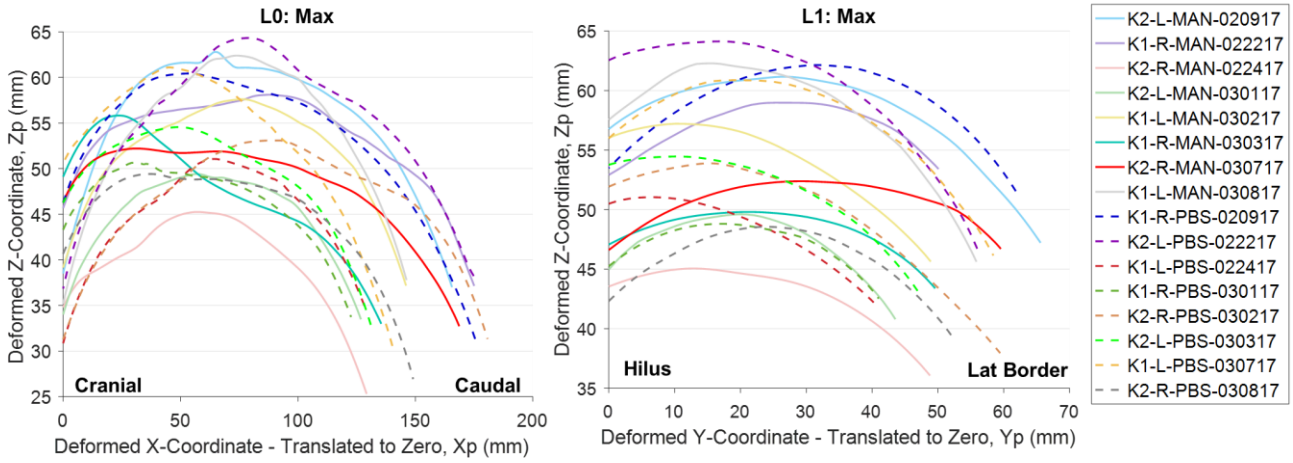

Figure 52. (Left) L0 and (right) L1 line slices at the maximum collection time for all kidneys. For the most part, the PBS kidneys are the same shape as the mannitol kidneys.

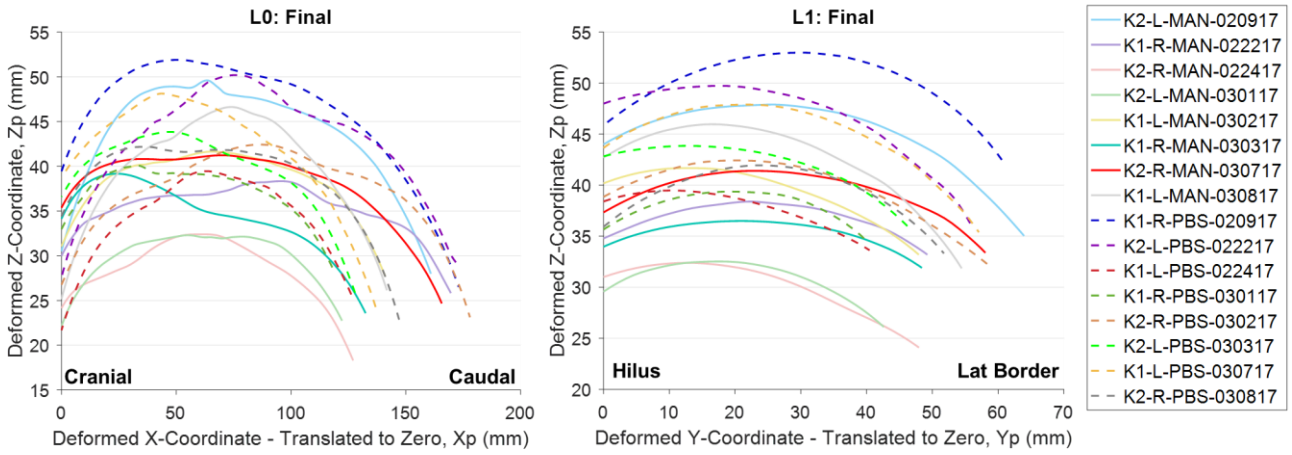

Figure 53. (Left) L0 and (right) L1 line slices at the final collection time for all kidneys. For the most part, the PBS kidneys are larger than the mannitol kidneys, but not to the same extent as was present in the initial collection time.

Chapter 5 - Conclusions

From these experiments and from this data, I can conclude that perfusate tonicity yields significantly different renal morphologies as a result of machine perfusion. While the magnitude of change in renal size (deformed z-coordinate, volume) is apparent due to perfusate tonicity, the way in which the kidneys swell (maximum z-displacement tracking) and their shape (line slices) do not appear to be affected by perfusate tonicity.

Average measurements of surface displacement (z-coordinate displacement) and size (deformed z-coordinate, volume) were used to describe renal morphology. Three different methods (i.e., point analysis, average analysis, and estimated volume analysis) yielded the same trends. Kidneys perfused with mannitol had a larger percent increase and percent decrease in size

(deformed z-coordinate, volume) during the perfusion and no perfusion intervals, respectively. This means that the kidneys perfused with mannitol have a more elastic response and are more responsive to perfusion. Kidneys perfused with mannitol also experienced larger changes in in size at the maximum collection time and they retained a larger final size compared to the initial size. Both kidneys perfused with mannitol and kidneys perfused with PBS did not fully return to their original size, indicating that fluid is retained during machine perfusion regardless of perfusate tonicity. Kidneys perfused with mannitol were smaller in size at the initial and final collection times than kidneys perfused with PBS. Additionally, maximum renal size was the same for kidneys perfused with mannitol and kidneys perfused with PBS. This suggests that regardless of perfusate type, there is a threshold, perhaps defined by renal capsule, which limits the amount of swelling that can occur. Also, it is very apparent that the initial flush performed shortly after procurement impacts renal size since mannitol kidneys are smaller than PBS kidneys at the initial data collection time. The maximum location of z-displacement, P0, showed the same trends as when the entire renal surface was used in the analysis. This suggests that the location of maximum z-displacement, which differs in location for each kidney, can act as a point that represents the entire kidney.

The movement of maximum z-displacement with respect to the renal anatomy during machine perfusion was variable for all kidneys; there were no patterns in the data other than 3 out of 8 kidneys perfused with PBS had maximum displacements that did not deviate from the hilus. Renal shape showed no significant differences between kidneys perfused with mannitol and kidneys perfused with PBS. This highlights one of the largest difficulties to tackle when working with biological tissues: there is extreme heterogeneity in the sample population. Even for the same kidney pair, the relative size is similar (prior to perfusion) but the renal shapes are quite different, which is most likely caused by differing supportive environments *in vivo*.

The osmolality and Raman measurements collected from the renal fluids (filtrate, venous outflow) assisted in understanding how the kidneys interact with the perfusate stream. Osmolality measurements of the renal fluids for PBS and mannitol both on average trended towards the control osmolality during the perfusion interval. This suggests that during the 15 minute machine perfusion interval the kidneys were still actively being flushed (i.e., there were biological fluids still present within the vasculature); the osmolality measurements collected at the beginning of perfusion are on average most different from the control osmolality. The Raman measurements proved that the kidneys were still functional during the machine perfusion interval since there was mannitol (osmotic agent) present in the ureter discharge (i.e., filtrate).

Specimen biopsies were used to understand how perfusate tonicity impacts the kidneys at the cellular level. There are distinct differences between the histologic changes that manifest from perfusion with PBS and perfusion with the mannitol solution. Kidneys perfused with PBS tended to have more instances of acute tubular necrosis and vacuolation; both are associated with cell swelling. However, kidneys perfused with the mannitol solution showed definite signs of lumen tubule dilation and epithelial cell shrinkage; both are associated with cell dehydration. These biopsy results correlate well the DIC measurements. Kidneys perfused with PBS showed signs of edema due to a limited range of motion captured with DIC. Additionally, kidneys

perfused with mannitol went through a larger range of motion measured with DIC when the cells were essentially dehydrated. This means that the surface measurements collected for the kidneys perfused with mannitol show swelling due to fluid reintroduction and drainage; whereas kidneys perfused with PBS show swelling due to fluid reintroduction and drainage for edematous tissue.

There are obvious limitations to this study, most importantly being the short perfusion interval (15 minutes). The perfusion interval was limited due to excessive surface wetting, which impacts DIC image collection. Thus, the conclusions from this thesis can only be applied to kidneys that are perfused for a short period of time. However, the short perfusion interval also highlights how quickly/how short of a time interval is needed to create conditions within the kidney that create a permanent deformation (even after 120 minutes without perfusion). Also, the size measurements (deformed z-coordinate, volume) at the initial data collection time are still relevant, regardless of the perfusion interval. The impact of perfusate type on the organ flush is quite apparent. Even with long ischemic intervals (see Appendix D) there is still a statistically significant difference between the kidneys perfused with mannitol and those perfused with PBS. It would be interesting to conduct a series of experiments that measured surface displacement over a typical perfusion interval of at least 12 hours. This would require the development of a different experimental procedure that mitigates surface wetting. Additionally, it would be beneficial to use a perfusion system with automatically adjusting flow rates. With the peristaltic pump, the flow was set in the first two minutes and not re-adjusted; changes in the renal resistance were allowed to change the pressure. A system with the capability to adjust the flow rate to maintain a systolic/diastolic pressure would be desired.

References

[1] Overbeck, I., Bartels, M., Decker, O., Harms, J., Hauss, J., and Fangmann, J., 2005, "Changes in Quality of Life After Renal Transplantation," Transplant. Proc., **37**, pp. 1618–1621.

[2] Wolfe, R. A., Ashby, V. B., Milford, E. L., Ojo, A., Ettenger, R. E., Agodoa, L. Y. C., Held, P. J., and Port, F. K., 1999, "Comparison of Mortality in All Patients on Dialysis, Patients on Dialysis Awaiting Transplantation, and Recipients of a First Cadaveric Transplant," N. Engl. J. Med., **341**(23), pp. 1725–1730.

[3] Lee, C. Y., and Mangino, M. J., 2009, "Preservation methods for kidney and liver," Organogenesis, **5**(3), pp. 105–12.

[4] Organ Procurement and Transplantation Network, 2014, "The New Kidney Allocation System: Resources for Protocols and Processes."

[5] Rao, P. S., and Ojo, A., 2009, "The Alphabet Soup of Kidney Transplantation: SCD, DCD, ECD - Fundamentals for the Practicing Nephrologist," Clin. J. Am. Soc. Nephrol., **4**, pp. 1827–1831.

[6] Guibert, E. E., Petrenko, A. Y., Balaban, C. L., Somov, A. Y., Rodriguez, J. V., and Fuller, B. J., 2011, "Organ preservation: Current Concepts and New Strategies for the Next Decade," Transfus. Med. Hemotherapy, **38**, pp. 125–142.

[7] Shi, S., and Xue, F., 2016, "Current Antioxidant Treatments in Organ Transplantation," Oxid. Med. Cell. Longev., **2016**.

[8] Thuluvath, P. J., Guidinger, M. K., Fung, J. J., Johnson, L. B., Rayhill, S. C., and Pelletier, S. J., 2010, "Liver transplantation in the United States, 1999-2008," Am. J. Transplant., **10**(Part 2), pp. 1003–1019.

[9] Organ Procurement and Transplantation Network, "How Organ Allocation Works" [Online]. Available: https://optn.transplant.hrsa.gov/learn/about-transplantation/how-organ-allocation-works/. [Accessed: 19-Apr-2016].

[10] Fuller, B. J., and Lee, C. Y., 2007, "Hypothermic perfusion preservation: The future of organ preservation revisited?," Cryobiology, **54**, pp. 129–145.

[11] Jochmans, I., Moers, C., Smits, J. M., Leuvenink, H. G. D., Treckmann, J., Paul, A., Rahmel, A., Squifflet, J. P., Van Heurn, E., Monbaliu, D., Ploeg, R. J., and Pirenne, J., 2011, "The Prognostic Value of Renal Resistance During Hypothermic Machine Perfusion of Deceased Donor Kidneys," Am. J. Transplant., **11**, pp. 2214–2220.

[12] Tojimbara, T., Wicomb, W. N., Garcia-Kennedy, R., Burns, W., Hayashi, M., Collins, G., and Esquivel, C. O., 1997, "Liver Transplantation From Non-Heart Beating Donors in Rats: Influence of Viscosity and Temperature of Initial Flushing Solutions on Graft Function.," Liver Transplant. Surg., **3**(1), pp. 39–45.

[13] Wszola, M., Kwiatkowski, A., Diuwe, P., Domagała, P., Górski, L., Kieszek, R., Berman, A., Perkowska-Ptasińska, A., Durlik, M., Pączek, L., and Chmura, A., 2013, "One-year results of a prospective, randomized trial comparing two machine perfusion devices used

for kidney preservation," Transpl. Int., **26**, pp. 1088–1096.

[14] Lindell, S. L., Muir, H., Brassil, J., and Mangino, M. J., 2013, "Hypothermic Machine Perfusion Preservation of the DCD Kidney: Machine Effects," J. Transplant., **2013**(8), pp. 1–7.

[15] Jochmans, I., O'Callaghan, J. M., Pirenne, J., and Ploeg, R. J., 2015, "Hypothermic machine perfusion of kidneys retrieved from standard and high-risk donors," Transpl. Int., **28**, pp. 665–676.

[16] Yuan, X., Theruvath, A. J., Ge, X., Floerchinger, B., Jurisch, A., García-Cardeña, G., and Tullius, S. G., 2010, "Machine perfusion or cold storage in organ transplantation: Indication, mechanisms, and future perspectives," Eur. Soc. Organ Transplant., **23**, pp. 561–570.

[17] Metzger, R. a, Delmonico, F. L., Feng, S., Port, F. K., Wynn, J. J., and Merion, R. M., 2003, "Expanded criteria donors for kidney transplantation," Am. J. Transplant., **3**(Suppl. 4), pp. 114–125.

[18] Moers, C., Smits, J. M., Maathuis, M.-H. J., Treckmann, J., van Gelder, F., Napieralski, B. P., van Kasterop-Kutz, M., Homan van der Heide, J. J., Squifflet, J.-P., van Heurn, E., Kirste, G. R., Rahmel, A., Leuvenink, H. G. D., Paul, A., Pirenne, J., and Ploeg, R. J., 2009, "Machine Perfusion or Cold Storage in Deceased-Donor Kidney Transplantation," N. Engl. J. Med., **360**(1), pp. 7–19.

[19] "2007 Annual Report of the U.S. Organ Procurement and Transplantation Network and the Scientific Registry of Transplant Recipients: Transplant Data 1997-2006."

[20] Chandran, K. B., Rittgers, S. E., and Yoganathan, A. P., 2012, Biofluid Mechanics: The Human Circulation, CRC Press, Boca Raton.

[21] Collins, G. M., Bravo-Shugarman, M., and Terasaki, P. I., 1969, "Kidney Preservation for Transportation: Initial Perfusion and 30 Hours' Ice Storage," Lancet, **294**(7632), pp. 1219–1222.

[22] Ploeg, R., Goossens, D., McAnulty, J., Southard, J., and Belzer, F., 1988, "Successful 72-hour cold storage of dog kidneys with UW solution," Transplantation, **46**(2), pp. 191–196.

[23] Ploeg, R. J., Hajo van Bockel, J., Langendijk, P. T. H., Groenewegen, M., Van der Woude, F. J., Persijn, G. G., Thorogood, J., and Hermans, J., 1992, "Effect of preservation solution on results of cadaveric kidney transplantation," Lancet, **340**(8812), pp. 328–337.

[24] Agarwal, A., Murdock, P., and Fridell, J. a, 2006, "Comparison of Histidine-Tryptophan Ketoglutarate Solution and University of Wisconsin Solution in Prolonged Cold Preservation of Kidney Allografts," Transplantation, **81**(3), pp. 480–482.

[25] Caon, M., 2008, "Osmoles, osmolality and osmotic pressure: Clarifying the puzzle of solution concentration," Contemp. Nurse, **29**(1), pp. 92–99.

[26] Pearson Education, "Concept 2 Review: Isotonic, Hypotonic, and Hypertonic Solutions" [Online]. Available: http://www.phschool.com/science/biology_place/biocoach/biomembrane1/solutions.html.

[Accessed: 16-Apr-2017].

[27] Scallan, J., Huxley, V., and Korthuis, R., 2010, "Pathophysiology of Edema Formation," Capillary Fluid Exchange: Regulation, Functions, and Pathology, Morgan & Claypool Life Sciences, San Rafael, CA.

[28] Warner, L., Yin, M., Glaser, K. J., Woollard, J. a, Carrascal, C. a, Korsmo, M. J., Crane, J. a, Ehman, R. L., and Lerman, L. O., 2011, "Noninvasive In Vivo Assessment of Renal Tissue Elasticity During Graded Renal Ischemia Using MR Elastography," Invest. Radiol., **46**(8), pp. 509–514.

[29] Helfenstein, C., Gennisson, J.-L., Tanter, M., and Beillas, P., 2015, "Effects of pressure on the shear modulus, mass and thickness of the perfused porcine kidney," J. Biomech., **48**(1), pp. 30–37.

[30] Loss, J., Drewitz, K. P., Schlitt, H. J., and Loss, M., 2013, "Accept or refuse? Factors influencing the decision-making of transplant surgeons who are offered a pancreas: results of a qualitative study," BMC Surg., **13**(1).

[31] Wolfe, R. a., LaPorte, F. B., Rodgers, a. M., Roys, E. C., Fant, G., and Leichtman, a. B., 2007, "Developing Organ Offer and Acceptance Measures: When 'Good' Organs Are Turned Down," Am. J. Transplant., **7**(Part 2), pp. 1404–1411.

[32] Libertiaux, V., Pascon, F., and Cescotto, S., 2011, "Experimental verification of brain tissue incompressibility using digital image correlation," J. Mech. Behav. Biomed. Mater., **4**(7), pp. 1177–1185.

[33] Siebert, T., Becker, T., Spiltthof, K., Neumann, I., and Krupka, R., 2007, "High-speed digital image correlation: error estimations and applications," Opt. Eng., **46**(5), p. 051004:1-7.

[34] Sutton, M. A., 2008, "Digital Image Correlation for Shape and Deformation Measurements," Springer Handbook of Experimental Solid Mechanics, W.N. Sharpe, ed., Springer, pp. 565–600.

[35] Correlated Solutions, 2016, "Vic-3D v7: Reference Manual."

[36] Lecompte, D., Smits, a., Bossuyt, S., Sol, H., Vantomme, J., Van Hemelrijck, D., and Habraken, a. M., 2006, "Quality assessment of speckle patterns for digital image correlation," Opt. Lasers Eng., **44**, pp. 1132–1145.

[37] Correlated Solutions, 2016, "Subset, Step Size and Strain Filter Selection" [Online]. Available: http://www.correlatedsolutions.com/support/index.php?/Knowledgebase/Article/View/10/1/subset-step-size-and-strain-filter-selection. [Accessed: 14-Apr-2017].

[38] Pan, B., Xie, H., and Wang, Z., 2010, "Equivalence of digital image correlation criteria for pattern matching," Appl. Opt., **49**(28), pp. 5501–5509.

[39] Correlated Solutions, 2016, "Minimizing Noise and Bias in 3D DIC."

[40] Correlated Solutions, 2016, "Resolution and Accuracy" [Online]. Available:

http://www.correlatedsolutions.com/support/index.php?/Knowledgebase/Article/View/8/1/resolution-and-accuracy. [Accessed: 14-Apr-2017].

[41] Lionello, G., Sirieix, C., and Baleani, M., 2014, "An effective procedure to create a speckle pattern on biological soft tissue for digital image correlation measurements," J. Mech. Behav. Biomed. Mater., **39**, pp. 1–8.

[42] Wilson, A. J., Chin, B. C., Hsu, V. M., Mirzabeigi, M. N., and Percec, I., 2015, "Digital Image Correlation: A Novel Dynamic Three-Dimensional Imaging Technique for Precise Quantification of the Dynamic Rhytid and Botulinum Toxin Type A Efficacy," Plast. Reconstr. Surg., **135**(5), p. 869e–876e.

[43] Zhang, D., Eggleton, C. D., and Arola, D. D., 2002, "Evaluating the Mechanical Behavior of Arterial Tissue using Digital Image Correlation," Exp. Mech., **42**, pp. 409–416.

[44] Gao, Z., Lister, K., and Desai, J., 2010, "Constitutive Modeling of Liver Tissue: Experiment and Theory," Ann. Biomed. Eng., **38**(2), pp. 505–516.

[45] U.S. National Library of Medicine, 2011, "MANNITOL- mannitol injection, solution," Dly. Med [Online]. Available: https://dailymed.nlm.nih.gov/dailymed/drugInfo.cfm?setid=74e9108e-8540-4442-82bc-4f46c6bdd334. [Accessed: 17-Apr-2017].

[46] de Veij, M., Vandenabeele, P., De Beer, T., Remon, J. P., and Moens, L., 2009, "Reference database of Raman spectra of pharmaceutical excipients," J. Raman Spectrosc., **40**, pp. 297–307.

Appendices

Appendix A: Phosphate Buffered Solution (PBS) Recipe

The recipe for 1X PBS used for machine perfusion is shown in Table A1. All reagents were added to 1.0 L of RO water.

Table A1: PBS recipe (1X stock)

Reagent	Amount to add (g)
NaCl	8.00
KCl	0.20
Na_2HPO_4	1.44
KH_2PO_4	0.24
$CaCl_2$ $2H_2O$	0.133
$MgCl_2$ $6H_2O$	0.10

Appendix B: Perfusate pH

The measured perfusate pH for each experiment date is shown in Table B1. The target pH for PBS is 7.4. All measurements were collected of chilled (i.e., refrigerated) perfusate.

Table B1: PBS and mannitol pH

Experiment Date	PBS pH	Mannitol pH
02-09-17	7.41	7.32
03-08-17	7.45	7.35
02-22-17	7.44	7.35
02-24-17	7.43	7.35
03-01-17	7.43	7.33
03-02-17	7.44	7.33
03-03-17	7.43	7.33
03-07-17	7.45	7.36

Appendix C: DIC Calibration Scores

The calibration score for each experiment date is shown in Table C1. A calibration is considered satisfactory if the calibration score is less than 0.05 pixels.

Table C1: Calibration scores

Experiment Date	Calibration Score (pixels)
02-09-17	0.037
03-08-17	0.029
02-22-17	0.025
02-24-17	0.029
03-01-17	0.031
03-02-17	0.029
03-03-17	0.027
03-07-17	0.027

Appendix D: Cold Storage Intervals

The cold storage interval for each experiment is shown in Table D1. The cold storage interval is the elapsed time between procurement and the start of machine perfusion. Procurement was 7:15 AM for all kidneys.

Table D1: Ischemic interval

Experiment Date	Kidney Sample ID	Ischemic Interval (h)
02-09-17	K1-R-PBS-020917	11.0
	K2-L-MAN-020917	14.5
03-08-17	K1-L-MAN-030817	8.75
	K2-R-PBS-030817	11.75
02-22-17	K1-R-MAN-022217	10.5
	K2-L-PBS-022217	13.5
02-24-17	K1-L-PBS-022417	10.25
	K2-R-MAN-022417	13.0
03-01-17	K1-R-PBS-030117	10.0
	K2-L-MAN-030117	12.75
03-02-17	K1-L-MAN-030217	8.25
	K2-R-PBS-030217	11.25
03-03-17	K1-R-MAN-030317	9.0
	K2-L-PBS-030317	12.0
03-07-17	K1-L-PBS-030717	9.25
	K2-R-MAN-030717	12.5

Appendix E: Perfusion Pressure

The initial and final perfusion pressures (systolic/diastolic) are shown in Table E1. The pressure along with the peristaltic pump RPMs are listed. A change in pump RPMs indicate that there was a large increase in pressure and the RPMs had to be changed. This occurred for four kidneys: K1-L-PBS-022417, K1-R-PBS-030117, K2-L-MAN-030117, and K1-L-MAN-030217.

Table E1: Initial and final perfusion pressures

Experiment Date	Kidney Sample ID	Initial Pressure [sys/dia] (mm Hg)	Final Pressure [sys/dia] (mm Hg)
02-09-17	K1-R-PBS-020917	123/113 @ 10 RPM	134/119 @ 10 RPM
	K2-L-MAN-020917	125/109 @ 12 RPM	142/129 @ 12 RPM
03-08-17	K1-L-MAN-030817	120/106 @ 8 RPM	124/106 @ 8 RPM
	K2-R-PBS-030817	115/93 @ 6 RPM	106/76 @ 6 RPM
02-22-17	K1-R-MAN-022217	115/109 @ 34 RPM	122/113 @ 34 RPM
	K2-L-PBS-022217	121/116 @ 16 RPM	123/118 @ 16 RPM
02-24-17	K1-L-PBS-022417	126/105 @ 10 RPM	137/120 @ 8 RPM
	K2-R-MAN-022417	120/99 @ 15 RPM	127/108 @ 15 RPM
03-01-17	K1-R-PBS-030117	124/108 @ 5 RPM	138/126 @ 4 RPM
	K2-L-MAN-030117	123/108 @ 8 RPM	131/121 @ 6 RPM
03-02-17	K1-L-MAN-030217	104/97 @ 28 RPM	103/95 @ 26 RPM
	K2-R-PBS-030217	114/100 @ 16 RPM	112/99 @ 16 RPM
03-03-17	K1-R-MAN-030317	122/107 @ 14 RPM	136/122 @ 14 RPM
	K2-L-PBS-030317	118/101 @ 6 RPM	132/118 @ 6 RPM
03-07-17	K1-L-PBS-030717	118/104 @ 12 RPM	125/112 @ 12 RPM
	K2-R-MAN-030717	111/92 @ 20 RPM	108/98 @ 20 RPM

Appendix F: Statistical Significance p-values

P-values for all three analysis types (P0, average, estimated volume) are in Table F1, Table F2, and Table F3, respectively.

Table F1: P-values for P0

P0 Parameter	Null Hypothesis (H_0)	Alternative Hypothesis (H_a)	p-value	Conclusion (Reject H_0 if p-value < 0.05)
Max W	$\delta = 0$	$\delta > 0$	<0.0001*	MAN > PBS
Final W	$\delta = 0$	$\delta > 0$	0.0510	MAN = PBS
Initial Zp	$\delta = 0$	$\delta < 0$	0.0074*	MAN < PBS
Max Zp	$\delta = 0$	$\delta \neq 0$	0.6936	MAN = PBS
Final Zp	$\delta = 0$	$\delta < 0$	0.0165*	MAN < PBS
Max Per Diff	$\delta = 0$	$\delta > 0$	0.0001*	MAN > PBS
Final Per Diff	$\delta = 0$	$\delta > 0$	0.0210*	MAN > PBS
Per Inc	$\delta = 0$	$\delta > 0$	0.0001*	MAN > PBS
Per Dec	$\delta = 0$	$\delta < 0$	0.0004*	MAN < PBS

Table F2: P-values for average method

Avg Parameter	Null Hypothesis (H_0)	Alternative Hypothesis (H_a)	p-value	Conclusion (Reject H_0 if p-value < 0.05)
Max W	$\delta = 0$	$\delta > 0$	<0.0001*	MAN > PBS
Final W	$\delta = 0$	$\delta > 0$	0.0119*	MAN > PBS
Initial Zp	$\delta = 0$	$\delta < 0$	0.0004*	MAN < PBS
Max Zp	$\delta = 0$	$\delta \neq 0$	0.4999	MAN = PBS
Final Zp	$\delta = 0$	$\delta < 0$	0.0039*	MAN < PBS

Max Per Diff	$\delta = 0$	$\delta > 0$	<0.0001*	MAN > PBS
Final Per Diff	$\delta = 0$	$\delta > 0$	0.0082*	MAN > PBS
Per Inc	$\delta = 0$	$\delta > 0$	<0.0001*	MAN > PBS
Per Dec	$\delta = 0$	$\delta < 0$	0.0035*	MAN < PBS

Table F3: P-values for estimated volume

Vol Parameter	**Null Hypothesis (H_0)**	**Alternative Hypothesis (H_a)**	**p-value**	**Conclusion (Reject H_0 if p-value < 0.05)**
Initial Vol	$\delta = 0$	$\delta < 0$	<0.0001*	MAN < PBS
Max Vol	$\delta = 0$	$\delta \neq 0$	0.2309	MAN = PBS
Final Vol	$\delta = 0$	$\delta < 0$	0.0131*	MAN < PBS
Max Per Diff	$\delta = 0$	$\delta > 0$	<0.0001*	MAN > PBS
Final Per Diff	$\delta = 0$	$\delta > 0$	0.0094*	MAN > PBS
Per Inc	$\delta = 0$	$\delta > 0$	<0.0001*	MAN > PBS
Per Dec	$\delta = 0$	$\delta < 0$	0.0066*	MAN < PBS

Appendix G: Measured Displacement Accuracy

The measured displacement accuracy calculated using the sixth static image collected of each kidney is shown in Table G1.

Table G1: Measured displacement accuracy

Kidney Sample ID	MeanU: Img 6 (μm)	StdU*2: Img 6 (μm)	MeanV: Img 6 (μm)	StdV*2: Img 6 (μm)	MeanW: Img 6 (μm)	StdW*2: Img 6 (μm)	Avg Abs Dev U: Img 6 (μm)	Avg Abs Dev V: Img 6 (μm)	Avg Abs Dev W: Img 6 (μm)
K1_R_PBS_020917	-4.319	5.327	4.868	4.178	2.223	9.908	4.823	4.868	6.065
K2_L_MAN_020917	-2.015	3.387	1.473	2.407	7.557	6.438	2.701	1.940	7.557
K1_R_MAN_022217	1.210	1.571	0.412	0.814	-1.768	3.702	1.390	0.613	2.735
K2_L_PBS_022217	-1.005	0.947	1.179	0.938	3.942	4.675	1.005	1.179	4.309
K1_L_PBS_022417	0.564	2.062	-1.430	1.565	-6.046	5.450	1.313	1.497	6.046
K2_R_MAN_022417	-0.661	1.623	-0.451	1.133	3.448	10.388	1.142	0.792	6.918
K1_R_PBS_030117	-0.847	4.705	-1.497	2.804	7.595	10.555	2.776	2.151	9.075
K2_L_MAN_030117	0.029	1.396	0.820	0.876	0.387	4.723	0.713	0.848	2.555
K1_L_MAN_030217	-0.139	7.222	1.022	7.320	5.827	12.479	3.680	4.171	9.153
K2_R_PBS_030217	-2.552	4.062	1.054	3.235	9.062	9.673	3.307	2.144	9.367
K1_R_MAN_030317	-1.000	4.813	-2.298	5.956	-3.637	9.030	2.906	4.127	6.334
K2_L_PBS_030317	-6.359	7.341	-2.350	6.421	4.971	11.946	6.850	4.386	8.458
K1_L_PBS_030717	1.082	3.426	-1.249	3.836	-0.071	6.724	2.254	2.543	3.397
K2_R_MAN_030717	4.324	6.144	-1.444	3.316	-17.766	17.059	5.234	2.380	17.766
K1_L_MAN_030817	1.739	5.559	4.540	6.262	-1.986	10.983	3.649	5.401	6.485
K2_R_PBS_030817	2.106	3.229	-0.188	3.316	-0.992	5.700	2.668	1.752	3.346

Appendix H: Biopsy Scoring Results

Each renal biopsy was scored by Dr. John Robertson using a semi-quantitative scoring method. The results are shown in Table H1, with the following numeric scale:

- 1 = minimal feature change,
- 2 = mild feature change,
- 3 = moderate feature change,
- 4 = marked feature change,
- 5 = severe feature change.

A dash indicates no feature change. The lines highlighted in red were biopsies collected from kidneys excluded from the study.

Table H1: Biopsy scoring results

Sample ID	Total Ischemic Interval (h)	Acute Tubular Necrosis (ATN)	Vacuolation (VAC)	Tubule Lumen Dilation (DIL)	Tubule Shrinkage (SHRINK)	Hyaline Droplets (H/D)
K1-R-PBS-020917	11.0	+3 / +4	+2 / +3	-	-	-
K1-L-PBS-022417	10.25	+1 / +2	+2 / +3	-	-	-
K1-R-PBS-030117	10.0	+1	+1	-	-	-
K1-L-PBS-030717	9.25	+1	+1	-	-	-
K2-R-PBS-030817	11.75	+1 / +2	+2 / +3	-	-	-
K2-R-PBS-021717	13.5	+2	+2	-	-	-
K2-L-PBS-022217	13.5	+1	+1	-	-	-
K2-R-PBS-030217	11.25	+2	+2 / +3	-	-	-
K2-L-PBS-030317	12.0	+3	+3	-	-	-
K1-L-MAN-021717	10.25	+1	-	+3	+3	-
K1-R-MAN-022217	10.5	-	-	+3	+3	+2
K1-L-MAN-030217	8.25	-	-	+3	+3	+1
K1-R-MAN-030317	9.0	+2	-	+3	+3	+1
K1-L-MAN-030817	8.75	-	-	+3	+3	+1
K2-L-MAN-020917	14.5	-	-	+3	+3	+1
K2-R-MAN-022417	13.0	-	-	+3	+3	-
K2-L-MAN-030117	12.75	-	-	+3	+3	+1
K2-R-MAN-030717	12.5	-	-	+3	+3	-

Appendix I: Maximum Z-displacement Tracking

Maximum z-displacement tracking with legend and xy-plane definition for all kidneys are in Figure I1-I8.

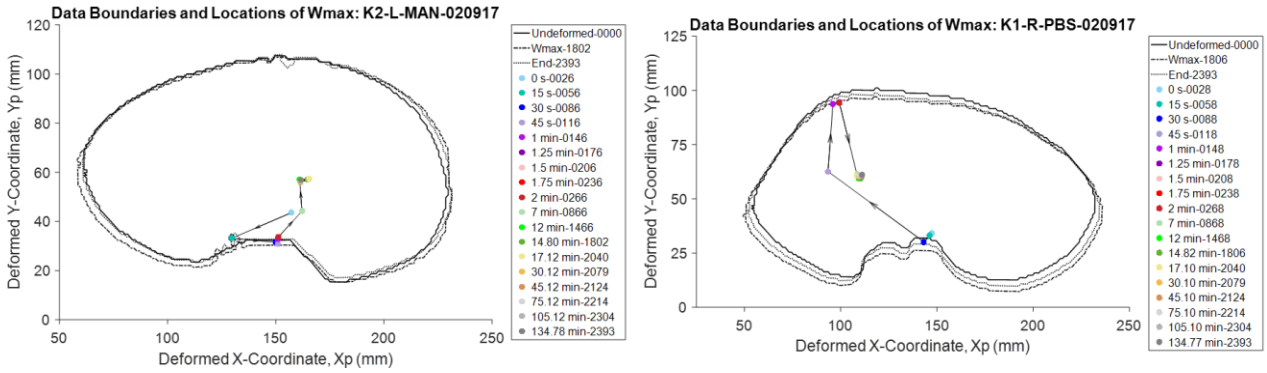

Figure I1. Data boundaries and locations of maximum z-displacement for Experiment 02-09-17.

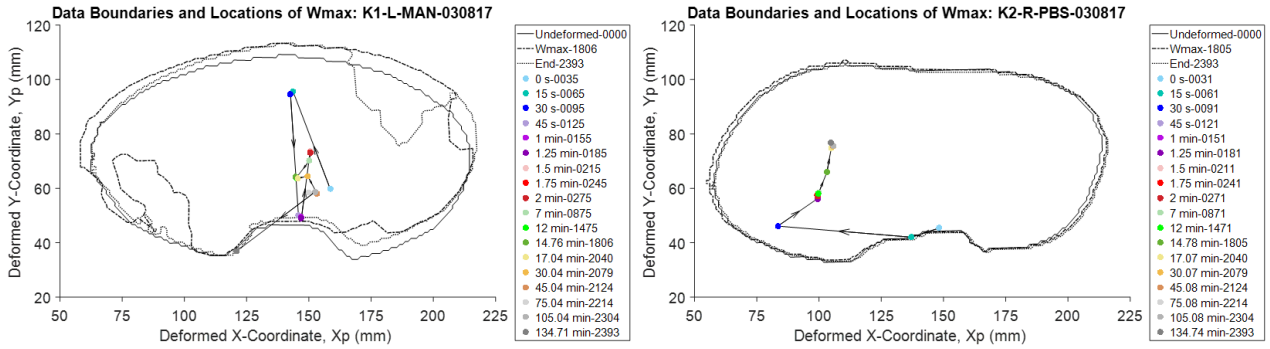

Figure I2. Data boundaries and locations of maximum z-displacement for Experiment 03-08-17.

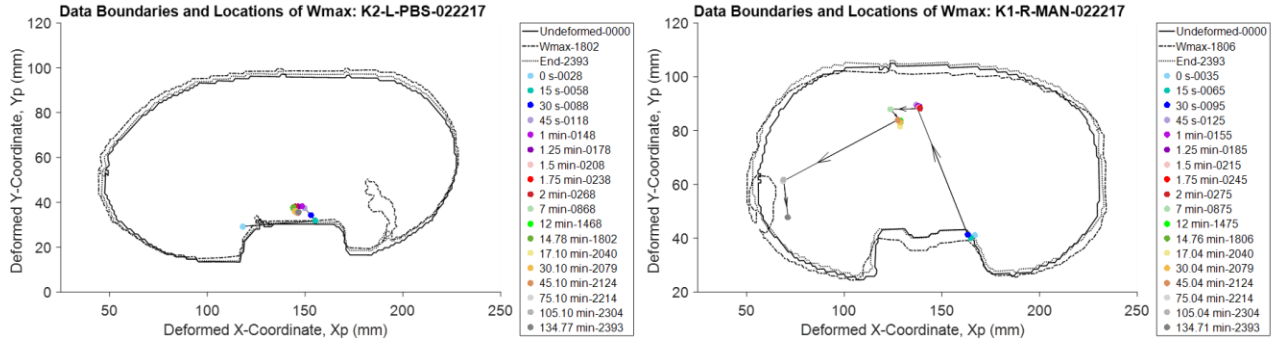

Figure I3. Data boundaries and locations of maximum z-displacement for Experiment 02-22-17.

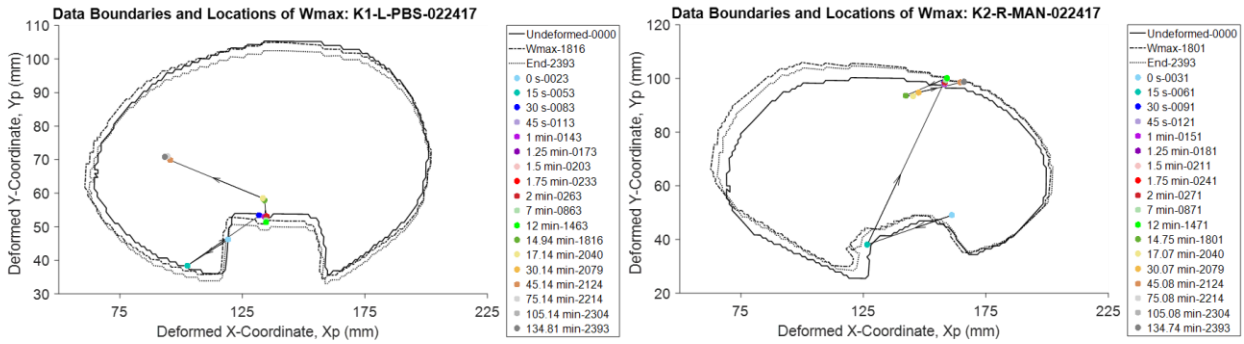

Figure I4. Data boundaries and locations of maximum z-displacement for Experiment 02-24-17.

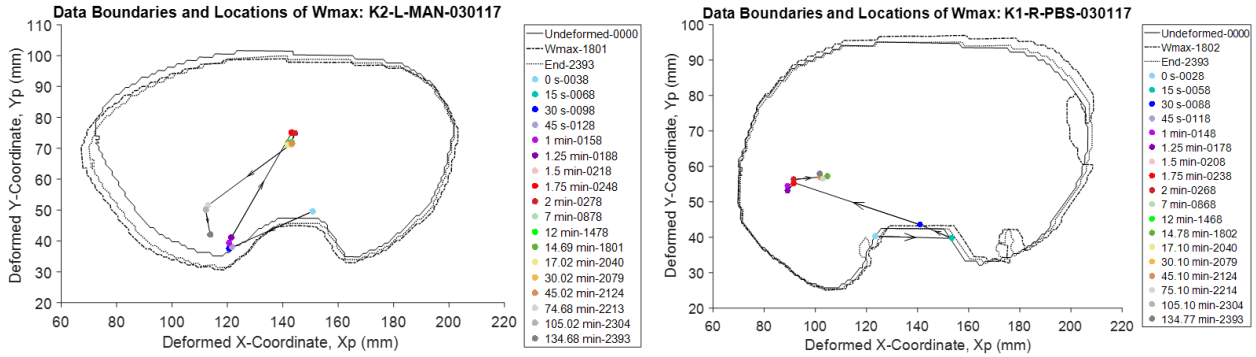

Figure I5. Data boundaries and locations of maximum z-displacement for Experiment 03-01-17.

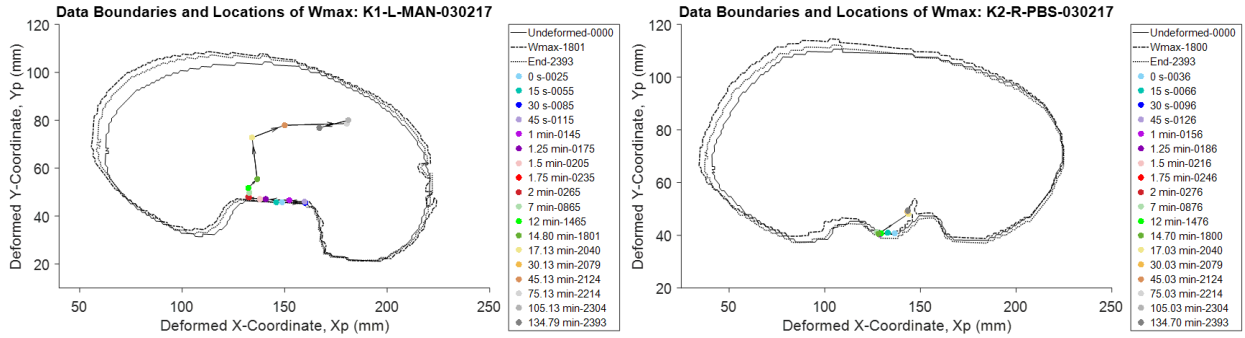

Figure I6. Data boundaries and locations of maximum z-displacement for Experiment 03-02-17.

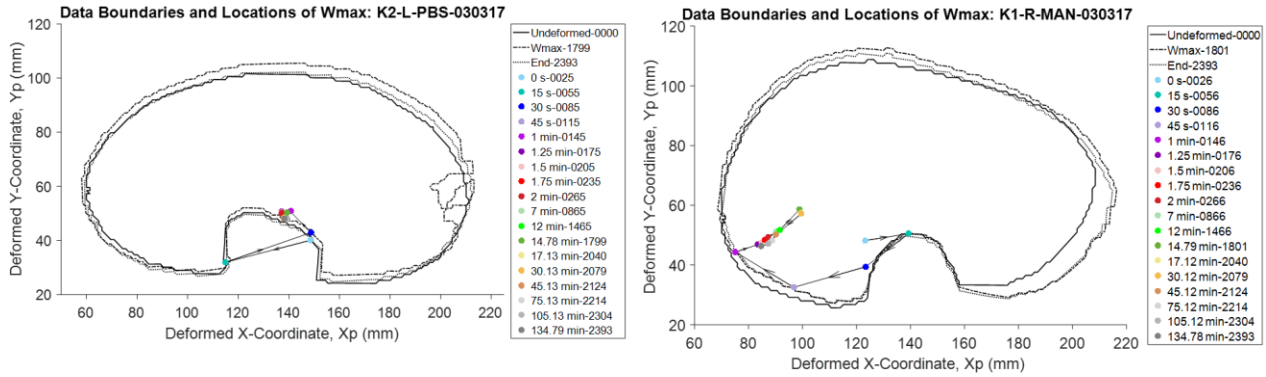

Figure I7. Data boundaries and locations of maximum z-displacement for Experiment 03-03-17.

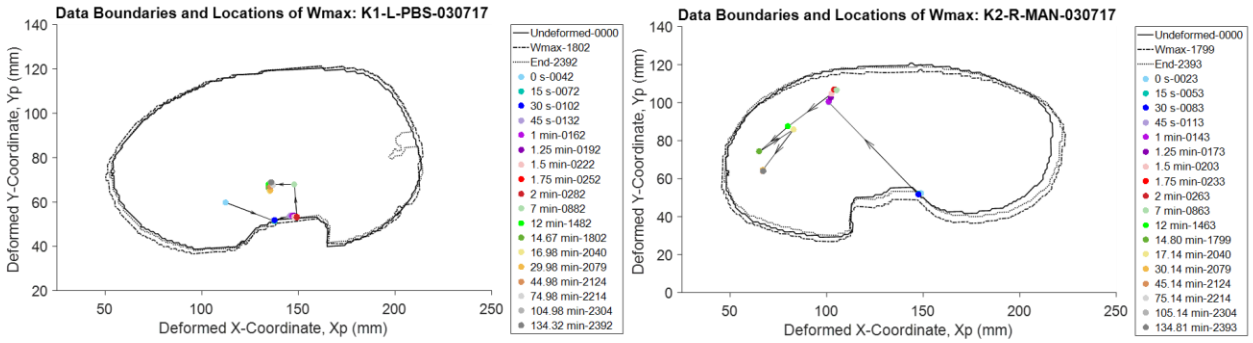

Figure I8. Data boundaries and locations of maximum z-displacement for Experiment 03-07-17.